“Ultra-thin Films of a Ferroelectric Copolymer: P(VDF-TrFE)”

Von der Fakultät für Mathematik, Naturwissenschaften und Informatik
der Brandenburgischen Technischen Universität Cottbus
zur Erlangung des akademischen Grades
Doktors der Naturwissenschaften
(Dr. rer. nat)

genehmigte Dissertation
vorgelegt von

Master of Science in Physics
Master of Technology in Materials Science & Engineering

Dipankar Mandal
Geboren am 21. Juni 1978 in Chapri, Indien

Gutachter: Prof. Dr. rer. nat. habil. Dieter Schmeißer (BTU, Cottbus)
Dr. habil. Rudi Danz (Fraunhofer Institut für Angewandte Polymerforschung)
Prof. Dr. rer. nat. habil. Ch. Pettenkofer (HMI, Berlin)

Tag der mündlichen Prüfung: 25. September 2008

"Ultra-thin Films of a Ferroelectric Copolymer: P(VDF-TrFE)"

Dipankar Mandal

Brandenburgische Technische Universität Cottbus, Germany, 2008

Zusammenfassung

Dünne durch Spin Coating abgeschiedene Filme des ferroelektrischen Copolymers P(VDF-TrFE) sind attraktiv für viele Anwendungen. Für diese Filme stellt sich die Frage, ob eine Abhängigkeit der ferroelektrischen Funktionalität von der Schichtdicke des ferroelektrischen Materials existiert. In dieser Arbeit wurden erfolgreich ultradünne P(VDF-TrFE)-Schichten herunter bis zu einer Dicke von 0.35 nm abgeschieden, was als sehr aussichtsreich für „low-cost"-Ansätze in der elektronischen Industrie anzusehen ist.
Diese Arbeit fokussiert auf die Präparation und Charakterisierung von ultradünnen P(VDF-TrFE)-Schichten, um eine wissenschaftliche Orientierung für mögliche nichtflüchtige Speicheranwendungen zu erarbeiten.

Anfangs wird zunächst die Präparation dargestellt. Dabei wird speziell auf die Optimierung der Temperparameter eingegangen. Die Bestimmung der Schichtdicke des Copolymers kann sehr präzise für die untersuchten ultradünnen Schichten durchgeführt werden.

Ausführlich wurde in der Arbeit die Charakterisierung der Filme mit der Photoelektronenspektroskopie durchgeführt. Dabei wurde zusätzlich festgestellt, dass für längere Röntgenstrahlungsexpositionszeiten der Filme eine Phasenumwandlung von der ferroelektrischen zur paraelektrischen Phase stattfinden kann. Deshalb wurde die Bestrahlungszeit hinsichtlich der unverfälschten Auswertbarkeit der spektroskopischen Ergebnisse optimiert.

Mit der Photoelektronenspektroskopie wurde die Grenzflächenchemie zwischen P(VDF-TrFE) und verschiedenen Elektrodenmaterialien untersucht. Die Grenzflächen von Aluminium/P(VDF-

TrFE) und PEDOT:PSS/P(VDF-TrFE) wurden verglichen. PEDOT:PSS (Poly(3,4-Ethylendioxithioph):Poly(Styrensulfonat) ist ein leitfähiges Polymer. Die Daten zeigen, dass sich eine Grenzflächenschicht bei Aluminiumelektroden bildet, eine Grenzflächenreaktion zeigt sich sowohl für Top- als auch für Bottomelektroden. Im Gegensatz dazu zeigt das organische PEDOT:PSS keine chemische Wechselwirkung mit dem P(VDF-TrFE). Dies zeigt eine verbesserte Funktionalität von dünnen organischen ferroelektrischen Filmen.

Für "low-cost"- Ansätze der Elektronik, die auf organischen Bauelementen basiert, ist die Einführung von organischen nichtflüchtigen Speichern von großer Bedeutung. P(VDF-TrFE) Copolymer ist ein Material mit einer sehr hoffnungsvollen Perspektive.
Ergebnisse elektrischer Messungen an P(VDF-TrFE)-Schichten werden in einem weiteren Abschnitt dieser Arbeit dargestellt. Mit Kapazitäts-Spannungsmessungen (CV) bei erhöhten Temperaturen wird der Curie-Punkt untersucht. Bei der Benutzung von Aluminiumelektroden wird eine Abnahme der Polarisation für Schichten kleiner 100 nm gefunden. Mit inerten Elektroden war eine Herunterskalierung bis zu 10nm mit einem kleinen Koerzitivfeld möglich. Das ist wichtig, da das relativ hohe Koerzitivfeld des P(VDF-TrFE) (>50 MV/m) eine ultradünne Schichtdicke für geringe Betriebsspannungen erfordert. Eine Voraussetzung für Speicheranwendungen ist eine hohe Retentionszeit, dies wurde auch gezeigt.

Die ferroelektrische Dipolorientierung wurde mit NEXAFS-Untersuchungen (Near edge X-ray Absorption Spectroscopy) untersucht. Bei Benutzung eines PEDOT:PSS-Substrates konnte auch für 0.35 nm dicke P(VDF-TrFE)-Filme eine durchschnittliche Dipolorientierung senkrecht zur Substratoberfläche) nachgewiesen werden.

Die ferroelekrischen Eigenschaften wurden für Filme bis zu 10 nm mit spektroskopischen (F1s NEXAFS) und elektrischen (CV) Methoden untersucht. Die Resultate zeigen, dass ein extrinsischer Schaltmechanismus vorliegt, der bei einer wesentlich kleineren Spannung als beim kollektiven intrinsischen Effekt stattfindet. Beide unabhängigen Methoden zeigen, dass keine kritische Dicke für Spincoating-Filme bis herunter zu 10 nm gefunden wird, wenn adaptierte Elektroden benutz werden.

"Ultra-thin Films of a Ferroelectric Copolymer: P(VDF-TrFE)"

Dipankar Mandal

Brandenburgische Technische Universität Cottbus, Germany, 2008

Abstract

Spin-cast films of the ferroelectric copolymer P(VDF-TrFE) are attractive for various applications. For such films the question arises whether there exists a depending on film thickness of ferroelectric functionality. In this work, ultra-thin films of P(VDF-TrFE) up to 0.35nm of thickness have been successfully spin coated, which is quite promising in respect of low cost approach in the electronic industry.

This thesis focuses on the preparation of the ultra-thin P(VDF-TrFE) copolymer film and its characterizations to find out a scientific guideline for the suitable application as a non-volatile memory element. Therefore, the ultra-thin film preparations have been investigated initially. Optimization of annealing parameters has been done to get the ferroelectric beta phase and thickness determination is also done carefully. The copolymer layer thickness could be determined down to about 0.35 nm.

Photoelectron spectroscopy is used extensively for the characterization of the thin film. Eventually, longer time X-ray irradiation of the P(VDF-TrFE) sample may cause a phase change from ferroelectric to paraelectric. Therefore the X-ray irradiation time was also optimized.

With photoelectron spectroscopy, the interface chemistry of the P(VDF-TrFE) copolymer and different electrode materials was studied. The interfaces aluminum/P(VDF-TrFE) and PEDOT:PSS/P(VDF-TrFE) are compared. PEDOT:PSS is a conducting polymer, Poly(3,4-ethylenedioxidethiophene): poly(styrenesulfonate). This data suggested that an interface layer is

formed for electrodes, made of aluminum. An interface reaction occurs in both cases: for aluminum as top and as bottom electrode. In contract, the organic PEDOT:PSS electrode shows no chemical interaction with the P(VDF-TrFE) copolymer. The much lower reactivity of organic electrode, compare to aluminum, gives a direct hint to improved functional properties of thin organic ferroelectric films.

In terms of a low cost approach for electronics, based on organic devices, the introduction of organic non volatile memories is of great importance. P(VDF-TrFE) copolymer is the material with a very hopeful perspective.
In next part electrical measurements with P(VDF-TrFE) have been done. By capacitance voltage measurements, the ferroelectric behavior of the polymer by measurements at elevated temperatures (Curie-Point) is confirmed, a threshold for remanent poalrization for films below 100 nm is found, if aluminum electrodes are used, but with inert electrodes, a downscaling of a low coercitive field was possible down to ten nm. This is very important, because due to the high coercitive field of the copolymer (>50 MV/m), ultrathin films for low operation voltages are needed. A prerequisite for memory applications is a high retention time, this was also confirmed.

By the help of Near edge X-ray Absorption Spectroscopy (NEXAFS) the possible ferroelectric dipole orientation have been also investigated. The average dipole orientation (perpendicular to the substrate) is observed up to 0.35 nm P(VDF-TrFE) copolymer films when PEDOT:PSS/Si substrate is used.

The ferroelectric properties of ultrathin films down to a layer thickness of 10nm were characterized using spectroscopic (F1s NEXAFS) and electrical methods (Capacitance voltage). The results indicates an extrinsic switching mechanism with a much lower operation voltage than for a collective intrinsic switching. Both independent methods agree that there is no critical thickness for spincoated copolymer films down to 10 nm, if an adapted system of electrodes is used.

Contents

Chapter 1. Introduction

1.1 P(VDF-TrFE) copolymer : background…….....1

1.2 Structures of PVDF and its co-polymer: P (VDF-TrFE)……2

1.3 Basic properties of P(VDF-TrFE)……...7

1.4 Motivation of the work.....10

Chapter 2. Experimental

2.1 Fourier Transformed Infra-Red Spectroscopy (FTIR)……..19

2.2 X-Ray Diffraction.....21

2.3 Atomic Force Microscopy.....22

2.4 X-ray Photoelectron Spectroscopy (XPS)……26

2.5 NEXAFS Spectroscopy.....31

2.6 Thin film preparation.....47

2.7 Thickness determination.....50

2.8 Surface morphology.....53

2.9 Beta phase identification.....55

2.10 Effect of Annealing.....57

2.11 Optimization of the X-ray irradiation time……...61

2.12 Experimental setup for external electric field……...66

Chapter 3. Aluminum and PEDOT: PSS interaction with P(VDF-TrFE)

3.1 Introduction.....75

3.2 XPS results.....77

3.3 Discussions.....83

Chapter 4. Summary of the electrical characterizations of the thin films

4.1 Introduction.....87

4.2 Results and discussion of electrical characterizations……..87

Chapter 5. Orientation of the ferroelectric dipoles

5.1 Introduction.....95

5.2 Peak assignment of NEXAFS spectra……..96

5.3 Dipole Orientation Evaluation by Angular Dependent NEXAFS……...100

5.4 Results and discussion…….103
5.5 Electric Field Induced Polarization.....111
5.6 Results.....112
5.7 Further results of ultra thin film (10 nm thickness)…….116
5.8 Discussion.....118

Chapter 6. Summary and outlook……..127

Appendix

Chapter 1. Introduction

Ferroelectric polymer polyvinylidene fluoride (PVDF) and its copolymer P(VDF-TrFE), both of them have attracted due to excellent properties and for their utility. Since last 30 years, P(VDF-TrFE) is mostly extensive studied ferroelectric polymer [1]. It has tremendous applications in electronic industry such as soft transducers, infrared imaging, and compact capacitors and most promisingly as a non volatile memory.

1.1. P(VDF-TrFE) copolymer : background

Ferroelectrics are the field of interest among researcher since almost 80 years [2]. This class of materials belongs to the pyroelectric family of which the direction of spontaneous polarization can be reversed by an electric field. In 1894, Pockels reported the anomalously large piezoelectric constant of Rochelle salt. From initial investigations of Rochelle salt by Valasek in the early 1920s [2, 3], ferroelectric materials are focus on research area. Starting from Rochelle salt, typical examples include potassium dihydrogen phosphate (KH_2PO_4), sodium nitrite ($NaNO_2$), and barium titanate ($BaTiO_3$). Most of them are stiff crystalline solids. In the last decade, some new ferroelectric members have been introduced those are somewhat different from the traditional ones in various points of view. One of them is a series of liquid crystalline ferroelectrics those are non-solid and rod like structure. Mayer *et al.* have synthesized a liquid crystal, called DOMAMBC, and have demonstrated ferroelectric polarization reversal behavior [4].

PVDF is not a newly synthesized polymer and it has been known over almost 50 years. Initially it was familiar as a polymer having a large dielectric constant and diverse crystalline polymorphs phase. Strong piezoelectricity was discovered by Kawai in 1969 for uniaxially-drawn and poled film [5]. Thereafter, in 1971, Bergman, McFree and Crane have accounted finding of pyroelectricity and non-liner optical behaviour in the same polymer [6]. These effects lead the idea that PVDF is not only a chemically stable structural material but also a functional polymer which perform as energy transducer. An extensive effort has been mature to basic understanding and the technical applications of PVDF [7-11]. After commercialize the product of PVDF as piezoelectric and pyroelectric flexible transducers, there had been continuing arguments regarding the origin of these effect, especially, whether they arises from oriented molecular dipoles or trapped space charges.

In the late 1970s, however, evidence for possible reorientation of crystalline dipoles induced by poling was demonstrated by means of X-ray and IR techniques [9, 12-14]. First switching

phenomena and hysteresis loops were demonstrated and explain by Furukawa *et al*., which gave much clear picture in this field that PVDF is a ferroelectric polymer [15, 16]. In 1980s, the existence of a Curie point, which is one of the evidence of ferroelectricity has been observed in copolymer of PVDF, namely, poly (vinylidene–trifluorethylene) (P(VDF-TrFE)) [15, 17, 18]. Afterwards, many scientific observations, interpreted as ferroelectric behavior of P (VDF-TrFE) were published [16, 19-23].

1.2. Structures of PVDF and its co-polymer: P (VDF-TrFE)

PVDF, a nonconjugated linear fluorinated hydrocarbon consists of a repeating unit of CH_2CF_2. It has a polar structure associated with positive hydrogen and negative fluorine atoms. The value of net dipole moment (μ_v) is about 7×10^{-30} Cm in vacuum [24, 25]. The orientations of dipoles are directly controlled by the conformation and packing of molecules, as the dipoles are rigidly attached to main backbone of the carbon chain. Figure 1.1 shows the unit structure (I), the molecular conformation (II), the crystalline structure (III), and the bulk structure (IV) of PVDF in its ferroelectric phase. In the *all-trans* conformation the CH_2CF_2 dipoles are aligned in the zigzag plane and perpendicular to the chain axis. In this case, *all-trans* molecules prefer to be packed in a parallel fashion to form a crystal called β phase. To generate the highest spontaneous polarization value, the molecular dipoles in the β phase are entirely aligned in one direction. If one consider μ_v is 7×10^{-30} Cm, then crystalline polarization for unit volume becomes $P_0 = 2\mu_v/abc = 130$ mC/m^2, where *a, b,* and *c* are orthorhombic lattice constants and the typical value in this case, $a = 0.858$ nm, $b = 0.491$ nm and $c = 0.256$ nm. The β phase is responsible for the ferroelectricity of PVDF, as the direction of P_0 has been shown to be switchable by action of the electric field. The bulk sample of PVDF is a mixture of crystalline and amorphous regions. It was found that ferroelectricity comes from the crystalline region, but the noncrystalline region is also more or less influenced [26].

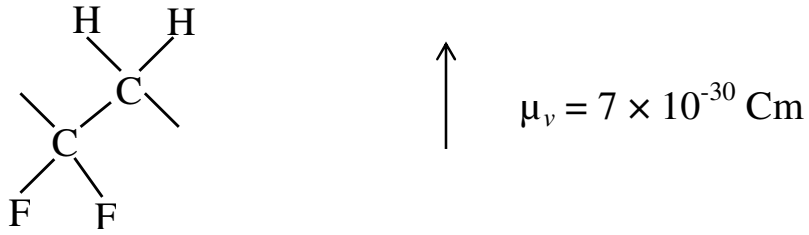

(I) Polar unit

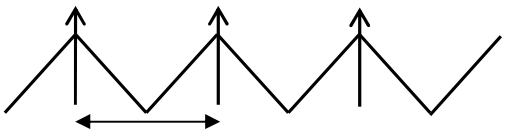

$c = 0.256$ nm

(II) All-trans conformation

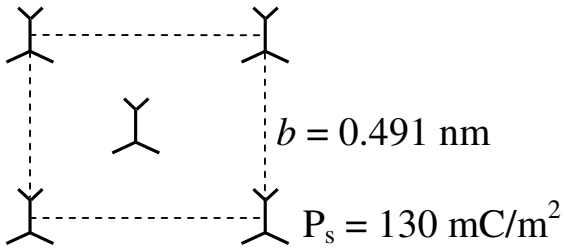

(III) Parallel packing

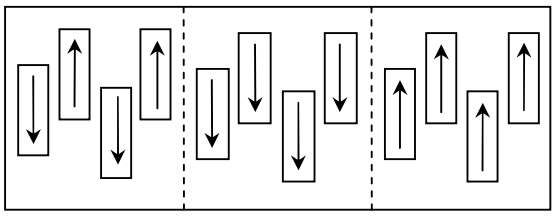

(IV) Polycrystalline bulk

Figure 1.1. *Unit (I), molecule (II), crystal (III), and bulk (IV) structure of PVDF [1, 35].*

Molecular and crystalline structure

PVDF have usually four different types of polymorphs. The *all-trans* (*TTTT*) β phase (phase I) is one of the diverse crystalline structure. The most common polymorph is the α phase (phase II) which consists of alternating *trans-gauche* $TGT\overline{G}$ molecules packed in antiparallel fashion [27, 29, 37]. There is an intermediate conformation T_3GT_3G which favors a parallel packing to generate the γ phase (phase III) [28]. The parallel version the α phase is known as δ phase (phase α_p or IV) [30, 31]. Figure 1.2 shows the molecular conformations and crystalline forms of PVDF. The polymer chain confirmations can be explained in the sequence of dihedral bond angles. The *trans* bond (*T)* has a dihedral angle of approximately ~ 180^0 and the left and right *gauche* bonds (*G* and $\overline{G}$) have dihedral angles of approximately ± 60^0. Therefore in summary, the most common conformations are *all-trans TTTT* (figure 1.2a), alternating left-right trans-gauche $TGT\overline{G}$ (figure 1.2b) and helical *TGTG* or $T\overline{G}T\overline{G}$. All three conformations form straight cylindrical chains that crystallize in a quasi-hexagonal packing.

In the β phase, the *all-trans* (*TTTT*) conformation crystallizes in an orthorhombic *m2m* structure with chains along the crystal c-axis and the dipoles aligned approximately along the crystal *b*-axis as shown in figure 1.2 [32-36]. The β phase is polar and uniaxial ferroelectric, as the polarization can be repeatably switched between opposite but energetically equivalent directions along the 2-fold *b*-axis. The β phase unit cell nominally consists of two $-(CH_2-CF_2)-$ formula units, one along the c-axis parallel to the chains (see figure 1.2a). The unit cell dimension is approximately: c = 0.256 nm along the chain axis, b = 0.491 nm along the polarization direction which is the 2-fold axis and a = 0.858 nm perpendicular to the chain axis and to the polarization [35]. It is possible that the unit cell is twice as big, containing two monomers along the chain, because a ± 7^0 dihedral tilt-ordering would make the *c*-axis period two monomers long or $c \approx 0.512$ nm [34].

The complete crystalline α phase structure shown in figure 1.2 (d) consist of opposing polar sublattices of the *trans-gauche* chains, resulting no net polarization in both parallel and perpendicular to the chain axis. The α phase unit cell nominally consists of four $-(CH_2-CF_2)-$ units, two along the *c*-axis parallel to the chains and two in the plane perpendicular to the *c*-axis. The unit cell dimensions are approximately: a = 0.964 nm, b = 0.496 nm, c = 0.462 nm [37].

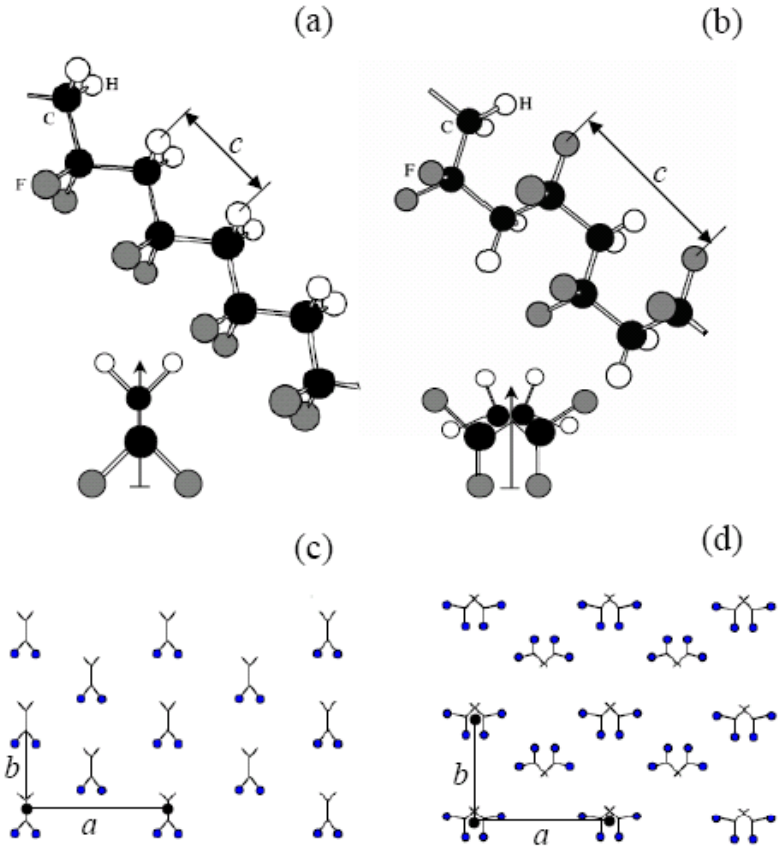

Figure 1.2. *Diagram of crystalline forms of PVDF (a) in the all-trans conformation (inset, end view of a chain); (b) in the alternating trans-gauche conformation (inset, end view of a chain); (c) end-on view of the crystal structure of the ferroelectric β phase, composed of close-packed all-trans chains; (d) end-on view of the crystal structure of the paraelectric α phase, composed of close-packed trans-gauche chains [32,36].*

It is possible that the α phase structure is antiferroelectric but published reports proposed only direct conversion to the *all-trans* conformation in the β phase on the application of an electric field [38-41], no rotation of the *trans-gauche* dipoles into the polar alternating *trans-gauche* α_p, or phase IV, which may be only metastable [34, 35, 42].

The paraelectric phase is composed of chains with the alternating *trans-gauche* ($TGT\overline{G}$) conformation (figure 1.2 b), packing with no macroscopic polarization. The crystal structure of the paraelectric phase has been variously described as orthorhombic *mmm* [37, 43], monoclinic *2/m* [34, 44, 46], and hexagonal [45, 47]. It has been proposed that the macroscopic paraelectric phase is composed of a random packing of the trans-gauche chain or a mixture of microcrystalline regions, each with different packing [42]. The paraelecteric phase structure includes a helical conformation in hexagonal packing [42], though infrared and Raman spectroscopes indicate a preponderance of *trans-gauche* conformation [48, 50]. Some observations pointed out, that especially PVDF and its copolymer exhibit a number of metastable crystalline phases that are difficult to separate from the true equilibrium phase [35, 51, 52].

It was found that 3-6 % unavoidably introduce monomer reversal defects with structure $-(CH_2-CF_2)-(CF_2-CH_2)-(CH_2-CF_2)-$ by the standard synthetic methods [53-55]. PVDF can also be copolymerized, apparently in random sequence, with trifluoroethylene (TrFE) $-(CHF-CF_2)-$ and tetrafluoroethylene (TeFE) $-(CF_2-CF_2)-$. The reversed monomers and the intentionally incorporated TrFE or TeFE units function as defects, tending to lower the melting and ferroelectric phase transition temperatures, as can chain ends, bends, and folds. The copolymer also has a slightly larger unit cell and a smaller average dipole moment than pure PVDF, owing to the replacement of some of the hydrogen atoms by the larger fluorine atoms. A molecular modeling of PVDF and its copolymers have determined stable conformations, crystal structures, band structures and other physical properties [57, 58]. Farmer *et al*. investigated the stability of crystal structures of the two main conformations, *all-trans* and alternating *trans-gauche*, finding that at least 14 % defects (e.g., TrFE monomers, head-head defects, chain ends) are needed to stabilize the α phase [34]. This was a reasonable agreement with experimental observations which showed that to produce a stable paraelectric α phase at below the melting point, the minimum requirement of TrFE was 20 % [53, 56]. Karasawa and Goddard found that the *trans-gauche* conformation could crystallize in four different packing arrangements with nearly identical energies, and proposed that the actual paraelectric α phase is a statistical mixture of these four packing arrangements [42]. The microscopic models have so far proven not sufficient enough for studying the ferroelectric-paraelectric phase transition because they neglect dipole-dipole interactions and treat interchain interactions only in the mean field approximation. Modern computers and codes are much more powerful and will likely produce greatly improved models of the structure and dynamics of ferroelectric polymers [59]. It was observed that PVDF essentially does not

crystallize from the melt and crystallizes only poorly from solution [60]. Films must be treated mechanically by stretching to align the polymer chains, and electrically to align the polarization axes of the crystallites. A mechanical and electrical alignment process leads to macroscopic behavior, although the film still having almost 50 % amorphous material and the crystallites are incompletely oriented [53, 60, 61]. On the other hand, copolymers of PVDF with trifluoroethylene (TrFE) and tetrafluoroethylene (TeFE) crystallize readily from the melt and can be stretched and electrically polarized to over 90 % crystallinity [53, 61, 62]. Films formed by spinning on texture Teflon have shown particularly good crystallinity and orientation which allow to detailed studies of intrinsic elastic anisotropy [63]. Several attempts (such as uniaxially drawing, annealing) successfully showed the significantly improved crystallinity in copolymer films, apparently eliminating amorphous material and lamellae, and producing a single crystalline phase with highly oriented crystallites [45, 47, 64]. Although much has been learned about the fundamental nature of ferrolectricity and related properties of PVDF copolymers, due to limit of processing of crystallization and as well as accuracy of measurements, many questions relating the fundamental properties are still not clear.

1.3. Basic properties of P(VDF-TrFE)

Ferroelectricity

The most promising property of P(VDF-TrFE) co-polymer is ferroelectricity, which is eventually useful for the application as non-volatile memory element. The evidence of the ferrolectricity arises due the presence of the component of TrFE with PVDF [24], which do exhibits a clear ferroelectric-paraelectric phase transition. P(VDF-TrFE) crystallize into various crystal forms depending on their molar content rations of VDF (x) and TrFE (1-x), and on crystallization conditions [25, 26, 32]. Under ordinary pressure, the α crystal form consisting of *TGTG* chains is stable for the VDF homopolymer (PVDF), while the β phase crystal consisting of *all-trans* chains becomes more stable on introducing TrFE sequences into VDF chains [34]. The β phase crystal is well known to be ferroelectric from its D-E hysteresis loops [15, 40], polarization switching [65], temperature behavior of the dielectric constant [15, 65-67], and anomalous X-ray dispersion [68]. Addition of the larger and less molar ratio of TrFE ruined the transition temperature by reducing the average dipole moment of the chains, expanding the lattice, and introducing defects. This ruined of ferroelectricity on addition of TrFE which indicates the resulting decrease in transition temperature [56]. In our study we choose the composition of 70% VDF and 30 % TrFE molar ratio, because it has the

most distinct ferroelectric properties and can be made mostly crystalline without stretching treatments. As the crystallinity is increased, the depolarization field is much reduced and therefore reasonably hysteresis loops occurs, a result from the 65 % VDF and 35 % TrFE molar ratio of P(VDF-TrFE) copolymer which has a crystallinity of ca. 80% [60].

Ferroelectric switching

The ferroelectric switching process gives the information about the dynamic characteristic of the polarization reversal.

The switching time of a ferroelectric follow the flowing relations

- $\tau_s = \tau_{s0} \exp(E_a / E)$, an exponential law 1.1
- $\tau_s = AE^m$, a power law 1.2

where E is the applied electric field, E_a is the activation field, τ_{s0} is the switching time at infinite field, know as 'time factor'. The experimental observation showed that ferroelectric polymers such as PVDF and the copolymer P(VDF-TrFE) follow the exponential law up to a sustainable field [23, 86, 87, 88], whereas $BaTiO_3$ follows the exponential law for fields from 0.3 to 3.0 MV/m, while it follow the power law at higher fields up to 10 MV/m [89, 90]. Most importantly, it is not found such a transition in P(VDF-TrFE) copolymers over a broad range of the applied field. It is noted that the applied sustainable field is much lower than that for the copolymer. The copolymers, especially in their very thin films, allow the application of a very high electric field.

For low fields where the nucleation of domains persists, the switching time is phenomenologically described by equation 1.1. A switching kinetic like this is called ***extrinsic switching***. For extrinsic switching process two mechanisms are play the most important role. One is nucleation of domains with opposite polarization when a reverse field is applied and another is growth of these small domains accompanied by domain wall motion.

In the higher field strengths, the nucleation of the new domains is so fast that the switching time is primarily determined by the time it takes to move the domain walls. In this case, τ_{ex} is described by

$$\tau_{ex} = \frac{1}{\mu(E - E')} \qquad 1.3$$

Where μ is the mobility of the domain walls and E' is a limiting field defining the range of validity of equation 1.3 and it is similar to coercive field strength. Therefore, in this case, a minimum critical size for ferrolectricity should exist, and a thermally activated process might be expected [94].

Some studies using P(VDF-TrFE) copolymer Langmuir-Boldgett films [95, 96] the switching kinetics follows different rules. This type of switching is called ***intrinsic switching***. For ultra-thin Langmuir Blodgett ferroelectric films of P(VDF-TrFE) with a thickness below 15 nm, the kinetics of polarization switching exhibit a critical behavior characterized by a pronounced slowing just above the coercive field [95, 96]. This phenomenon is called the intrinsic switching mechanism and the associated threshold field the intrinsic coercive field. Apart from the nucleation driven process of ferroelectricity, this field shows an enormous magnitude. In such a system, the dipoles in the crystal are highly interconnected and intended to switch coherently or not at all. Due to a reduced film thickness the nucleation volume limits and that does not allow nucleation. As a result extrinsic switching is inhibited.

Piezoelectricity and pyroelectricity

A change in polarization can occur through changes in either the moment or the volume. Piezoelectricity and pyroelectricity arises due to mechanical and thermal stresses respectively. PVDF has large (relative to inorganic and metallic materials) compressibility and thermal expansion coefficients, and with aligned dipoles present, can yield large polarization changes through changes in volume [69, 70]. Since the discovery of PVDF, several investigations have been done on piezoelectric and pyroelectric properties of uniaxially drawn PVDF [7, 8, 71-74]. As PVDF is a ferroelectric polymer as well which have switchable dipoles [14, 75-77], the piezoelectric and pyroelectric activities can be naturally ascribed to the cooperative orientation of crystalline dipoles. PVDF is a complicated material in the context that samples used for the measurements are subjected to uniaxial drawing before poling. Uniaxial drawing results in a strong mechanical anisotropy, especially in large Poisson's ratios [78]. In analogous to PVDF, the P(VDF-TrFE) copolymer basically adopt an all-trans structure of β phase in melt-crystallized or solution cast films [33, 79, 80]. As a result P(VDF-TrFE) copolymer shows piezoelectric and pyrolectric properties in undrawn samples [81]. This arises due to aligned crystalline dipoles. The degree of dipole orientation, equivalently the remanent polarization P_r, is the most crucial quantity determining the magnitudes of these activities. Furukawa and Wen have proposed a model to explain the possibility that stress induces the changes in dipole orientation due to an electrostrictive coupling in the crystalline phase of P(VDF-TrFE) cast film [85]. Some observations reported that the poled copolymers

with higher PVDF contains (70-80 mole %) exhibit strong piezoelectric effects and conspicuous ferroelectric phenomena [82]. In uniaxial constrained films, the effective pyroelectric coefficient depends on the pyroelectric coefficients and also on the piezoelectric and elasticity tensors, because the thin film constrained on a rigid substrate is stress-free normal to the film, but strain-free in the film plane [83, 84].

1.6. Motivation of the work

This work addresses the possibility of using organic materials to make nonvolatile memory device by combining a ferroelectric and conducting polymer. It is conceivable that such a memory device could be made by solution-processing techniques, which would enable its use in ultra-low-cost applications. One of the main applications that one can conceive for such polymer memory devices in low-cost mass data storage. For this application it would have to compete with Flash memory technology by offering lower production costs. Another major application is the integrated memory. For the merit of such kind of research, it is expected that it is unattaionable by traditional Si-technology. Therefore, there are many challenges to understand the basic properties of the behavior of the ferroelectric polymer in the contest of 'non-volatile memory' element.

Therefore, we have much concentrated to make ultra thin film of the P(VDF-TrFE) copolymer and understand the ferroelectric dipole orientation mechanism by the use of NEXAFS spectroscopy.

References

1. T. Furkawa, "Ferroelectric properties of Vinylidene fluoride copolymers", *Phase Transitions 18 (1989) 143*.
2. J. Valasek, "Piezo-electric and allied phenomena in Rochelle salt", *Phys. Rev. 15 (1920) 537.*
3. J. Valasek, "Piezo-electric and allied phenomena in Rochelle salt", *Phys. Rev. 17 (1921) 475.*
4. R. B. Meyer, L. Liebert, L. Strzelecki, and P. Keller, "Ferroelectric liquid crystals", *J. de Phys. Lett. 36 (1975) L69*.

5. H. Kawai, "The piezoelectricity of poly(vinylidene fluoride)", *Jpn. J. Appl. Phys. 8 (1969) 975.*
6. J. G. Jr. Bergman, J. H. McFree, and G. R. Crane, "Pyroelectricity and optical second harmonic generation in polyvinylidene fluoride films", *Appl. Phys. Lett. 18 (1971) 203.*
7. Y. Wada and R. Hayakawa, "Piezoelectricity and pyroelectricity of polymers", *Jpn. J. Appl. Phys. 15 (1976) 2041.*
8. R. G. Kepler, "Piezoelectricity, pyroelectricity and ferroelectricity in organic materials", *Ann. Rev. Phys. Chem. 29 (1978) 497.*
9. A. J. Lovinger, "Poly(vinylidene fluoride). Developments in crystalline polymers-1" *Ed. by D. C. Bassett. Appl. Sci. London, 1981.*
10. M. G. Broadhurst, and G. T. Davis, "Piezo- and pyroeleccric properties. Topics in modern electret", *Ed. by G. M. Sessler, Springer-Verlag, Berlin, 1980.*
11. G. M. Sessler, "Pizoelectricity in polyvinylidenefluride", *J. Acoust. Soc. Am., 70 (1981) 1596.*
12. M. Tamura, S. Hagiwara, S. Matsumoto, and N. Ono, "Some aspects of piezoelectricity and pyroelectricity in uniaxially stretched poly (vinylidene fluoride)", *J. Appl. Phys. 48 (1977) 513.*
13. M. Tamura, K. Ogasawara, N. Ono, and S. Haigiwara, "Piezoelectricity in uniaxially stretched poly(vinylide fluoride)", *J. Appl. Phys., 45 (1974) 3768.*
14. R. G. Kepler and R. A. Anderson, "Ferroelectricity in polyvinylidene fluoride", *J. Appl. Phys 49 (1978) 1232.*
15. T. Furukawa, M. Date and E. Fukada, Y. Tajitsu, and A. Chiba, "Ferroelectric behavior in the copolymer of vinylidene fluoride and trifluoroethylene", *Jpn. J. Appl. Phys., 19 (1980) L109.*
16. T. Furukawa and G. E. Johnson, "Dielectric relaxations in a copolymer of vinylidene fluoride and trifluoroethylene", *J. Appl. Phys. 52 (1981) 940.*
17. T. Yagi, M. Tatemoto, and J. Sako, "Transition behavior and dielectric properties in trifluoroethylene and vinylidene fluoride copolymers", *Polym. J. 14 (1980) 209.*
18. Y. Tajitsu, A. Chiba, T. Furukawa, M. Date, and E. Fukada, "Crystalline phase transition in the copolymer of vinylidene fluoride and trifluoroethylene", *Appl. Phys. Lett. 36 (1980) 286.*
19. T. Yamada, T. Ueda, and T. Kitayama, "Ferroelectric-to-paraelectric phase transition of vinylidene fluoride-trifluoroethylene copolymer", *J. Appl. Phys. 52 (1981) 948.*

20. A. J. Lovinger, G. T. Davis, T. Furukawa, and M. G. Broadhurst, "Crystalline forms in a copolymer of vinylidene fluoride and trifluoroethylene (52/48 mol%)", *Macromolecules 15(1982) 323.*
21. T. Furukawa and G. E. Johnson, "Dielectric relaxations in a copolymer of vinylidene fluoride and trifluoroethylene", *J. Appl. Phys. 52 (1981) 940.*
22. T. Furukawa, A. J. Lovinger, G. T. Davis, and M. G. Broadhurst, "Dielectric hysteresis and nonlinearity in a 52/48 mol% copolymer of vinylidene fluoride and trifluoroethylene", *Macromolecules 16(1983) 1885.*
23. T. Furukawa, M. Date, M Ohuchi, and A. Chiba, "Ferroelectric switching characteristics in a copolymer of vinylidene fluoride and trifluoroethylene", J. *Appl. Phys. 56 (1984) 1481.*
24. T. Yagi, M. Tatemoto, and J. Sako, "Transition Behavior and Dielectric Properties in Trifluoroethyleneand Vinylidene Fluoride Copolymers" *Polymer J. 12 (1980) 209.*
25. K. Tashiro, K. Takano, M. Kobayashi, Y. Chatani, and H. Tadokoro, "Structural study on ferroelectric phase transition of vinylidene fluoride-trifluoroethylene copolymers (III) dependence of transitional behavior on VDF molar content" *Ferroelectrics 57 (1984) 297.*
26. H. Ohigashi, Proc. 6th Int. meeting on Ferroelectricity, Kobe 1985, *Jpn. J. Appl. Phys. 24 (1985) 23*.
27. R. Hasegawa, M. Kobayashi, and H. Tadokoro, "Molecular conformation and packing of poly(vinylidene fluoride). Stability of three crystalline forms and the effect of high pressure" *Polym. J. 3 (1972) 591.*
28. S. Winhold, M. H. Litt, and J. B. Lando, "The crystal structure of the γ phase of poly(vinylidene fluride)" *Macromolecules, 13 (1980) 1178.*
29. R. Hasegawa, Y. Takahashi, Y. Chatani, and H. Tadokoro, "Crystal structure of the three crystalline forms of poly(vinylidene fluoride)", *Polym. J. 3 (1972) 600.*
30. G. T. Davis, J. E. McKinney, M. G. Broadhurst, and S. C. Roth, "Electric-field-induced phase changes in poly(vinylidene fluoride)", *J. Appl. Phys. 49 (1978) 4998.*
31. B. Servet and J. Rault, "Polymorphism of poly(vinylidene fluoride) induced by poling and annealing", *J. de Phys. 40 (1979) 1145.*
32. J. B. Lando and W. W. Doll, "The polymorphism of poly(vinylidene fluoride). I. the effect of head-to-head structure", *J. Macromolecular science-Physics B 2 (1968) 205.*

33. A. J. Lovinger, G. T. Davis, T. Furukawa, and M. G. Broadhurst, "Crystalline forms in a copolymer of vinylidene fluoride and trifluoroethylene (52/48 mol %)", *Macromolecules, 15 (1982) 323.*
34. B. L. Farmer, A. J. Hopfinger, and J. B. Lando, "Polymorphism of poly(vinylidene fluoride): potential energy calculations of the effects of head-to-head units on the chain conformation and packing of poly(vinylidene fluoride)", *J. Appl. Phys. 43 (1972) 4293.*
35. K. Tashiro, in "Ferroelectric polymers" (H. S. Nalwa, *Ed.*), *Macrel Dekker, New York (1995) p.63.*
36. J. F. Legrand, "Structure and ferroelectric properties of P(VDF-TrFE) copolymers", *Ferroelectrics 91 (1989) 303.*
37. M. A. Bachmann and J. B. Lando, "A reexamination of the crystal of phase II of poly(vinylidene fluoride)" *Macromolecules 14 (1981) 40.*
38. K. Kimura, and H. Ohigashi, "Ferroelectric properties of poly(vinylidenefluoride-trifluoroethylene) copolymer thin films", *Appl. Phys. Lett. 43 (1983) 834.*
39. T. Furakawa, A. J. Lovinger, G. T. Davis and M. G. Broadhurst, "Dielectric hysteresis and nonlinearity in a 52/48 mol copolymer of vinylidene fluoride and trifluoroethylene", *Macromolecules 16 (1983) 1885.*
40. G. T. Davis, M. G. Broadhurst, A. J. Lovinger, and T. Furukawa, "Hysteresis in copolymers of vinylidene fluoride and trifluoroethylene", *Ferroelectrics 57 (1984) 73.*
41. T. Kajiyama, N. Khuwattanasil and A. Takahara, "Electric field induced structural change for poly.vinylidene fluoride-co-trifluoroethylene. ultrathin films studied by scanning Maxwell stress microscope", *J. Vac. Sci. Tech. B 16(1998)121.*
42. N. Karaswa, and W. A. Goddard, "Force fields, structures, and properties of poly(vinylidene fluoride) crystals", *Macromolecules 25 (1992) 7268.*
43. V. V. Kochervinski, "The structure and properties of block poly(vinylidene fluoride) and systems based on it", *Russ. Chem. Rev. 65 (1996) 865.*
44. Y. Takahashi, Y. Matsubara, and H. Tadokoro, "Mechanisms for crystal phase transformations by heat treatment and molecular motion in poly(vinylidene fluoride)", *Macromolecules 15(1982) 334.*
45. H. Ohigashi, K. Omote, and T. Gomyo, "Formation of single crystalline films" of ferroelectric copolymers of vinylidene fluoride and trifluoroethylene", *Appl. Phys. Lett. 66 (1995) 3281.*

46. Y. Takahashi, M. Kohyama, Y. Matsubara, H. Iwane and H. Tadokoro "Tilting phenomena in forms II and III of poly(vinylidene fluoride): evidence for monoclinic structures", *Macromolecules 14 (1981)1841.*
47. H. Ohigashi, K. Omote, H. Abe, and K. Koga, "Chain motions in the paraelectric phase in single crystalline films of Vinylidene fluoride and trifluoroethylene copolymer P(VDF/TrFE)", *J. Phys. Soc. Jpn. 68(1999) 1824.*
48. K. Tashiro, R. Tanaka, K. Ushitora, and M. Kobayashi, "Annealing effect on ferroelectric phase transitional behavior of vinylidene fluoride-trifluoroethylene copolymers: An interpretation base on the concept of domain and trans-gauche conformational disorder", *Ferroelectrics 171 (1995) 145.*
49. G. T. Davis, T. Furukawa, A. J. Lovinger, and M. G. Broadhurst, "Structural and dielectric investigation on the nature of the transition in a copolymer of vinylidene fluoride and trifluoroethylene (52/48 mol %)", *Macromolecules 15(1982) 329.*
50. K. Tashiro and M. Kobayashi, "Ferroelectric properties of Vinylidene fluoride copolymers", *Phase Transitions 18 (1989) 213.*
51. A. J. Lovinger, "Polymorphic transformations in ferroelectric copolymers of Vinylidene fluoride induced by electron-irradiation", *Macromolecules 18 (1985) 910.*
52. A. J. Lovinger, G. E. Johnson, H. E. Bair, and E. W. Anderson, "Structural, dielectric, and thermal investigation of the curie transition in a tetraluoroethylene copolymer of vinylidene fluoride", *J. Appl. Phys. 56 (1984) 2412.*
53. T. T. Wang, J. M. Herbert, and A. M. Glass, Eds.,"The Application of Ferrolectric Poymers," *Chapman and Hall, New York, 1988.*
54. R. E. Cais and H. M. Kometani, "Synthesis and two-dimensional NMR of highly aregic poly(vinylidene fluoride)", *Macromolecules 18 (1985) 1354.*
55. R. E. Cais and H. M. Kometani, "Polymerization of vinylidene fluoride-d2. Minimal regiosequence and branch defects and assignment of preferred chain-growth direction from the deuterium isotope effect", *Macromolecules 17 (1984) 1887.*
56. K. Koga and H. Ohigashi, "Optical absorption of ZnSe-ZnS strained layer superlattices", *J. Appl. Phys. 59 (1986) 2142.*
57. J. J. Ladik, "Quantum Theory of Polymers as Solids." Plenum Press, New York, 1988.
58. B. Wunderlich, "Crystal Structure, Morphology, Defects", *Academic Press, New York, 1973.*
59. R. E. Cohen, Ed., "Fundamental Physics of Ferroelectrics", *Vol. 535. American Institute of Physics, Melville, New York, 2000.*

60. T. Furkawa, "Ferroelectric properties of Vinylidene fluoride copolymers", *Phase Transitions 18 (1989) 143.*
61. A. J. Lovinger, "Ferroelectric Polymers", *Science 220 (1983) 1115.*
62. A. J. Lovinger, in "Developments in Crystalline Polymers-I", *(D. C. Basset, Ed.), Applied Science, London, 1982*.
63. J. K. Krüger, B. Heydt, C. Fischer, J. Baler, R. Jimėnez, K.-P. Bohn, B. Servet, P. Galtier, M. Pavel, B. Ploss, M. Beghi, and C. Bottani, "Surface-induced organization of liner molecules on nanostructured polytetrafluoroethylene: Crystalline state of poly(vinylidenefluoride-trifluoroethylene)," *Phys. Rev. B 55 (1997) 3497.*
64. K. Omote, H. Ohigashi, and K. Koga, "Temperature dependence of elastic, dielectric, and piezoelectric properties of "single crystalline" films of vinylidene fluoride trifluoroethylene copolymer", *J. Appl. Phys. 81 (1997) 2760.*
65. Y. Tajitsu, T. Masuda, and T. Furukawa, "Switching phenomena in vinylidene fluoride/trifluoroethylene copolymers near curie point", *Jpn. J. Appl. Phys. 26 (1987) 1749.*
66. T. Furukawa, "Phenomenological aspect of a ferroelectric vinylidene fluoride/trifluoreethylene copolymer", *Ferroelectrics 57 (1984) 63.*
67. T. Furukawa, G. E. Johnson, H. E. Bair, Y. Tajitsu, A. Chiba, and E. Fukada,"Ferroelectric phase transition in a copolymer of vinylidene fluoride and trifluoroethylene", *Ferroelectronics 32 (1981) 61.*
68. Y. Takahashi, Y. Nakagawa, H. Miyaji, and K. Asai, "Direct evidence for ferroelectric switching in poly(vinylidene fluoride) and poly(vinylidene fluoride-trifluoroethylene) crystals", *J. Polym. Sci.,-Part C 25 (1987) 153.*
69. E. P. Adams, "On electrets", J. Franklin Inst. 204 (1927) 469.
70. F. I. Mopsik and M. G. Broadhurst, "Molecular dipole electrets", *J. Appl. Phys. 46 (1975) 4204.*
71. M. G. Broadhurst and G. T. Davis, "Topic in Modern Physics of Electrets", *Ed. by G. M. Sessler, Springer, West Berlin, 1980.*
72. E. Fukada and T. Furukawa, "Piezoelectricity and ferroelectricity in polyvinylidene fluoride", *Ultrasonics 19 (1981) 31*.
73. A. J. Lovinger, "Development in Crystalline Polymers 1, edited by D. C. Basset", *Applied Science, London, 1982*.
74. G. M. Sessler, "Piezoelectricity in polyvinylidene fluoride", *J. Acoust. Soc. Am. 70 (1981) 1956*.

75. D. Nagele and D. Y. Yoon, "Orientation of crystalline dipoles in poly(vinylidene fluoride) films under electric field", *Appl. Phys. Lett. 33 (1978) 132*.
76. T. Furukawa, M. Date, and E. Fukada, "Hysteresis phenomena in polyvinylidene fluoride under high electric field", *J. Appl. Phys. 51 (1980) 1135.*
77. T. Furukawa, G. E. Johnson, "Measurements of ferroelectric switching characteristics in polyvinylidene fluoride", *Appl. Phys. Lett. 38 (1981) 1027.*
78. S. Tasaka and S. Miyata, "The origin of piezoelectricity in poly(vinylidene fluoride)", *Ferroelectrics 32 (1981) 17.*
79. K. Tashiro, K. Takano, M. Kobayashi, Y. Chatani, and H. Tadokoro, "Structural study on ferroelectric phase transition of vinylidene fluoride-trifluoroethylene random copolymers", *Polymer 22 (1981) 1312.*
80. A. J. Lovinger, T. Furukawa, G. T. Davis, and M. G. Broadhurst, "Crystallographic changes characterizing the Curie transition in three ferroelectric copolymers of vinylidene fluoride and trifluoroethylene: 1. As-crystallized samples", *Polymer 24 (1983) 1225.* "Crystallographic changes characterizing the Curie transition in three ferroelectric copolymers of vinylidene fluoride and trifluoroethylene: 2. Oriented or poled samples", *Polymer 24 (1983) 1233.*
81. T. Furukawa, J. X. Wen, K. Suzuki, Y. Takashina, and M. Date, "Piezoelectricity and pyroelectricity in vinylidene fluoride/trifluoroethylene copolymers", *J. Appl. Phys. 56 (1984) 829.*
82. H. Ohigashi and K. Koga, "Ferroelectric copolymers of Vinylidenefluoride and trifluoroethylene with a large electromechanical coupling factor", *Jpn. J. Appl. Phys. 21 (1982) L455.*
83. K. Lefki and G. J. M. Dormans, "Measurement of piezoelectric coefficients of ferroelectric thin films", *J. Appl. Phys. 76 (1994) 1764.*
84. A. V. Bune, C. Zhu, S. Ducharme, L. M. Blinov, V. M. Fridkin, S. P. Palto, N. N. Petukhova, and S. G. Yudin, "Piezoelectric and pyroelectric properties of ferroelectric Langmuir–Blodgett polymer films", J. *Appl. Phys. 85 (1999) 7869.*
85. T. Furukawa, J. X. Wen, "Electrostriction and piezoelectricity in ferroelectric polymers", *Jpn. J. Appl. Phys. 23 (1984) L677.*
86. K. Matsushige, S. Imada, and T. Takemura, "Temperature effect on ferroelectric polarization switching in poly(vinylidene fluoride)", *Polymer J., 13 (1981) 493.*
87. Y. Takase and A. Odajima, "γ-ray radiation-induced changes in switching current of polyvinylidene fluoride", *Jpn. J. Appl. Phys. 22 (1983) L318.*

88. Y. Takase, A. Odajima, and T. T. Wang, "A modified nucleation and growth model for ferroelectric switching in form I poly(vinylidene fluoride)", *J. Appl. Phys. 60 (1986) 2920.*
89. W. Merz "Switching time in ferroelectric $BaTiO_3$ and its dependence on crystal thickness", *J. Appl. Phys. 27 (1956) 938.*
90. H. L. Stadler, "Ferroelectric switching time of $BaTiO_3$ crystals at high voltages", *J. Appl. Phys. 29 (1958) 1485.*
91. T. Furukawa, H. Matsuzaki, M. Shiina, and Y. Tajitsu, "Nanosecond switching in thin films of vinylidene fluoride/trifluoethylene copolymers", *Jpn. J. Appl. Phys. 24 (1984) L661.*
92. K. Kimura and H. Ohigashi, "Polarization behavior in Vinylidene fluoride-trifluoroethylene copolymer thin films", *Jpn. J. appl. Phys. 25 (1986) 383.*
93. M. E. Lines and A. M. Glass, "Principal and applications of ferroelectrics and related materials", *Clarendon Press, Oxford, 1977.*
94. H. Kliem and R. T.-Morgane, "Extrinsic versus intrinsic ferroelectric switching: experimental investigations using ultra-thin PVDF Langmuir-Blodgett films", *J. Phys. D: Appl. Phys. 38 (2005) 1860.*
95. G. Vizdrik, S. Ducharme, V. M. Fridkin, and S. G. Yudin, "Kinetics of ferroelectric switching in ultrathin films", *Phys. Rev. B 68 (2003) 094113.*
96. S. Ducharme, V. M. Fridkin, A. V. Bune, S. P. Palto, L. M. Blinov, N. N. Petukhova , and S. G. Yudin, "Intrinsic ferroelectric corecive field", *Phys. Rev. Lett.* ***84*** *(2000) 175.*
97. A. V. Bune, V. M. Fridkin, S. Ducharme, L. M. Blinov, S. P. Palto, A. V. Sorokin, S. G. Yudin, and A. Zlatkin, "Two-dimentional ferroelectric films", *Nature 391 (1998) 874.*

Chapter 2. Experimental

In this chapter we introduce the experimental techniques used to study for P(VDF-TrFE) copolymer films. 1st we discuss about Fourier Transformed Infrad-Red Spectroscopy (FTIR) in respect of principle and merit of the technique. Then we address about the principle of X-ray diffraction (XRD) technique. For morphological investigation, we used Atomic force microscopy (AFM), therefore we have discussed about the principle of the technique and merit of the different modes. Out of them, most of our experimental results based on photoemission spectroscopy, such as X-ray photoelectron spectroscopy (XPS), Near Edge X-ray Absorption Fine Structure (NEXAFS). Therefore we address the principle and realization of XPS of P(VDF-TrFE) copolymer. Furthermore, we concentrate on the interplay of NEXAFS spectroscopy. In NEXAFS spectroscopy, we discuss about the principle of the molecular transition associated from core level to the empty states. The description about instrumentation for NEXAFS measurements is also described. And we concentrate the principle and necessity of curve fitting of NEXAFS spectrum. In the next step, details of the sample preparations are described. Sample preparations involve the thin film preparation procedure, thickness determination of the films, surface morphology, identification of the ferroelectric phase, effect of annealing and the optimization of the X-ray irradiation time for the P(VDF-TrFE) copolymer film. Finally we demonstrate the experimental setup for external application of the electric field.

Experimental techniques and their interpretation

2.1. Fourier Transformed Infra-Red Spectroscopy (FTIR)

Infrared (IR) spectroscopy is one of the versatile techniques for the organic and inorganic field of research [1]. FTIR is measurement technique where spectra are collected based on measurements of the temporal coherence of a radiative source, using time-domain measurements of the electromagnetic radiation or other type of radiation.

A Fourier transform spectrometer is a Michelson interferometer with a movable mirror. By scanning the movable mirror over some distance, an interference pattern is produced that encodes the spectrum of the source, in fact, it turns out to be its Fourier transform. In its simplest form, a Fourier transform spectrometer consists of two mirrors located at a right angle to each other and oriented perpendicularly, with a beamsplitter placed at the vertex of the right angle and oriented at a 45^{o} angle relative to the two mirrors. Radiation incident on the beamsplitter from one of the two ports is then divided into two parts, each of which propagates down one of the two arms and is reflected off one of the mirrors. The two beams are then recombined and transmitted out the other port. When the position of one mirror is continuously varied along the axis of the corresponding arm, an interference pattern is swept out as the two phase-shifted beams interfere with each other. A simplified optical layout of FTIR interferometer is shown in figure 2.1.

Infrared spectroscopy exploits the fact that molecules have specific frequencies at which they rotate or vibrate corresponding to discrete energy levels. In vibrational mode, a molecule is IR active because of changes in the permanent dipole. Simple diatomic molecules have only one bond, which may stretch. More complex molecules have many bonds and vibration can be conjugated, leading to infrared absorptions at characteristic frequencies that are related to chemical groups. For example, the atoms in a CH_2 group, commonly found in organic compounds can vibrate in six different ways: symmetrical and antisymmetrical stretching, scissoring, rocking, wagging and twisting [3]. As each molecule has its own distinct quantized vibrational and rotational energy level and any transition within these levels is sensitive to electromagnetic energy corresponding to the mid-infrared region (4000 cm^{-1} – 400 cm^{-1}). Therefore, this technique is based on the principle that a molecule absorbs infrared radiation of the appropriate frequency to excite it from one vibrational or rotational level to another.

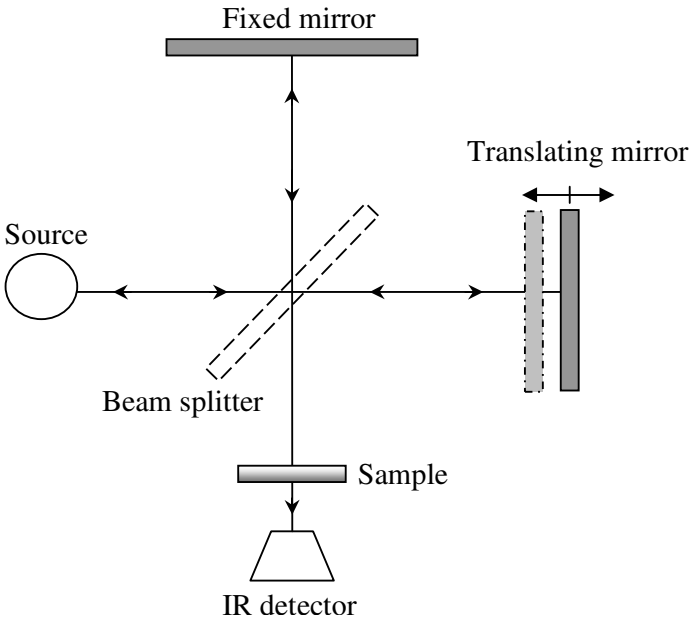

Figure 2.1. *Schematic layout of a typical FTIR interferometer [2]*

In this investigation, we used FTIR spectroscopy for distinguished different existing phases (i.e. ferroelectric, paraelectric phase) of P(VDF-TrFE) thin films. In figure 2.2, a typical FTIR spectrum is shown. It shows clearly visible peaks at 470 cm^{-1}, 848 cm^{-1}, 1184 cm^{-1} and 1292 cm^{-1} which are typical for the all-trans ferroelectric phase [4, 5].

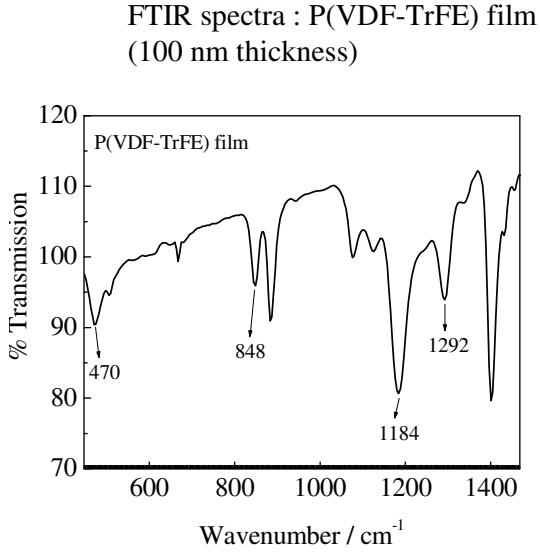

Figure 2.2. *A typical FTIR spectra of pristine thin film of P(VDF-TrFE).*

In this thesis, infared spectra were recorded with Bio-Rad FTS-60A Spectrometer, equipped with deuterated triglycine sulfate (DTGS) detector and Thermo-Nicolet Impact 410 Spectrometers. Spectra were taken at 4 cm^{-1} resolution and 100 scans are recorded.

2.2. X-Ray Diffraction

X-Ray Diffraction (XRD) has been used for the identification of the phases of the co-polymer P(VDF-TrFE) films, because generally P(VDF-TrFE) contains both, a ferroelectric and a paraelectric phase [6].

The principle of XRD is discussed shortly as follows: The atomic spacing of most of crystalline materials is of the same order as the wavelength of X-rays (0.5 Å – 2.5 Å). When a sample is illuminated with incident X-rays, the specimen's lattice spacing, its lattice shape, and the atom type all cause the incident X-rays to be diffracted in a characteristic manner. After penetration deep into the specimen, a typical diffraction pattern is build up by the X-rays. From this pattern it is possible to identify the crystal structure and we are able to distinguish the type of phase of the specimen. When a monochromatic X-ray beam is partially reflected from the specimen i.e. lattice plane, the interference of the reflected beam can be constructive only in specific directions.

The interference of the reflected beam would be constructive when the path difference AB + BC (see figure 2.3) is integral multiple of the wavelength of X-rays, given by the Bragg's equation:

$$n\lambda = 2d \sin\theta \qquad 2.1$$

where λ is the incident wavelength, θ is the angle of incidence, d is the interplanar spacing of atomic planes.

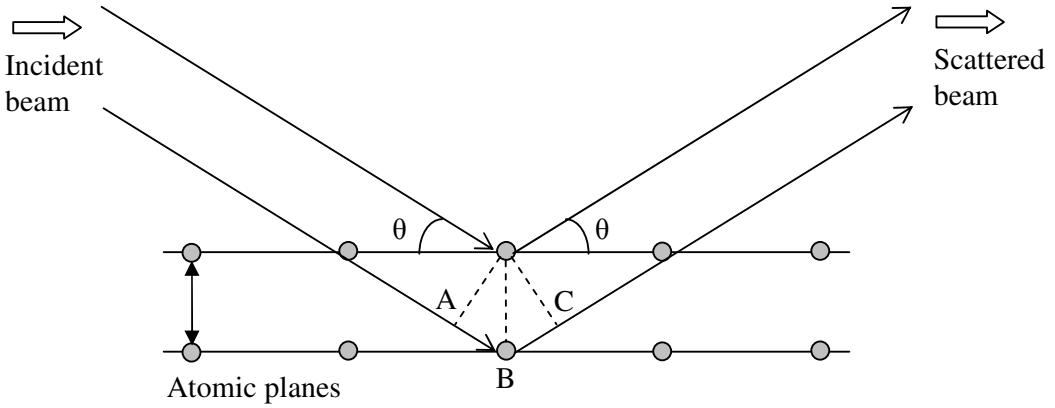

Figure 2.3. *X-ray diffraction of Bragg's law*

X-ray diffraction analysis was carried out in a "XRD 3000 TT" device (Seifert-FPM Ahrendsburg, Germany) in Bragg Brentano geometry. We used Co-K_α radiation (λ = 1.7902 Å) as the source at the X-ray operating voltage 40 kV and 30 mA emission current.

2.3. Atomic Force Microscopy

Atomic force microscopes (AFMs) belong to the family of scanning probe techniques [7] which probes the surface topography of a sample with a sharp tip scanned across the surface. The tip is located at the free end of a cantilever that is 100 to 200 µm long and less than 100 Å in diameter. The cantilever is usually made of silicon and exhibits a very low spring constant. Forces between the tip and the sample surface cause the cantilever to bend, or deflect. A detector measures the cantilever deflection as the tip is scanned. These deflections allow a computer to generate a map of the surface topography [8]. AFMs can be used to study insulators and semiconductors as well as electrical conductors.

Several forces typically contribute to the deflection of an AFM cantilever. The force most commonly associated with atomic force microscopy is an interatomic force as the van der Waals force. Discussion of the dependence of the van der Waals force upon the distance between the tip and the sample is important as it is determine the choice of mode of AFM operation. The force vs. distance curve is shown in figure 2.5 where two distinct regimes are distinguished: (1) the contact regime; and (2) the non-contact regime. In the contact regime,

the cantilever is held less than a few angstroms from the sample surface, and the interatomic force between the cantilever is held on the order of tens to hundreds angstroms from the sample surface and the interatomic force between the cantilever and sample is attractive (largely a result of the long-range van der Waals interactions).

In our experimental study mostly we used non-contact image techniques, because we investigate soft polymeric surfaces.

Contact mode

In contact mode, also know as repulsive mode, an AFM tip makes soft "physical contact" with the sample. The tip is attached to the end of a cantilever with a low spring constant, lower than the effective spring constant holding the atoms of the sample together. As the scanner gently traces the tip across the sample (or the sample under the tip), the contact force causes the cantilever to bend to accommodate changes in topography.

Most AFMs detect the position of the cantilever with optical techniques. In most common scheme, shown in figure 2.4, a laser beam bounces off the back of the cantilever onto a position-sensitive photodetector (PSPD). As the cantilever bends, the position of the laser beam on the detector shifts. The PSPD itself can measure displacements of light as small as 10 Å. The ratio of the path length between the cantilever and the detector to the length of the cantilever itself produces mechanical amplification. As a result, the system can detect sub-angstrom vertical movement of the cantilever tip.

Other methods of detecting cantilever deflection rely on optical interference. Once the AFM has detected the cantilever deflection, it can generate the topographic data set by operating in one of the two modes- constant-height or constant-force mode. In constant-height mode, the spatial variation of the cantilever deflection can be used directly to generate the topographic data set because the height of the scanner is fixed as it scans. In constant-force mode, the deflection of the cantilever can be used as input to a feedback circuit that moves the scanner up and down in z, responding to the topography by keeping the cantilever deflection constant. In this case, the image is generated from the scanner's motion. With the cantilever deflection held constant, the total force applied to the sample is constant. This mode often used for taking atomic-scale images of atomically flat surfaces, where the cantilever deflections and thus variations in applied force are small. This mode is also essential for recording real-time images of changing surfaces, where high scan speed is essential.

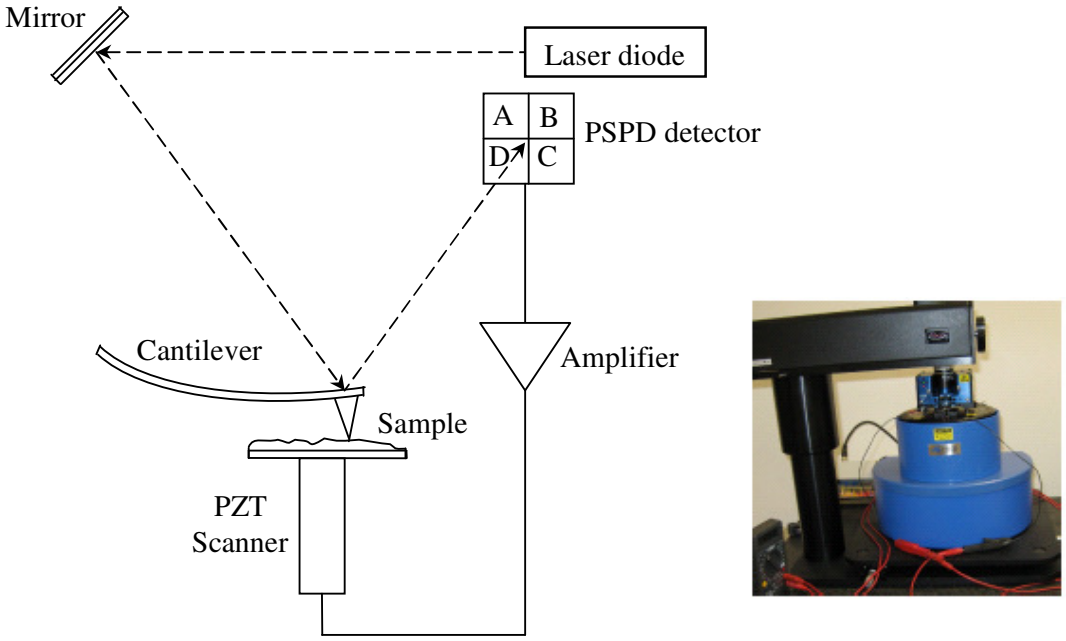

Figure 2.4. *Basic lay-out of an AFM (right side). VECCO Digital Instruments CP-II AFM (left side).*

Non-contact mode

The non-contact mode AFM (NC-AFM) is one of several vibrating cantilever techniques in which an AFM cantilever is vibrated near the surface of a sample. The spacing between the tip and the sample for NC-AFM is on the order of tens to hundreds of angstroms. This spacing is indicated on the van der Waals curve of figure 2.5 as the non-contact regime.

NC-AFM is desirable because it provides a means for measuring sample topography with little or no contact between the tip and the sample. Like contact mode AFM, non-contact mode AFM can be used to measure the topography of insulators and semiconductors as well as electrical conductors. The total force between the tip and the sample in the non-contact regime is very low, generally about 10^{-12} N. This low force is advantageous for studying soft or elastic samples [9]. A further advantage is that samples like silicon wafers or polymer thin films are not contaminated through contact with the tip.

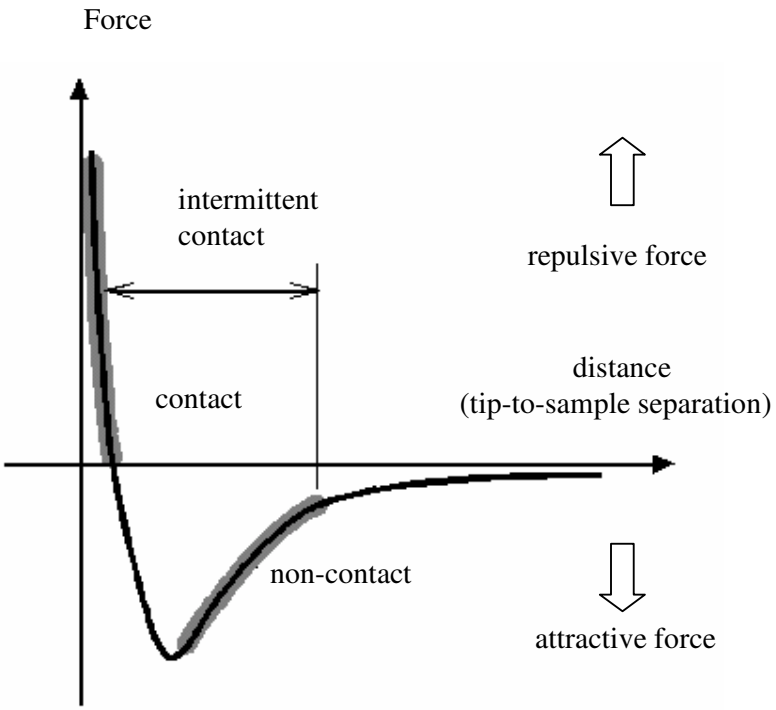

Figure 2.5. *Interatomic force vs. distance curve.*

Because the force between the tip and the sample in the non-contact regime is low, it is more difficult to measure than the force in the contact regime, which can be several orders of magnitude greater. In addition, cantilevers used for NC-AFM must be stiffer than those used for contact AFM because soft cantilevers can be pulled into contact with the sample surface. The small force values in the non-contact regime and the greater stiffness of the cantilevers used for NC-AFM are both factors that make the NC-AFM signal small, and therefore difficult to measure. Thus, a sensitive, AC detection scheme is used for NC-AFM operation.

In non-contact mode, the system excites a stiff cantilever near its resonant frequency (typically from 100 to 400 kHz) with amplitude of a few tens to hundreds of angstroms. Then, it detects changes in the resonant frequency or vibration amplitude as the tip comes near the sample surface. The sensitivity of this detection scheme provides sub-angstrom vertical resolution in the image, as with contact mode AFM.

For the AFM measurements presented in this thesis, VECCO Digital Instruments CP-II AFM is used.

2.4. X-ray Photoelectron Spectroscopy (XPS)

The history of XPS can be considered to begin in 1887 with the discovery of the photoelectric effect by H. Herz [9]. In 1907, P.D. Innes [11] described a kinetic-energy spectrum of photoelectrons excited by radiation of an X-ray tube with a platinum anode and registered by a spectrometer consisting of a magnetic analyzer and photographic detection. After development by Kai Siegbahn with colleagues of a high-resolution spectrometer, which allowed measuring accurately the binding energy levels of photoelectron peaks [12], the goal of using XPS for electronic structure investigation had been realized. Subsequently the same group observed the chemical shift effect for binding energy of core-level electrons [13, 14], which led to development of the whole field of electron spectroscopy named ESCA (electron spectroscopy for chemical analysis) [15, 16]. The work of K. Siegbahn was awarded by Nobel Prize in 1981 "for his contribution to the development of high-resolution electron spectroscopy". In 1969-70 commercial XPS instruments began to appear thanks to developing routine methods of obtaining UHV conditions. Starting from that time XPS can be considered as a widely used method for investigation of the surface of a solid sample. The possibility of estimation of chemical composition and of chemical state of elements together with a small information depth makes XPS an important method for microelectronics, polymer technology and metallurgy [17]. Therefore, it has wide range of practical implications in various scientific fields like surface chemistry, material science and solid state physics.

The basic elements of an XPS instrument are a light source, an electron energy analyzer and an electron detector as it is drawn on figure 2.6.
In this technique, the chemical analysis of the first few atomic layers of the sample is carried out by irradiating the sample with mono-energetic X-rays and analyzing the kinetic energies of the emitted electron. The X-rays (photon), possessing limited penetration depth, interact with atoms in the surface causing electron emission by the photoelectric effect.

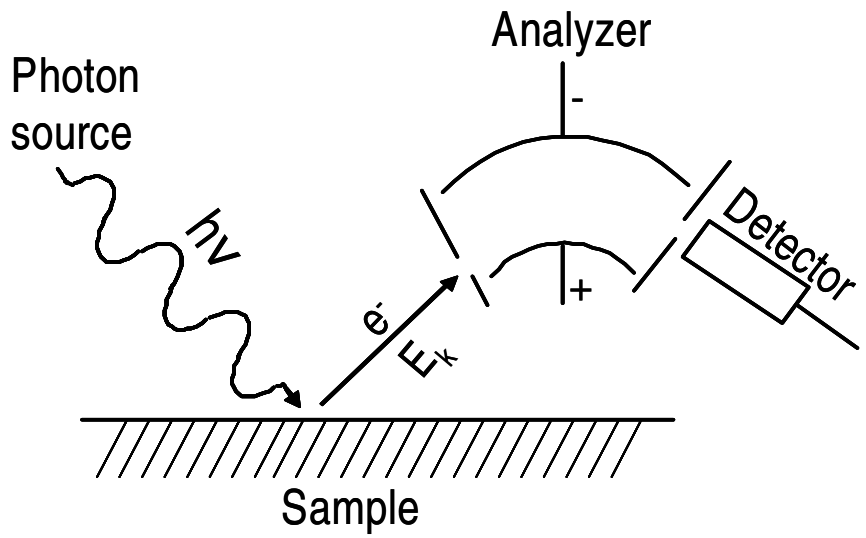

***Figure 2.6**. Basic elements of the XPS equipment [18].*

The physical principle of the photoemission process is demonstrated by figure 2.7.

In a laboratory XPS system, an X-ray tube usually with Al and Mg cathode are used. Development of synchrotrons made available the wide range of excitation energies between hard X-ray to visible light. Furthermore, the use of synchrotron light has several advantages comprising common laboratory X-ray sources. Besides a high photon flux and the possibility of focusing of an X-ray beam into a small spot, synchrotron light has the property of excitation energy tenability, which allow the changing the information depth and the photoelectric cross-section.

If no surface charge is present, the kinetic energy E_K of the photoelectron can be obtained from the Einstein equation for the photo effect:

$$E_K = h\upsilon - E_B - WF \qquad 2.2$$

Where $h\upsilon$ is the energy of the X-ray photon, E_B is the binding energy of the core level and WF is the work function of the sample. In the case of charging, the potential energy of the electron in the electromagnetic field should be subtracted from the right side of the equation. One should note that the value of the E_B is a difference of the initial and final atomic energies, which in general includes the relaxation component. The value of E_B is always lower than the energy of the orbital from where the photoelectron was emitted. Nevertheless, E_B is suitable for element analysis and chemical state identification.

As far as every chemical element has a characteristic XPS spectrum, the chemical composition can be identified. A binding energy of a core-level electron depends also on the surroundings of atoms. Non-equivalence of binding energies for an element in different chemical compounds can arise from various reasons: difference in a formal oxidation state, different molecular environment, and different lattice parameters for example.

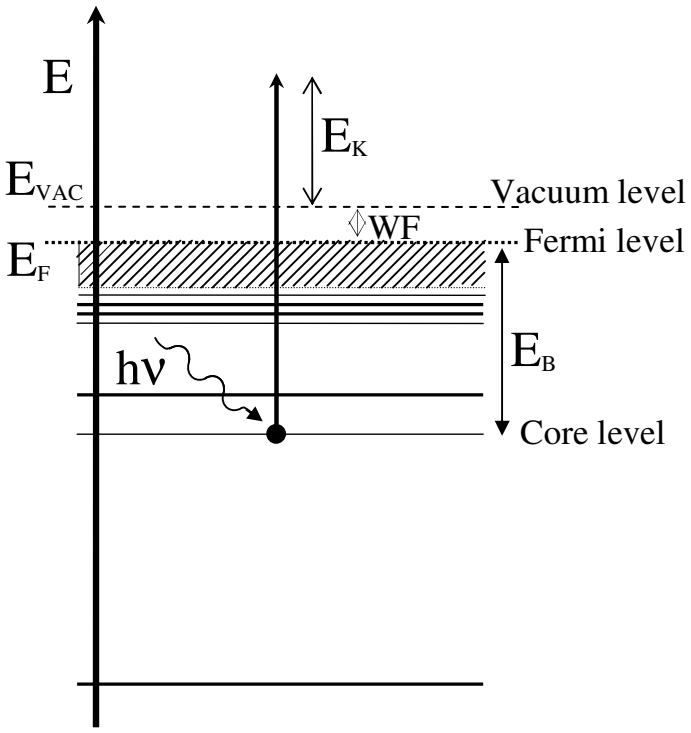

Figure. 2.7. *Schematic diagram of a core-level-photoelectron emission process.*

A binding energy shift due to environment effects, which is usually chemical shift, can be described by the simple equation [19]:

$$E_B\text{-}E_B(0) = IA + EA \qquad 2.3$$

Where $E_B(0)$ is the binding energy of the core-level electron in the isolated atom. The intra-atomic part IA can be described in terms of the effective charge q of the atom in a molecule or crystal as $IA = kq$, where k is a constant for the chemical element. The extra-atomic part EA is

the potential energy produced by the surroundings. This part is often referred as Madelung potential. The parts *IA* and *EA* acting opposite each other and the dependence of *EA* on type of solid sometimes makes problematic the identification of the chemical state of an atom by its chemical shift.

After escape from an atom, a photoelectron travels some distance inside the solid before escape to vacuum or relax. On the way it collides elastically or inelastically with lattice atoms. Elastic collisions do not change the electron kinetic energy while inelastic lead to a decrease in energy. Inelastically scattered electrons will form a spectrum background or will not escape from solid and thus, these electrons can be counted as lost for XPS analysis. It is assumed that there is constant probability of an inelastic scattering event in the depth per unit length and the probability of photoelectrons from the escape depth L is proportional to exp (-L/λ), where λ is usually named the inelastic mean free path and represents the first momentum of a probability distribution.

A typical structure of an XPS spectrum of P(VDF-TrFE) film is shown is figure 2.8, where Mg K_α (photon energy: 1253.6 eV) is used as an X-ray source. The spectrum consists of relatively narrow core-level photoelectron peaks, a broad Auger transition peak and a valence band spectrum. The spectrum background is formed by inelastically scattered electrons.

The transformations of photoelectron kinetic energy into binding energy by the Einstein equation (2.2), implies knowledge of the analyzer work function. For metallic compounds the Fermi level is the suitable binding energy reference. A submonolayer gold film is often deposited on a sample in order to use the Au4f peak as a binding energy reference. C1s is also often employed for binding energy calibration. Other suitable reference peaks can be used as well [20].

The width of XPS peak is defined as a full width at half maxima (FWHM) of the peak after background subtraction. The width DE is a combination of the following values:

$$\Delta E = (\Delta E(n)^2 + \Delta E(p)^2 + \Delta E(a)^2)^{1/2} \qquad 2.4$$

Where $\Delta E(n)$ is the natural width of a core level, $\Delta E(p)$ is the spectral width of photon source radiation, $\Delta E(a)$ is the analyzer resolution. Additionally, the peak can be broadened by sample inhomogeneity or by differential charging. The natural broadening and the analyzer broadening are described by the Lorenzian and Gaussian profiles respectively. Synchrotron X-ray radiation has the Gaussian spectral shape because of the instrumental broadening introduced by a monochromator.

An X-ray photoelectron spectrum of a solid-state sample always contains a background, which is formed by inelastically scattered photoelectrons. To estimate the peak shape and the stoichiometry from an experimental spectrum first the background should be subtracted.
Different models of background shape are in use. A simple linear type background can be used for fast spectra analysis, while for more accurate line shape and stoichiometry analysis more complicated background types should be used [21-23].

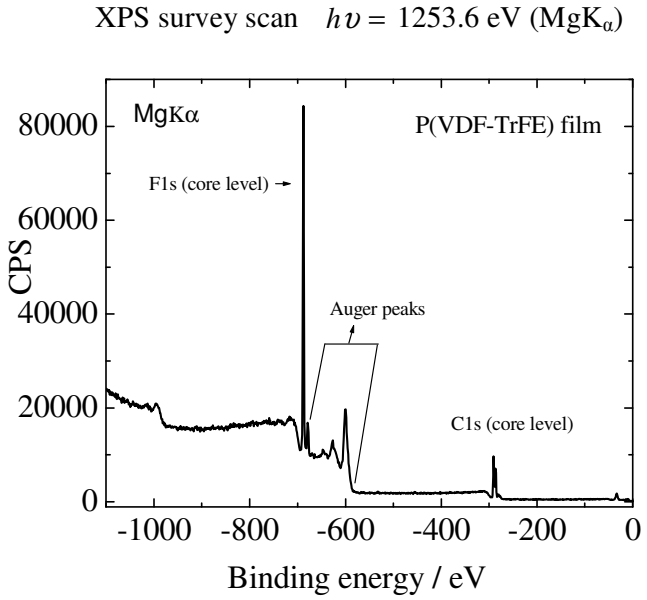

Figure 2.8. *Photoelectron spectrum of P (VDF-TrFE) film.*

The stoichiometry of the sample surface can be estimated from the area ratio of XPS peaks. The general formula for the XPS peak area [20] is

$$I = nf\sigma\theta y\lambda AT \qquad 2.5$$

Where n is the atomic concentration of the element, f is the X-ray flux, σ is the photoelectron cross-section for the atomic orbital of interest, θ is the angular efficiency factor for the instrumental arrangement, y is the efficiency in the photoelectronic process for formation of photoelectrons of the normal photoelectron energy, λ is the mean free path of the photoelectrons in the sample, A is the area of the sample from which photoelectrons are detected, T is the detection efficiency for electrons emitted from the sample.

In our XPS experiment, we have calculated the stoichiometric ratio ration of two element C and F in the P(VDF-TrFE) film as follows [11]:

$$\frac{n_C}{n_F} = \frac{I_C / \sigma_C y_C \lambda_C T_C}{I_F / \sigma_F y_F \lambda_F T_F} = \frac{I_C / S_C}{I_F / S_F} \qquad 2.6$$

where S_C and S_F are atomic sensitivity factor of carbon and fluorine respectively.

2.5. NEXAFS Spectroscopy

Introduction

Near-Edge X-Ray Absorption Fine Structure (NEXAFS) spectroscopy is an X-ray absorption technique which deals with the absorption cross section near the (1s) ionization step [24]. Omitting a background from electrons bound to different orbitals, two fundamental types can occur near the 1s edge. The final states can either be discrete molecular orbitals or may alternatively be free vacuum states if the exciting energy is sufficient to excite the electron above the Fermi level.

Although it is generally refers to the photon absorption process as an electronic transition, the rest of the molecule is also affected by such excitation. The hole in the inner shell of the molecule leaves this in an excited state which subsequently decays. Energy which is set free during this relaxation can either be discharge via the emission of a secondary photon (fluorescence) or can be transferred to another electron in a higher shell, enabling it to escape the molecule (Auger process). The latter is the predominant relaxation channel for atoms with low atomic numbers ($z \leq 15$) [25] and the number of Auger electrons is proportional to the number of primary excitations. For a constant flux of incoming photons the number of Auger electrons emerging from the sample hence quantifies the absorption cross-section in a non-normalized fashion [24].

The energy of NEXAFS resonances yields information on the chemical state of atoms within the probe depth. Additionally, the absorption cross-section into a molecular final state depends on the relative orientation of the electric field vector of the photon with respect to the direction of the transition dipole moment, which is in turn related to the charge distribution in a molecular orbital. If the photons are linearly polarized, then order structures, such as C-F dipoles for P(VDF-TrFE) co-polymer, produce spectra that inherently depend on the angle of photon incidence. Several work on NEXAFS study for organic molecule has been done in the group of **applied physics II – sensor technologies at the BTU Cottbus** [26-33].

For the NEXAFS technique, the differential cross-section of photon absorption by an electron is particularly interesting, since it is the basis of how to detect order in a molecular film. Fermi derived an expression for the electronic transition probability (P_{fi}) of a transition from an initial ($|i>$) to a final state ($|f>$) per unit time under the influence of a time-dependent perturbation (V(t)), which is known as "Fermi's golden rule" and is shown in equation 2.7. ρ_f (E) denotes the density of states in the region of the final state.

$$P_{fi} = \frac{1}{h}\left|<f\left|\overline{V}\right|i>\right|^2 \rho_f(E) \qquad 2.7$$

Although it was derived with the formalism of perturbation theory, this expression is believed to be universally valid and has indeed proven to be reliable experiment. Of course, the absorption of an X-ray photon may not strictly comply with the exact concept of mathematical perturbation. Within the frame of non-relativistic quantum mechanics, the absorption of the photon cannot be explained but its effect on an electron can nevertheless be calculated by inserting its electromagnetic potential into "Fermi's golden rule" (equation 2.7) as the perturbing potential. Equation 2.8 shows the vector potential for a linearly polarized photon ($\vec{e}$ stands for the unit vector in direction of its electric field) which propagates in the direction of the wave vector $\vec{k}$ and oscillates with the frequency ω/2π:

$$\vec{A} = A_0 \vec{e} \cos\left(\vec{k}.\vec{x} - \omega t\right) \qquad 2.8$$

After several mathematical steps, this explicit form of photon potential (equation 2.8) turns equation 2.7 into:

$$P_{fi} = \frac{\pi e^2}{2\hbar m^2 c^2} A_0^2 \left|< f\left|e^{ik.x}\vec{e}.\vec{p}\right|i>\right|^2 \qquad 2.9$$

Until now the calculation was exact apart from a possible misuse of perturbation theory. In a next step equation 2.9 will now be simplified by a linear approximation of the exponential function. This cut-off is well justified due to the very low values of $\left|\vec{k}.\vec{x}\right|$ ($k \leq 1$ nm^{-1}, $|r| \approx 1$ Å [24]) and we end up with the "dipole" approximation of the X-ray absorption cross-section:

$$P_{fi}\alpha\left|< f\left|\vec{e}.\vec{p}\right|i >\right|^2 \rho_f(E) \qquad 2.10$$

The final step is to express the momentum operator in its more intuitive spatial representation [24]:

$$\vec{p} = \frac{im(E_f - E_f)}{\hbar}\vec{r} \qquad 2.11$$

And hence:

$$\sigma_x \infty P_{fi} \infty \rho_f(E)\left|< f\left|\vec{e}.\vec{r}\right|i >\right|^2 = \rho_f(E)\left|\vec{e}.< f\left|\vec{r}\right|i >\right|^2 \qquad 2.12$$

The term $< f\left|\vec{r}\right|i >$ is known as 'transition dipole moment' (TDM).

The incident photon therefore can excite an electronic transition $\left|i > \rightarrow \right|f >$ if three conditions are all fulfilled. First of all, the density of states (ρ_f) in the energy region into which the photon could excite the electron has to be non-zero. Secondly, the vector of the transition dipole moment (TDM) has to be non-zero. This is a vectorial quantity which is determined by two states involved and reflects the symmetry of the system. Group theory states [24, 34] that the direct product of the irreducible representations of the initial and final states contains the irreducible representations of the x, y and z-coordinates. This requirement can be verified by a comparison with (readily available for standard molecular orbitals) character tables so that it is not necessary to analytically calculate the TDM in order to test whether a transition is symmetry allowed. For molecular states where the final orbital corresponds to a bond, the TDM normally points in a distinctive direction with respect to the involved atoms. (*e.g.* in the common transition 1s → σ it points along the intermediate axis). Due to this relation, the orientation of a TDM is directly related to that of its associated bond. The final requisite is that the vector of the TDM must have a component which is parallel to the electric field vector of the (linear polarized) photon in order for the scalar product to differ from zero.

Transitions into molecular orbitals

According to quantum mechanics, the energy spectrum of a molecular contains discrete levels. On the photon energy scale the individual transitions can hence be observed as a series

of peaks. As mentioned above, the transition dipole moment varies from zero if and only if the combination of initial and final moment varies exhibits the correct behavior under symmetry transformations. For TDMs which are fixed in space, the transition probability depends on the relative angle between the incident photon and the TDM. By measuring this angle dependence (i.e. with a series of spectra at different angles of incidence), we can hence conclude the absolute direction into which the TDM of an oriented molecular orbital is pointing.

Transitions into vacuum states – ionization

The energy spectrum of free particles is continuous and lacks any directional preferences due to the isotropy of space, so that the three requirements of six are always satisfy if the energy of the incoming photon is high enough to lift an electron above the Fermi level. Transitions into vacuum states show a relatively weak dependence (exponential decrease) on the energy of the photon [24] and are not influenced by the direction from which the photon hits the atom. They manifest themselves as step-like angular independent feature in the spectra.

Angular dependence of a NEXAFS signal

The following section is devoted to the way in which a NEXAFS signal can be analyzed to deliver the mean tilt angle of molecular orbitals. One can calculate the angle dependence of the NEXAFS signal of such a resonance for a concrete choice of coordinate system and partially linearly polarized light. The intensity of the experimental signal (I) is proportional to the transition probability (P_{if}) of the electronic transition. Assuming that the other conditions are satisfy ($\rho_f(E) > 0$, TDM $\neq \vec{0}$), the focus is turned towards the angle-dependent term in equation 2.12:

$$I \infty \left| \vec{e} < f \left| \vec{r} \right| i > \right|^2 \equiv \left| \vec{e}.\vec{o} \right|^2 \qquad 2.13$$

Like previously mentioned, $\vec{e}$ denotes a unit vector in the direction of the electric field vector and $|i>$, $|f>$ are the initial and final states of the transition respectively. As a direct result of Maxwell's equations the electric field vector of a photon is always perpendicular to its propagation direction. It is decomposed into a component in the plane of the electron (E^{II}) and one perpendicular ($E^{\perp}$), the sense of which will become clear from the electromagnetic field of a bending magnet. For light that is partially linearly polarized in the plane of the electron ring, then the two components are connected via the degree of polarization [35]:

$$P \equiv \frac{\left|E^{II}\right|^2}{\left|E^{II}\right|^2 + \left|E^{\perp}\right|^2} \qquad 2.14$$

We now obtain a form for equation 2.13 which explicitly uses these notations:

$$\begin{aligned} I \infty P\left|< f\left|\vec{e}^{\,II}.\vec{r}\right|i>\right|^2 + (1-P)\left|< f\left|\vec{e}^{\,\perp}.\vec{r}\right|i>\right|^2 \\ \equiv P.I^{II} + (1-P).I^{\perp} \end{aligned} \qquad 2.15$$

2.16

Where $\vec{e}^{\,II}$ and $\vec{e}^{\,\perp}$ are unit vectors of the in-plane and perpendicular electric field components. In the next step, equation 2.15 is evaluated for an explicit choice of direction for the incoming photon and of the TDM. This situation as well as the coordinates with which would subsequently describe this situation are shown in figure 2.9.

For this coordinate system the intensities can be rewritten for the in-plane and perpendicular components:

$$I^{II} \infty P(\cos^2\theta\cos^2\alpha + \sin^2\theta\sin^2\infty + 2\sin\alpha\cos\alpha\sin\theta\cos\theta\cos\phi)$$

$$I^{\perp} \infty (1-P)(\sin^2\alpha\sin^2\phi) \qquad 2.17$$

These expressions are the general forms of the two intensities. For transitions on substrates with three or higherfold rotational symmetry, the azimuthal (ϕ) dependence is, however, average out-thus simplifying the equation.

After simplification, the final, most simple form of equation 3.7 for the intensity emerges:

$$I = A(P(\cos^2\theta\cos^2\alpha + \frac{1}{2}\sin^2\theta\sin^2\alpha) + (1-P)(\frac{1}{2}\sin^2\alpha)) \qquad 2.18$$

The newly introduced scaling factor A contains all the physical experimental constants (e.g. overlap integral, detector efficiency). Molecular orbitals are sometimes divided into two categories called "vector" and "plane" type orbitals for practical reasons [24].

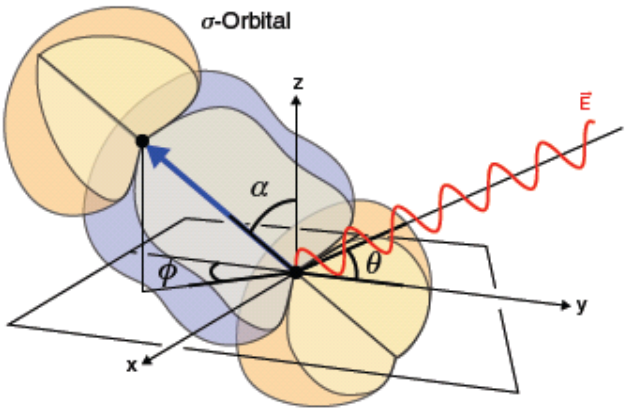

Figure 2.9. *A linearly polarized photon with a wave vector and electric field vector in the yz-plane that hits the sample and the TDM-vector for the transition it excites. The attention is drawn to the reference axis from where the different angles are measured.*

The dipole selection rules related to K-shell NEXAFS resonance intensities are quite simple: the resonance intensity associated with the specific molecular orbital final state is largest if the $\vec{E}$ vector points in the direction of that molecular orbital, i.e., lies in the nodal plane of the orbital. The σ^* resonance is most pronounced and the π^* resonance is smallest when the E vector is parallel to the surface. It would be useful to start with an example: In figure 2.10, the polarization dependence of resonances for oriented molecules CO on Mo(110) and C_2H_4 on Ag(100) is shown [36-38]. Since the π^* resonance is observed for $\vec{E}$ parallel to the surface and the σ^* resonance for $\vec{E}$ nearly perpendicular to the surface, the CO molecules stands up on the surface, as showed in the figure. Furthermore, the observed spectra clearly show peaks associated with the molecular nature of CO, such that the molecule remains intact bonding to the surface. The same principle can be applied for ethylene, as shown in the right side of the

figure 7. The π^* and σ^* resonances in the C_2H_4 NEXAFS spectra are affiliated with the C–C core of the molecule and show the opposite angular dependence to that for CO. The π^* resonance is observed for $\vec{E}$ nearly perpendicular to the surface and the σ^* resonance for $\vec{E}$ parallel to the surface. This clearly means that the molecule lying down on the surface, i.e., the C–C axis is oriented parallel to the surface. If we now consider the hydrogen atoms we expect another peak mentioned due to C–H* resonance associated with C–H bonds. The peak is observed in the spectrum when $\vec{E}$ is parallel to the surface, similar to the C–C σ^* resonance. The fact that the peak is stronger for this polarization shows that the C–H bonds lie in a plane parallel to the surface, or at least close to that plane.

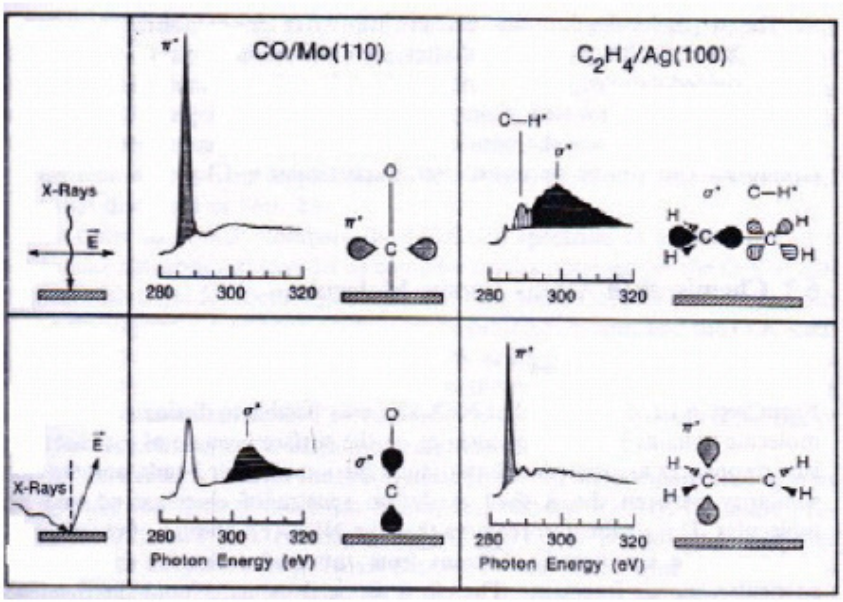

***Figure 2.10**. Polarization dependence of resonances for oriented molecules, illustrated for vertically oriented CO on Mo(110) and lying down ethylene (C_2H_4) on Ag (100) [adopted from ref. 24].*

Instrumentation

For the all part, NEXAFS experiments were performed under UHV conditions. As a nice side effect of this environment, unwanted contamination is substantially reduced so that the integrity of the samples is retained for a significant time (e.g. measuring time per sample approximately 40 minutes).

After synchrotron light (X-ray photon) coming from storage ring, the X-rays have to be guided to the sample. All optical components for X-rays are operated in reflection, because it is not possible to manufacture lenses for X-rays (insignificant contrast in refractive index [39]. Fairly stringent criteria apply to the materials that are used for the optical components. They have to be UHV-compatible, free from absorption features in their operational energy range and resistant to the intense X-ray irradiation. For an optimal throughput of the photons and in order to prevent an excessive heating of the optical components by refracted light, all instruments are operated close to or below the critical angle for total reflection, which is very grazing due to the high frequency of the photons [40]. From this optical arrangement, "precise workability" accrues as an additional requirement for the materials. The general scheme of their production is hence by a polishing and subsequent coating process.

On its way to the sample, the first optical device that the light encounters is a mirror which focuses it onto the entrance slit of the monochromator. Due to minor changes in the position of the electron beam, this mirror has to be adjusted after every injection to maximize the intensity of light that enters the monochromator.

In a next stage a monochromator selectively allows photons of only a single energy to pass through to the samples while all others are deflected. For this purpose, the incident beam is widened to a focused image in which the different wavelengths are spatially separated. This is achieved by diffraction at plane grating. In our case a special design called "plane grating monocromator" were used. Light emerging from the monochromator then hits a mirror which directs it onto the sample. Before hitting the sample the beam is collimated by a series of apertures and passes a nearly completely transparent gold grid. The radiation-induced electron signal on this grid is measured during each experiment and can be used as a situ monitor of the spectral transmission if the grid itself is free from (mainly hydrocarbon) contamination and its associated absorption features in the experimental energy region. We used the signal on this grid for the compensation of minor fluctuations of the photon flux (I_0). As the beam also grazes a tungsten wire, I_0 is occasionally monitored through the current of the emitted electrons and the associated absorption features are sending via an amperemeter to the experiment control unit.

In the end-station, the compact High Energy Photon Absorption Spectroscopy (HEPAS) set-up was installed [41], see figure 2.12. It is based on a 7 cm long cube like UHV vessel with a hollow sphere of 5 cm diameter with 6 flanges, where all other components like the detector, the manipulator, the fast load lock and the connections to the beamline and the final endstation are adapted to via CF 38 flanges. In figure 2.12, an outline of the set-up is

presented. In the HEPAS chamber, the beam hits the sample which is mounted on a 360° rotate-able manipulator. The electron yield mode can be measured by simple current, directed via amperemeter to the control unit. The impinging photons can hit the sample surface under variable grazing angles up to normal incidence, because in polymer samples, the molecular orbital orientation can be identified by varying the angle between sample and the beam [24].

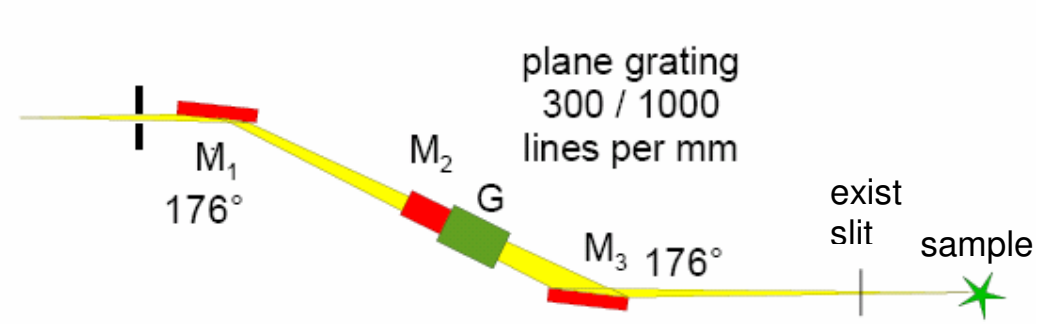

Figure 2.11. *Top view of the UG49/2 PGM 2 beam line (BESSY-II, Berlin, Germany) guiding system. Where M_1 & M2 is a platinum coated cylindrical mirror ($2\theta=176^o$) and plane mirror respectively, $G_{1,2}$ is plane grating having 300/1000 lines per mm and M_3 is gold coated cylindrical mirror ($2\theta=176^o$) which is vertical focusing to the exist slit. M_1, M_2, G is connected with water cooling system [Adopted from ref.41].*

The combined photon and electron detector is mounted rectangular to the photon beam. It is based on a commercial channeltron (BURLE), placed on a liner manipulator to change the detector working distance. To protect the channeltron from stray fields from scattered electrons, inherently present in this small set-up, a first metallic mesh is installed in front and grounded electrically. The mesh diameter of 1.5 cm determines the cone width of emitted photons and electrons to angle 15°. When the fluorescence mode is used, a voltage of 0 to 4 kV is applied to a second grid to suppress emitted electrons. For electron detection an acceleration voltage can be used to focus the charge carriers into the channeltron.

The complete detector is encapsulated into a pipe with 25 mm diameter and the grids cover the complete area, therefore no electrons or photons can pass at the sides. The conducting elements of the detector were protected by a polymeric layer against electrical short circuit

with the UHV chamber. This protection can sustain back out up to 200°C and is suitable for UHV applications.

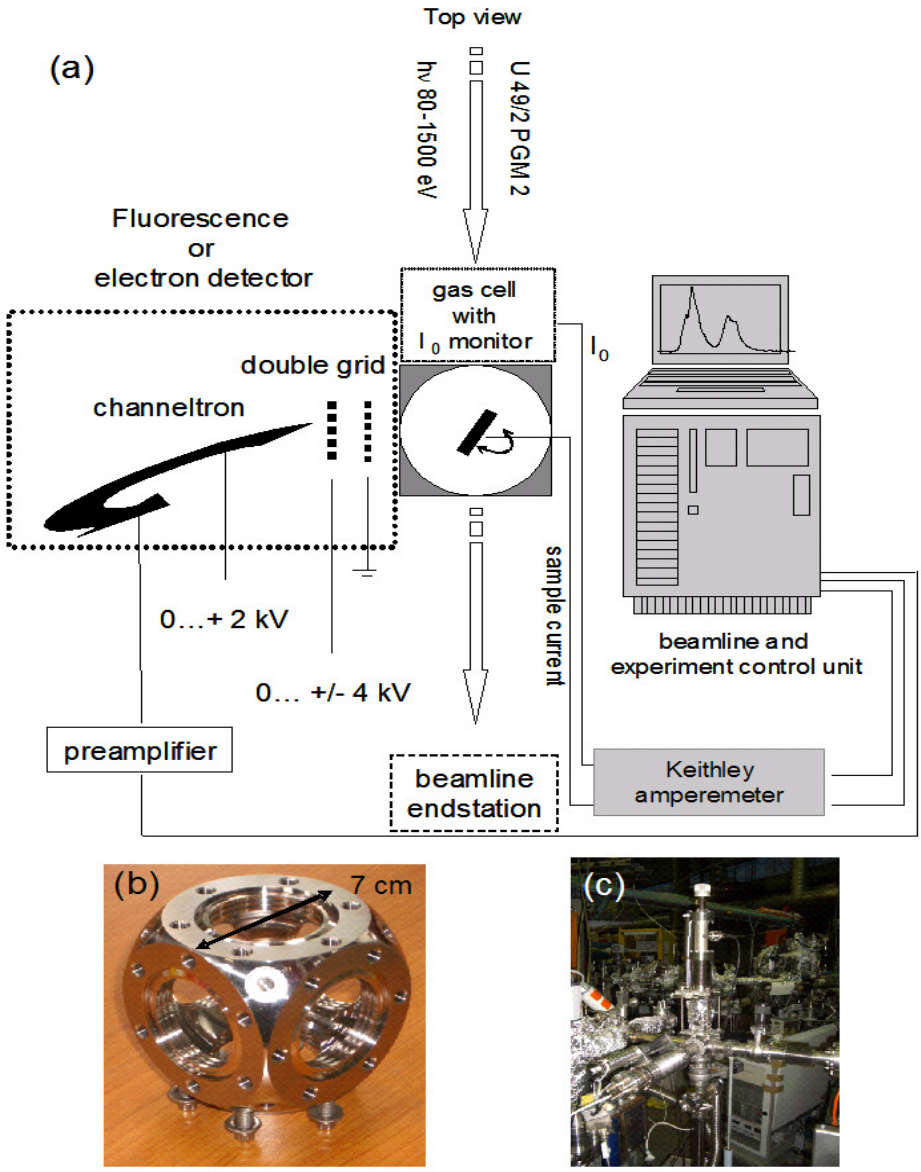

Figure 2.12. *Schematical drawing illustrating the main components of the XAS experiment in top view in (a). Central compact UHV vessel for the experiment in (b), the outer diameter is given. Present set-up integrated into the U49/2 PGM 2 beamline at BESSY II in (c). The beamline endstation is at the right hand side, the beamline with the impinging photons at the left. In front the moveable fluorescence and electron detector is shown [adopted from ref.42].*

The particles were detected in the channeltron and multiplied. The signal is send via decoupler unit and a preamplifier to a counter in the control unit. In this control unit, which is standard part of all BESSY beamlines, the photon energy is set and all detector signals, I_0, undulator and monochromator settings can be read out simultaneously.

One UHV load lock with liner manipulator connected with cube like chamber to transfer the sample into measuring chamber.

In our case, NEXAFS is mainly used to perform in Total Electron Yield (TEY) and Total Fluorescent Yield (TFY) mode for soft x-rays between 80 -1500 eV, but it is also possible to perform in higher photon energies.

As example, an N_2 absorption spectrum is shown in figure 2.13, which is taken in the gas cell at the undulator based U49/2 PGM2 beamline at BESSY when the photon energy scan through the N_2 absorption edge [41]. The two main absorption peaks arise around 400.9 and 401.15 eV which is fitted with a double Voigt profile with a Gaussian broadening of 59 meV. The operation photon energy resolution is found around E/ΔE: 6500-7000 over the complete spectral range of 80-1450 eV.

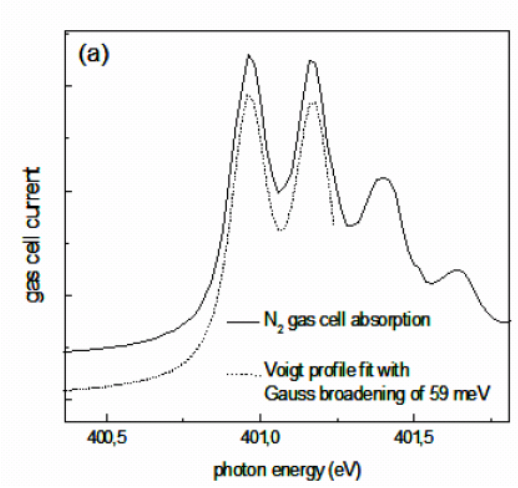

Figure 2.13. *N_2 edge NEXAFS spectra from the N_2 gas cell, the spectral resolution is determined with a Voigt profile fit (dashed line).*

When the energy is scanned through CK edge, it is very important to monitor the photon flux very precisely. In figure 2.12(b), the photon flux (I_0) is measured from a tungsten wire which shows an intensity drop of 83 % within an interval of below 20 eV from 280 eV. Two sharp

peaks at 283 and 287 eV arise due to carbon contamination of the optical elements and mirrors in the beamline. In the case of the N-Kedge and the O-Kedge, there is a similar but not such severe problem observed.

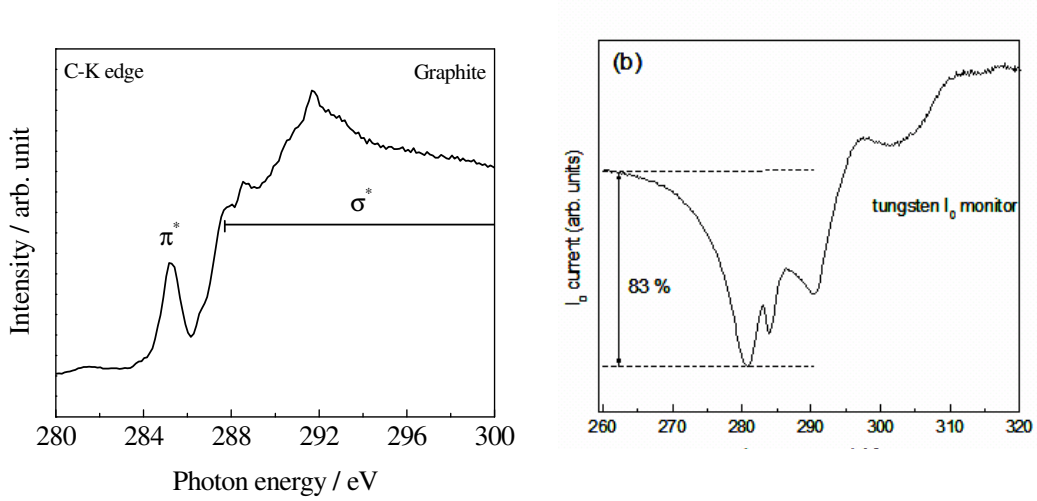

***Figure 2.14**. NEXAFS spectra of graphite at the C-K edge (recorded at the magic angle to eliminate angular effects (a). The photon flux vs. photon resolution is monitored with a tungsten wire at the C-Kedge (b)*

The Normalisation and background correction for carbon based samples must be done very carefully [24]. It is advisable to measure I_0 during each scan of measuring the sample simultaneously, especially at the C-Kedge.

Graphite provides crystalline solids of well-known bonding structure. Therefore it is always used as a calibration sample for the C-K edge NEXAFS spectra. In figure 2.14(a), one calibrated spectra of graphite is illustrated. For graphite, the C-K edge NEXAFS energy range can be subdivided into two regions: The first π* resonance around 285 ± 0.5 eV and a broad σ^* region above 289 eV, as indicated in the figure. The characteristic of the π* resonance can serve as a fingerprint of the local bonding, in contrast, the σ^* region is more complex [24, 43, 44].

Data analysis of NEXAFS

In most of the cases it is advantageous to use a curve fitting analysis method. In this case one should careful in performing the edge jump normalisation procedure. This method is

particularly valuable in the analysis of angular dependent NEXAFS spectra. It isolates the angular-dependent resonances by eliminating the isotropic components of the NEXAFS spectra such as the continuum step [45].

The curve fitting method provides valuable information on the existence of certain resonances and of their positions and line-shapes. The fit parameters of the resonance lineshapes may then be used in the fits of original data, which are in general, more complicated but also contain more information.

Curve fitting procedure

This section overviewed of the details importance and significance of the different lineshape of the peaks in the near edge spectrum. In particular, we consider typical lineshapes observed for core excitation resonances to discuss how to isolate the peaks so that the lineshape can be analysed.

Gaussian, Lorentzian and Voigt Funcations

In the first step of the curve fitting procedures to analyze core excitation spectra, an analytical function must be used. This function can identify the lineshapes of the individual peaks. If the monochromator resolution has dominant character then peaks will have a Gaussian lineshape, which describe by:

$$I_G = Me^{-1/2((E-P)/(\Gamma_G/c))^2} \qquad 2.19$$

Where M is the maximum value of the function, T_G is the FWHM of the peak, P is the position of the peak, E is the energy which is an independent variable and c is constant of value 2.355.

Another common lineshape encountered in curve fitting procedure is the Lorentz-curve. If the monochromator resolution is small compared to the intrinsic lifetime-related width of a peak, this lineshape will be described by the Lorentzian function:

$$I_L = M\left(\frac{(\Gamma_L/2)^2}{(E-P)^2 + (\Gamma_L/2)^2}\right) \qquad 2.20$$

A third lineshape function often used is the Voigt profile which convolutes a Gaussian and a Lorentzian lineshape [24]. This profile is useful in cases where instrumental and lifetime widths are comparable and the lineshape is given by:

$$I_V = M\left[\eta\left(\frac{(\Gamma/2)^2}{(E-P)^2+(\Gamma/2)^2}\right)+(1-\eta)e^{-1/2((E-P)/(\Gamma/c))^2}\right] \qquad 2.21$$

Here η is the Lorentzian fraction and Γ is the FWHM of the Voigt profile. *Wertheim et. al.* have showed that it is possible to determinate the components widths Γ_L and Γ_G from the fit parameters η and Γ.

The most resolute peaks in the K-shell NEXAFS spectra are the bound state resonances in the form of π^* or Rydberg resonances. An example is shown in figure 2.15, high resolution spectrum of N_2 molecule [46]. Here both the vibrational fine structure of the π^* resonance and various Rydberg resonances, merging into the ionization potential, are shown. In addition, the double excitation feature around 415 eV is found to exhibit a detailed fine structure. The dashed lines represent the fitted curve by Voigt functions.

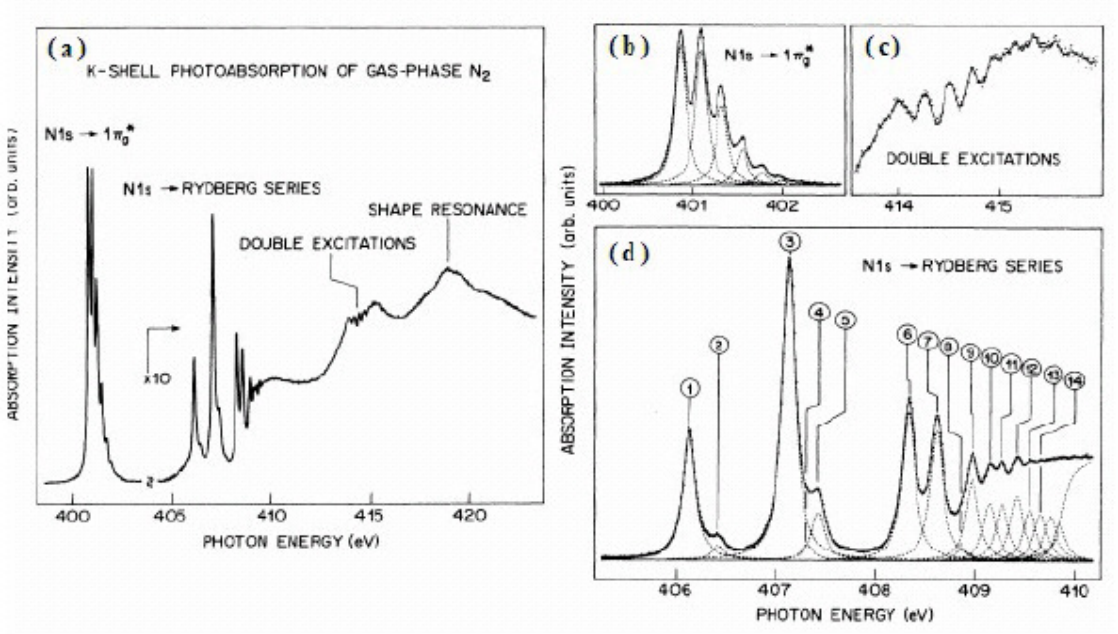

Figure 2.15*. (a) NEXAFS spectra of the nitrogen molecule in the gas phase. (b) Vibrational fine structure in the π^* resonance, fitted profile shown dashed. (c) Blow-up of the double excitation feature, showing vibrational fine structure. (d) Rydberg series fitted with Voigt*

profiles, merging into the ionisation continuum with a step-like onset at 409.938 eV [adopted from ref. 46].

Figure 2.16 shows an example of fits of π^* resonances in lower resolution (1.1 eV), namely the C=C π^* resonance of condensed allyl alcohol (CH_2=$CHCH_2OH$) on a Si(111) surface at 285.0 eV [47]. It was clearly visible that the Gaussian lineshape provide a reasonable fit whereas the Lorentzian fit is poor because the base of the Lorentzian is too broad. As the intrinsic lifetime width of this peak is so narrow that the instrumental resolution imposes the Gaussian lineshapes upon the peak.

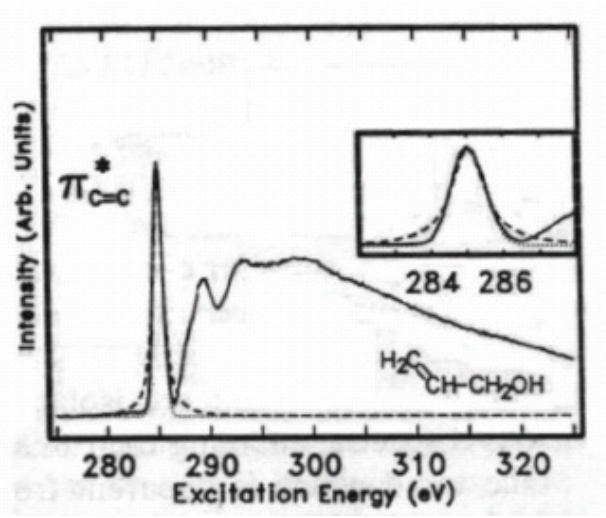

Figure 2.16. *Fit of the C=C π^* resonance in the NEXAFS spectrum of condensed allyl alcohol [adopted from ref. 47].*

Asymmetric Gaussian and Lorentzian Lineshapes

In NEXAFS spectra, it is commonly seen that many resonances are not isolated like π^* resonances but overlap with the ionization continuum and other resonances. The asymmetry increases with increasing energy, since the lowest energy peaks are well accounted for by symmetric Gaussians while the highest energy peak has a quite distinct high-energy tail. As example, a NEXAFS spectrum of a P(VDF-TRFE) film on PEDOT:PSS/Si(100) substrate is

shown in figure 2.17. The increase in width of resonances with increasing energy can be attributed to lifetime broadening. That is, the higher the energy of the final state, the shorter its lifetime and hence the broader the peak.

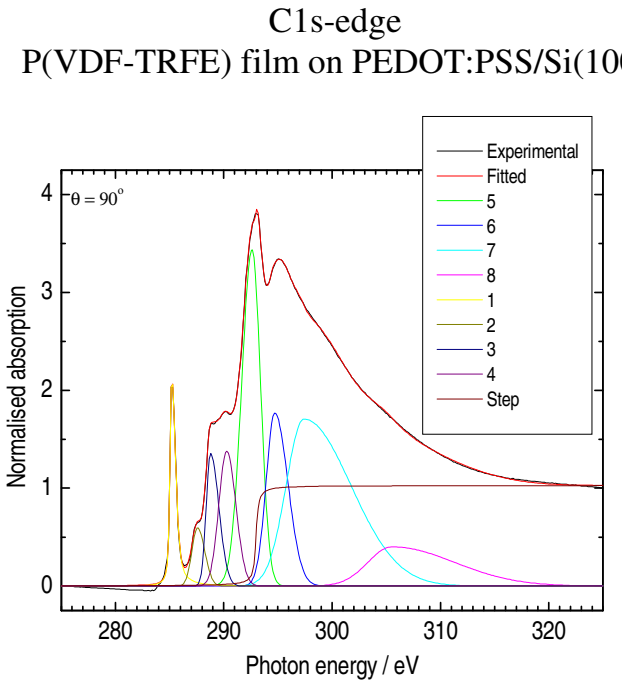

Figure 2.17. *The C-K edge NEXAFS spectrum of P(VDF-TRFE)films on PEDOT:PSS/Si(100)[inset, fitted curve 1 attributed for* π^* *resonance and rest of the fitted curves (2-8) are arises due to* σ^* *resonances.*

Step function

In addition to peaks, NEXAFS spectra contain one or more step-like features referred to as continuum steps. This arises due to excitation of the core electron to a continuum or quasi-continuum of final states, e.g., to the smooth density of states. Experimentally steps are difficult to examine, because they are almost always obscured by other spectral features. In particular, the position and shape of the edge are difficult to distinguish from experiment, as is evident from figure 2.15 (d), where the density of Rydberg resonances becomes so high that a continuum-like smooth cross section is observed well below the accurately known ionisation potential at 409.938 eV [46], where the continuum step is located. It is also visualised by fitted curve in figure 2.17.

Sample preparation

2.6. Thin film preparation

Substrate cleaning prior to spin coating

p type Si(100)-wafers (Wacker-Chemitronic GmbH) were used as main substrate for our experiments. Before the preparation of polymer spin coated films, pieces of Si-wafers were cleaned through a standard RCA-1 cleaning procedure. This wet cleaning procedure is useful to remove organic contamination and particles from the surface of the Si substrate [48]. The experimental set-up and the cleaning procedure are descried as follows:

- Removing the photoresist from the Si-wafer if necessary by rinsing with acetone and iso-propanol (IPA) followed by drying with N_2 blowing
- Repeating the above step at least two times for better cleaning
- Preparation of a mixture of NH_4OH, H_2O_2 and di-ionized water (DI-water) with 1:2:10 ratio respectively. The solution is called RCA-1 solution
- Arranging of shaped pieces of wafers (size: ~15 × 15 mm^2) in a sample holder and immersion in the RCA-1 solution (see figure 2.18)
- Maintaining of the temperature at 70 ± 5^oC for 20 minutes. The solution will bubble vigorously after 1-2 minutes, indicating that it is started to work
- After 20 minutes, the Si-wafers pieces along with wafer stand need to take out and soak into another beaker containing DI-water. This transfer should be faster to prevent wafers from drying up
- This previous step has to be done three-four times for a complete removal of the residual RCA-1 solution
- Taking out the wafer one by one and rinse with DI-water followed by rinse with IPA and afterwards blows up by N_2 flow. This step is useful to dry up the wafer faster and prevent water mask
- Transfer of the whole set of wafers to the Glove box for spin coating

These treatments were followed for every set of samples prior to the organic thin film making procedure.

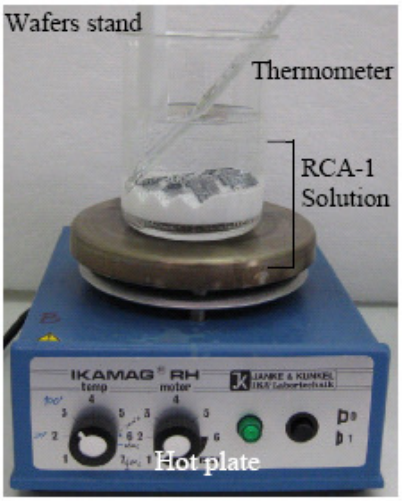

Figure 2.18. *Experimental set-up for RCA-1 cleaning for Si-wafers*

Spin coating procedure

Spin coating is a widely used technique in the semiconductor industry for the deposition of polymer resist layers which take part in the lithographic patterning process [49].

For our ultra thin polymer film deposition, a WS-400B-6NNP/LITE spin coating unit is used (see figure 2.19B) which is kept inside glove box. A photograph of the glove box is shown in figure 2.19A. The glove box has a large antechamber and a single gas purifier with single gas blower, manual isolation valves, and an evacuatable glove port cover. Purifier regeneration and antechamber evacuation and refill are manually controlled.

The purposes of the glove box are as follows: substrates need to be protected from contamination, especially before making thin film, and the contamination can include oxygen as well as moisture and particulate. The glove box creates a mini-environment that can be controlled to varying the degree of purity.

In the glove box, RCA-1 cleaned Si wafer pieces and necessary chemicals are inserted into an antechamber which is purged with argon. The atmosphere in the glove box is pure argon that has the oxygen and moisture removed by recirculation the argon through an absorbing chamber. Before any processing commences, the moisture level within the box is maintain less than 10 ppm, with the oxygen level less than 100 ppm.

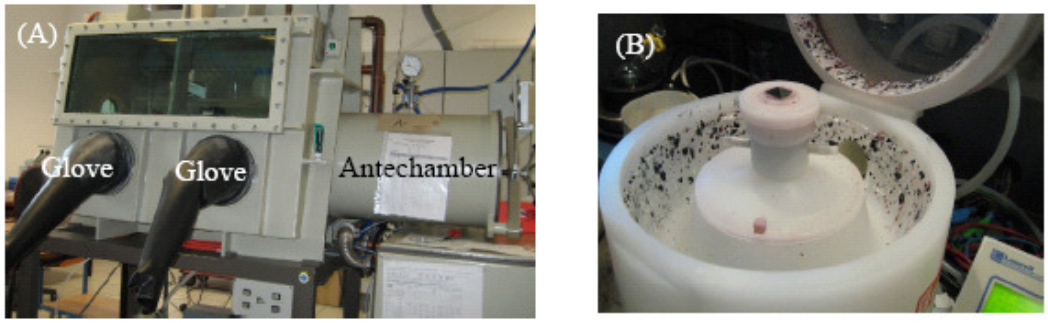

Figure 2.19 *(A) Photograph of Glove-box for spin coating; (B). Photograph of spin-coating unit (Model: WS-400B-6NPP/LITE)*

Our spin coating is a process which involves depositing a small puddle of an organic solution onto the centre of a substrate (see figure 2.20), which is then spun around at a high speed so that the solution is spread out by the centrifugal force. Excess solution flies off the substrate and simultaneously, some of the solvent evaporates. The evaporation process raises the concentration and viscosity of the remaining solution. This high viscosity prevents the solution from exiting the substrate and a thin film of solution remains. Continued spinning evaporates the rest of the solvent after which a thin film of polymer is obtained. The spinning speed is ranging from 1000 to 6000 rpm, depending on the interest of the film thickness.

Figure 2.20. *Illustration of the spin coating technique. A solution containing a polymer is deposited on a substrate, which is then spun at a high speed.*

The co-polymer, we use P(VDF-TrFE) with molar ratio of VDF and TrFE is 70:30. The material is supplied as film by Piezotech S.A., France. There are some selective solvent available for making P(VDF-TrFE) solution for spin coating. We choose 2- butanone as solvent for spin coating, as it allow us to make homogeneous solution and the solvent is not harmful for health. We prepare different concentrations of P(VDF-TrFE) as weight percent, say for example from 0.1 % to 2.5 % . By controlling the concentration of P(VDF-TrFE) and spin speed, we can able to make different film thickness on RCA-1 cleaned Si wafer. The calibration curve of spin coating (film thickness versus spinning speed) is shown in figure 2.21. After spin coating, the film was annealed at 135^{o}C for 2.0 hours to improve the crystallinity. But to investigate the annealing effect, we have also varied the annealing duration which is mentioned in the corresponding results.

Apart from different thickness (down to 10 nm or so) of P(VDF-TrFE) films on Si-wafer, we also make different film with PEDOT:PSS on Si-wafer as substrate for P(VDF-TrFE) films to investigate interaction of P(VDF-TrFE) films with PEDOT:PSS films. The purpose and spin coating steps is discussed in each concerning section of result and discussion.

To investigate interaction of aluminum layer with P(VDF-TrFE), we deposited a thin 'Al' layer by a thermal evaporation process in UHV condition.

For the effect of an electric field on P(VDF-TrFE) films, we prepare a layer structure on the Si-wafer. In this case, 1st we deposited 'Al' on the Si-wafer and then spin-coated PMMA solution on it to avoid leakage current during application of the electric field. Thereafter, the PMMA/Al/Si staking is annealed at 100^{o}C for 30 minutes. And finally, different concentrations of P(VDF-TrFE) films are spin coated on the PMMA/Al/Si staking followed by further annealing at 135^{o}C for 2.0 hours.

2.7. Thickness determination

The thickness of the spin coated P(VDF-TrFE) copolymer films is measured by Taylor Hobson profilometer (Talystep). The thickness below 15 nm is calculated on the based on XPS results.

Measured by Profilometer

As mentioned in thin film preparations section, the thickness of the spun polymer can be varied by spin speed and concentration of the solution in a wide range. In figure 2.21 the film thickness versus the spinning speed is shown for different concentrations of the solution. In [49], [50] models for spin coating process have been developed taking into account the solvent evaporation and the non-Newtonian character of the rheological behavior of the resists. Jenekhe [50] introduced a parameter α, which is describing the influence of solvent evaporation on the viscosity of the fluid during spin coating. A general dependence $t \sim \omega^{-p}$ with $p=2/(2+\alpha)$, where t is the final thickness and ω is the angular frequency, was described. By analyzing a log-log plot of the thickness versus the speed (inset of figure 2.21) we determined mean values of p of 0.23 in the concentration range of 0.5-2.5%, while for the thicker solution of 5% a value of 0.48 was found, which is in the typical range of 0.40-0.82 for resists discussed by Jenekhe [50].

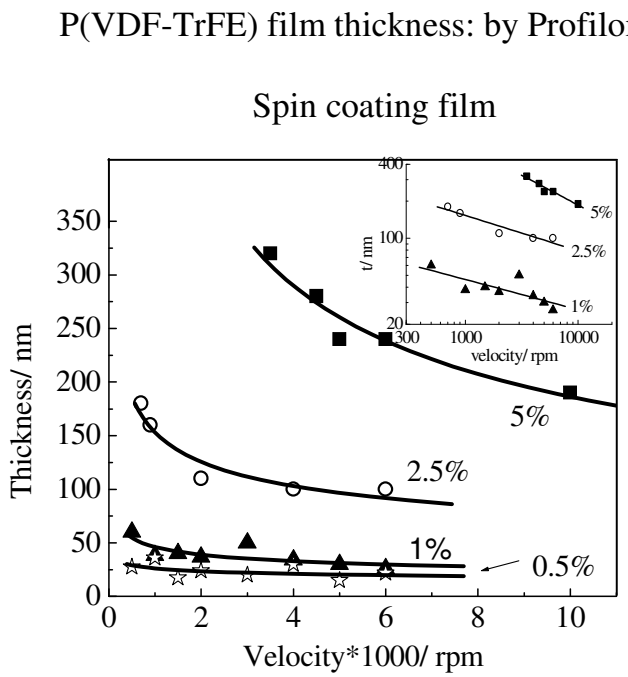

Figure 2.21. *Calibration curve of thickness determination (measured by Profilometer) versus spinning speed of different weight concentration of P(VDF-TrFE) copolymer with 2-butanone as a solvent.*

Generally we find an increased slope p by increasing the concentration of the solution. This is in good agreement with the modulations in [49] and attributable to the increased fluid viscosity and therefore to the more prominent non-Newtonian behavior at higher concentrations [49].

Determined from XPS results

The layer thickness of P(VDF-TrFE) copolymer ultra thin films has been determined from the XPS results. In this case, the P(VDF-TrFE) copolymer layer is on the substrate PEDOT:PSS/Si-wafer. The detail of the thickness estimation is described in XPS section of this thesis. The plot of layer thickness versus copolymer thickness is shown in figure 2.22.

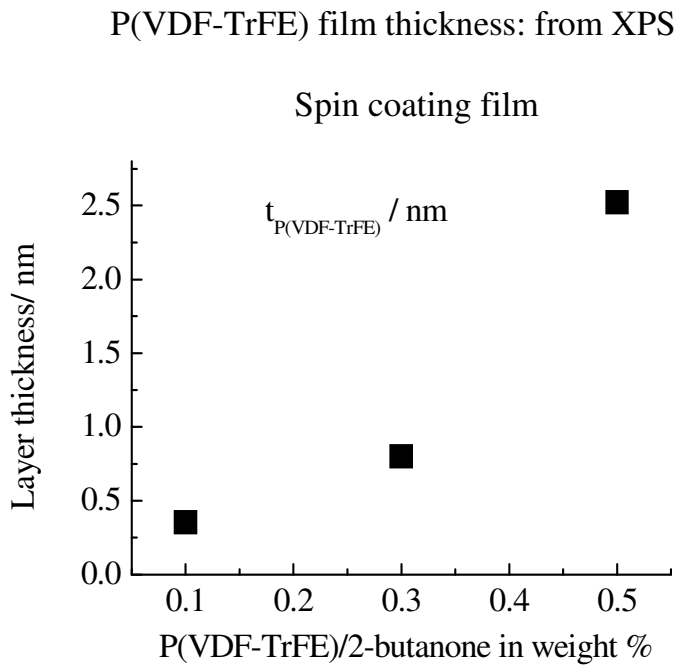

Figure 2.22. *The determine values of layer thickness of P(VDF-TrFE) films on the based on XPS results. Where the weight concentration of P(VDF-TrFE) copolymer make with 2-butanone as a solvent.*

2.8. Surface morphology

For morphological investigation, the spin coated film of P(VDF-TrFE) (100 nm thick film) is investigated by scanning electron microscope (SEM) of pristine and after annealing (see figure 2.23). The annealing is undertaken at 135^{o}C for 2.0 hours as mentioned in thin film preparations section of this thesis. First of all, we noticed that there are many pin holes are distributed for pristine film. After annealing, most of the pin holes are dramatically removed and reduces from the film. Therefore it is conformed that after annealing the film becomes more homogeneous. To investigate the surface roughness morphology, we have employed the non-contact mode AFM which gives us an opportunity to study in lower scale than SEM.

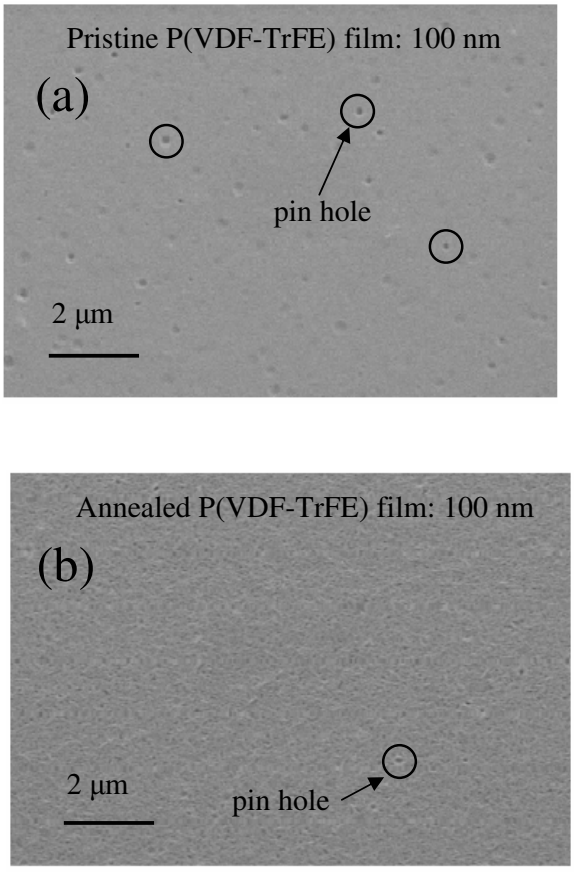

***Figure 2.23**. SEM images of a 100 nm thick P(VDF-TrFE) copolymer film on Si(100) substrate; (a) pristine film and (b) annealed film (135^{o}C for 2.0 hours).*

Figure 2.24 (a) shows a non-contact mode (NC) AFM topographical image of the 100 nm thickness of P(VDF-TrFE) copolymer spin coated film (pristine film). A pin whole distribution is observed for the pristine film as expected, which is also observed in SEM images (see figure 2.23 a). Figure 2.24 (b) shows a NC-AFM topographical image for the annealed film. After annealing the pin holes are significantly removed and shows the well grown lamellar crystalline region, which is very typical for P(VDF-TrFE) [51-53]. In average, the dimensions of the lamellae, measured by AFM line profile, are around 70 nm in length and 60 nm in width (see figure 2.25).

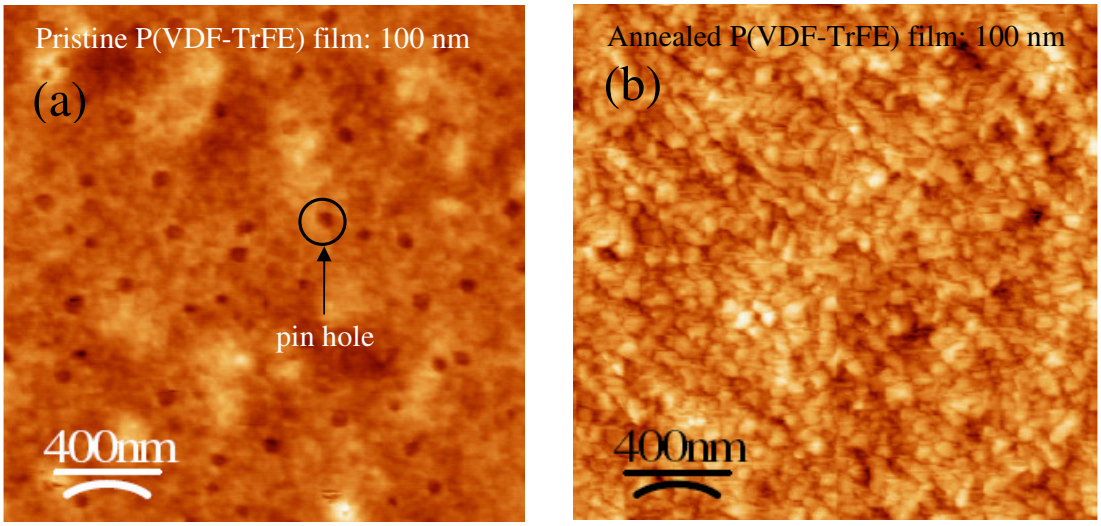

Figure 2.24. *Non-contact mode AFM topographic images (Scan area: 2 μm × 2 μm) of a 100 nm P(VDF-TrFE) copolymer film on Si(100) substrate (a) pristine film (RMS surface roughness ~1.3 nm) and (b) annealed film,135°C for 2.0 hours (RMS surface roughness ~ 3.2 nm).*

The root mean square (RMS) surface roughness is found about 1.3 nm for pristine film whereas RMS value of annealed film is about 3.2 nm. Thus, AFM topographic images confirm that our annealing steps improve the crystallinity. Although because of the long molecular chain structure of polymeric materials, a fully crystalline state is usually hard to obtain. From FTIR and XRD study shows that our spin coated P(VDF-TrFE) copolymer films

also show a semicrystalline structure, where the polar crystalline β phase and amorphous phases coexist, has been described in the next section of this chapter.

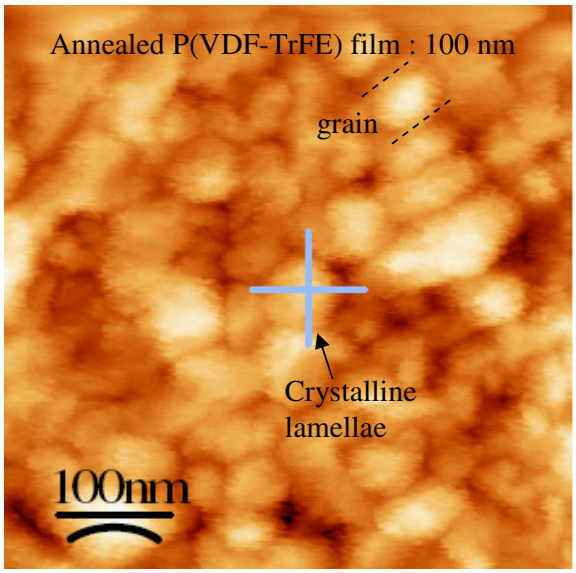

Figure 2.25. *Non-contact mode AFM topographic image (Scan area: 0.5 μm × 0.5 μm) of the annealed film.*

2.9. Beta phase identification

From the structural point of view, we have made some attempt to investigate the existence of different phases of P(VDF-TrFE) copolymer film. As a part of measurement, FTIR spectroscopy is employed to characterize the chain confirmation of a 70/30 VDF/TrFE copolymer. Infra-red spectroscopy can accurately determine localized structures. When the vibrations are well characterized, the identification of chemical groups can be determined. Even though the copolymers are known to have a large fraction of amorphous phase, there are few vibrations which can be definitely assigned to either the amorphous phase or the crystalline phase [54]. The vibrational modes of the polymer chains can also be used to distinguish the two phases. Certain vibrational modes exist only in one conformation, either the *all-trans* conformation of the ferroelectric phase, or the alternating *trans-gauche* conformation [55-59]. It is difficult to obtain infrared data for the 9-μm thick P(VDF-TrFE) copolymer films (which we brought from Pizotech, France) for quantitative analysis since many bands show high absorbance values (see the figure 2.26 B). Therefore, we make different thickness of thin film until 100 nm thickness on Si-wafers followed by annealing.

'Si' is penetrable for infrared radiation. The detailed procedure of the thin film making is described in the sample preparations section. The analysis of vibrational spectra has been carried out for poly(tetrafluoroethylene) [60-64] and for PVDF [59, 65, 66]. These studies have proven to be enormously useful to select the vibrations in order to interpret the molecular structure of P(VDF-TrFE) copolymer. Due to the large mass of the fluorine atom, most infrared-active vibrations for the copolymer are concentrated in a rather narrow region, 1500–400 cm^{-1} (see the figure 2.26 A). Several vibrational bands for the copolymer have been assigned to specific conformations by Tashiro *et al*. [55, 59, 65, 67] and these assignment are useful to analysis of our study.

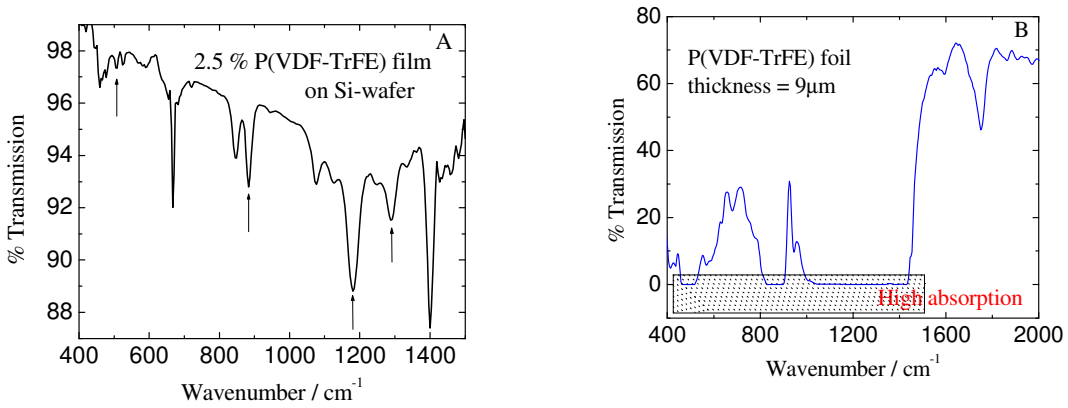

Figure 2.26. *FTIR spectrum of a (A) spin coated film of P(VDF-TrFE) on a Si-wafer, solvent: 2-butanone. film thickness: 100nm (B) 9 µm thickness of P(VDF-TrFE) foil.*

The 506 cm^{-1} band, may correspond to the 510 cm^{-1} CF_2 bending band observed for *trans* sequences associated with either the β or γ phases of PVDF. However, Davis *et al*. have observed a band at this position of P(TrFE) [68], making it difficult to employ for structural interpretation. The 1290 cm^{-1} band has been assigned the symmetric CF_2 stretching vibration coupled to the backbone stretching and bending vibrations [69, 70]. It is assigned to sequences of four or more VDF units corresponding to *trans* isomer sequences four or more units long and is therefore characteristic of the chain extended or β structure [55, 56, 67]. This band is absent in the paraelectric phase. The 883, 845 (doublet), and 612 cm^{-1} bands, assigned to CH_2 symmetric stretching, and the CF_2 bending coupled to skeletal bending, respectively, are

useful to structural characterization [65, 69-71]. Although not use extensively in our study, the 802 cm^{-1} band assigned to the CF_2 symmetric stretching vibration is extremely strong in the Raman spectrum of these copolymers [72, 65]. It should be emphasized that these vibrations are characteristic for the conformations of PVDF sequences. Strictly speaking we cannot directly interpret the overall chain conformation; however we feel the molecular response of the co-monomers cannot be separated. The two bands near 845 cm^{-1}, similar to the 1290 cm^{-1} band, are characteristic of long sequences of al least three *trans* isomers [55, 56, 67]. In contrast, the bands at 802 and 612 cm^{-1} are characteristic of gauche conformations [55, 56, 65, 72]. There has been controversy regarding the assignments of the bands for the position at 883 and 845 cm^{-1}. Originally, the assignments of those aforesaid bands for PVDF were unclear [71]. Tashiro et al. showed by poling experiment and normal vibrational analysis, the new assignment is consistent with polarized Raman studies on rolled PVDF films, with the 883 cm^{-1} band assigned to the CH_2 rocking, CF_2 asymmetric stretching, and CF_2 rocking vibrations, while the 845 cm^{-1} band is assigned to the CF_2 symmetric stretching mode [69].
In summary, figure 2.26 A the bands, market with arrows, at 505 cm^{-1}, 845 cm^{-1}, 1184 cm^{-1}, 1290 cm^{-1} gives evidence for *all-trans* ferroelectric phase. No indication for alternating *trans-gauche* conformation is observed. For this phase, a strong absorption feature at 802, 612 and 1196 cm^{-1} occurs, for example.

2.10. Effect of Annealing

FTIR results

After conforming the ferroelectric β phase in the FTIR study for the 100 nm thickness of P(VDF-TrFE) films, we anneal the films at 135^{o}C for 2.0 hrs. We have also employed to realize the effect of crystallinity as a function of annealing duration for the same annealing temperature. Care has been taken to understand the effect, after spin coating of copolymer on Si wafer, the samples are breaks into several pieces for different annealing durations. There might be effect of crystallinity if we do annealing several times for the sample and of course as a result it is timid to make conclusion. Figure 2.27 (A) showing the effect of annealing duration. In all spectra, illustrate the evidence for all-trans ferroelectric phase (see the previous analysis). The three arrow marked bands at 1400 1250, and 1100 cm^{-1} are due to contributions from the amorphous region of the copolymer films [73, 74]. All such three bands are more prominent for unannealed sample and 1250 cm^{-1} absorption band is diminishes even for 10 min. annealing. The rest two bands (1400 and 1100 cm^{-1}) exist for all samples even after 240 min. annealing but the absorption intensity are changing significantly

until 120 min, annealing. For realizing the improvidence of the degree of crystallinity, we have taken 1400 cm^{-1} band (the most prominent absorption) as reference. Figure 2.27 (B) shows that after 30 min. annealing, the crystallinity improved about 40 % with respect to unannealed film and afterwards the change is not significant.

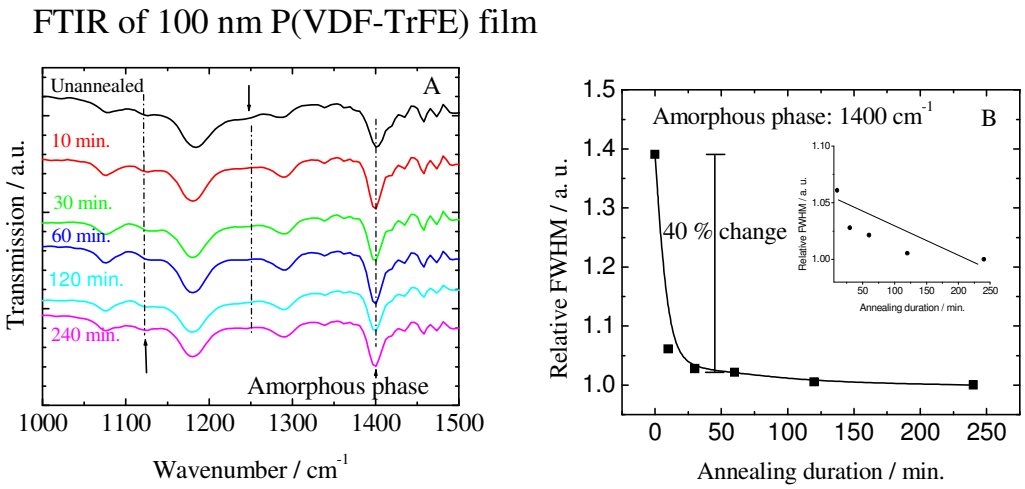

Figure 2.27. *(A) FTIR spectrum (1000 – 1450 cm^{-1}) of spin coated films of P(VDF-TrFE) on a Si-wafer (solvent: 2-butanone. film thickness: 100nm) as function of annealing duration at temperature 235^{o}C. Arrow marks showing the amorphous phase; (B) Representation of the relative change of FWHM (at 1400 cm^{-1} of FTIR spectrum, from figure 6.1 A) with respect to annealing duration, (inset: without unannealed data for showing the relative change more prominently, the straight line is for eye guide.*

Topographical investigations

We have conformed from the FTIR study that the amorphous phase is not reducing significantly after 2 hour annealing. From the AFM topographical images, we found that the average size of crystalline lamellae structure is not improving significantly for longer time annealing. The topographical images of unannealed and annealed films are shown figure 2.24, the results revel that the crystalline lamellae structure improves significantly after annealing. The AFM topographical images for longer time annealing (4 and 40 hours) of the copolymer film is illustrate in figure 2.28. Here we found that the grain sizes of the crystalline region are not improved significantly after 2 hours annealing.

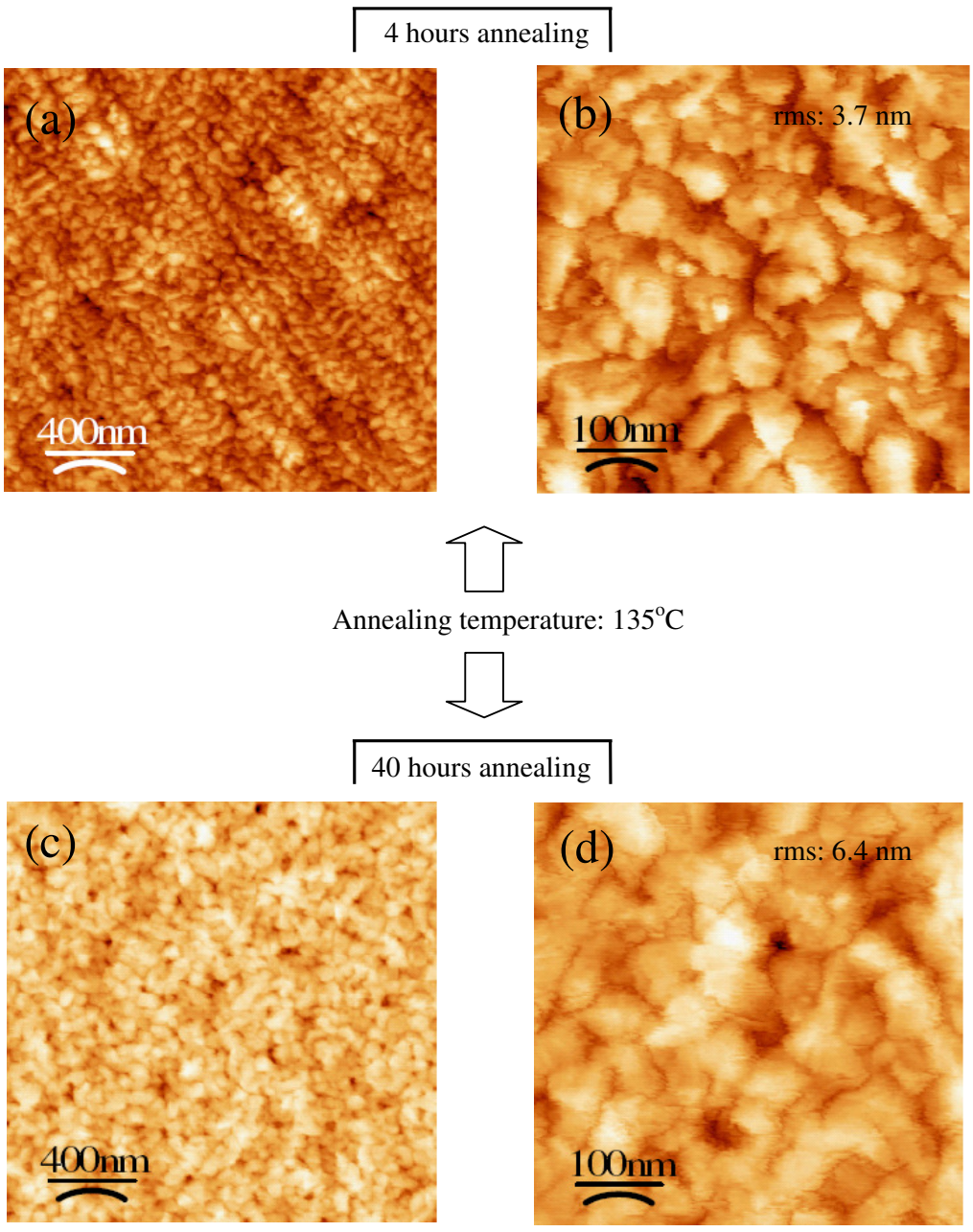

***Figure 2.28**. Non-contact mode AFM topographic images annealed P(VDF-TrFE) copolymer film on Si(100) substrates. Scan area: 2 μm × 2 μm (a) and (c); scan area: 0.5 μm × 0.5 μm (b) and (d). The annealing temperature and duration is mentioned in the figure.*

CV measurement

Here we will show the effect of the annealing step to our current-voltage (CV) measurements.

Experimental set-up

The measurements of capacitance versus voltage (CV) are carried out with an Agilent 4284A LCR meter at a frequency of 1 MHz with a 25mV (RMS value) test signal level while sweeping the DC bias with rates from 12.5 mV/s to 100 mV/s. The sample is hold in a sample holder under dark condition. Measurements are mostly performed at room temperature.

Results of CV measurement

In our current-voltage (CV) measurements, we observed much more symmetric behavior in the flat-band voltage shift inside one CV loop after annealing, while the CV loops of non-annealed samples additionally shift due to a probable charge injection [75]. We also found that annealing lead to a higher polarization value. The flat-band voltage shifts normalized to the thickness of the films deliver a polarization proportional value [75]. In figure 2.29, we show these values versus the applied electrical field window of the CV loop for one annealed and one non-annealed sample. We observe much higher values of the polarizability for the -

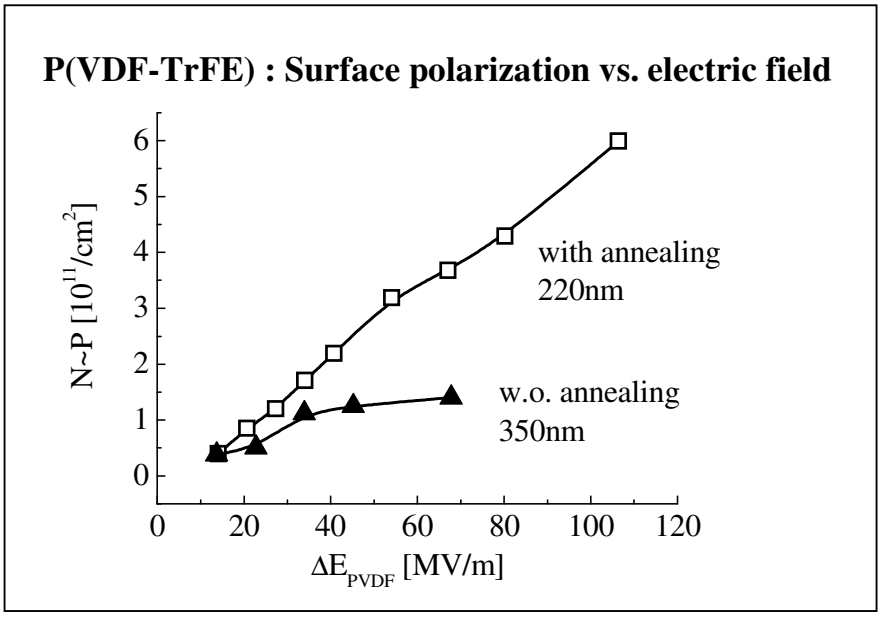

Figure 2.29. *Polarization proportional values versus applied electrical field window of the CV loop for one annealed and one non-annealed sample.*

annealed sample, while the non-annealed sample already shows saturation even here, where a thick SiO_2 buffer layer of 235 nm is used. A strong effect of annealing for improving the crystallinity of P(VDF-TrFE), which results in higher polarization values by a factor of 3 to 4, was clearly discussed [76]. Our results are in good agreement with this statement.
Therefore we have taken as template the annealing condition at 135^{o}C for 120 minute for our further investigations.

2.11. Optimization of the X-ray irradiation time

We have optimized the X-ray (Mg K_α) irradiation time of XPS analysis for P(VDF-TrFE) copolymer film. Therefore, we have employed the effect of X-ray irradiations on P(VDF-TrFE) copolymer films. It has been found that the fluoropolymers are sensitive to radiation [77- 80]. The X-ray photoelectron spectroscopy (XPS) is an extensive tool for the structural evaluation of P(VDF-TrFE) copolymer [81, 82] but none of investigation was reported for irradiation effect of the X-ray photon. For the structural evolution of the copolymer films, we exposed the X-ray on the copolymer sample for different duration and finally optimized the parameters for further investigation.
X-ray irradiation is carried out with *in-situ* environment in ultra high vacuum (base pressure 10^{-9} mbar) chamber using an X-ray tube (Mg K_α) with an operating voltage of 10 kV and a filament current of 10 mA.
Figure 2.30 (A) shows the FTIR spectra for pristine and X-ray irradiated samples for 1.0 and 6.0 hours. There is a significant change of some bands are noticed as shown with arrow marks (see figure 2.30 A). Interestingly, all such bands are the characteristic of evidence of the *all* trans ferroelectric phase [55, 56, 67]. On the other hand, the characteristic of the alternating trans-guache conformations are appears after 1.0 hrs of X-ray irradiation. The absorption band positions of trans-gauche conformations are shown in the figure 2.30 (A) with oval shape mark. It has been proven that alternating trans-gauche conformations are the unique evidence of paraelectric phase [55, 56, 65, 72]. Therefore we are suspecting that after 1.0 hrs of X-ray irradiation led to phase change from ferroelectric to paraelectric (F to P). To supporting such observation we have undertaken the adjacent investigation by the help of an X-ray diffraction (XRD) study.
From the XRD measurement, it is clear that the P(VDF-TrFE) films shows the crystalline region with co-existance phase of amorphous region (see figure 2.30 B). As is known P(VDF-TrFE) with a VDF/TrFE with molar ratio is a semicrystalline copolymer which consists of a

ferroelectric crystalline β-phase embedded in an amorphous matrix, and the β-phase has quasi-hexagonal close packing with orthorhombic *mm2* structure [83]. As seen in the figure 2.30 (B), the pristine copolymer sample exhibit an intense diffraction peak at $2\theta = 23.4^{o}$ which is a characteristic diffraction peak of the ferroelectric polar β-phase of the overlapping (110) and (200) plane reflections [83-87].

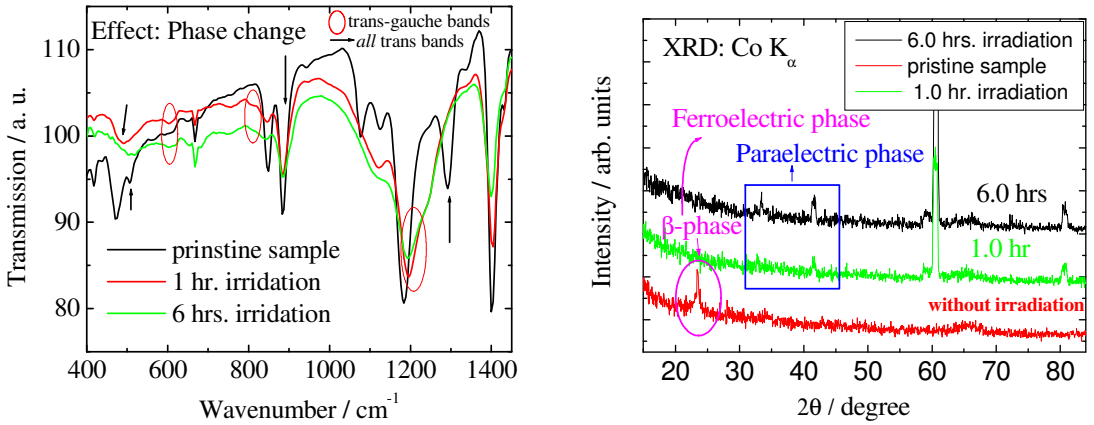

Figure 2.30. (A) *FTIR spectrum of 100 nm thickness of P(VDF-TrFE) thin film on Si-wafer, for showing the effect of X-ray irritation. (X-ray source: Mg* K_{α}*).* (B) *X-ray diffraction scans from the pristine, 1.0 hour and 6.0 hours X-ray irradiated P(VDF-TrFE) sample.*

In addition to the sharp peaks in the XRD pattern caused by crystalline phase, there is a broad peak with a much lower intensity that is caused by the amorphous phase in the films. Thus the XRD patterns for the pristine sample can be decomposed into one crystalline peak, which is from the polar β- phase, and the amorphous halo contribution. It is important to note that most of the reported XRD investigation for P(VDF-TrFE) copolymer films are measured by Cu K_{α} radiation of wavelength $\lambda = 1.5418$Å [84-88]. Therefore it is obvious that the diffraction peak position (2θ) are different in our present study but of course the inter planner distance (*d*) of the crystalline plane is comparable. For example, for the (110)/(200) reflection plane at peak position $2\theta = 23.4^{o}$, the *d* value is 4.41 Å for XRD with Co K_{α} wavelength (1.7902 Å), which is comparable with other reported values [83-88].

In contrast to the pristine sample, after 1.0 hour X-ray irradiation, the diffraction peak at 2θ = 23.4^o due to the ferroelectric polar β - phase is totally diminishes and some additional diffraction peaks (at 2θ = 33.4 and 41.6^o) arises. Furthermore, after 6.0 hours irradiation, this additional peaks intensity becomes more intense (see the figure 2.30 B). The peaks at 2θ = 33.4 and 41.6^o are the characteristic of the paraelectric α phase for the *d* value of 2.51 and 3.12 Å, respectively [84, 85]. The peak at 2θ = 33.4 corresponds to (130) reflection and the diffraction plane at 2θ = 33.4 is associated with strong unresolved (210)/(040)/(200) reflections.

Therefore, taking into infrared spectroscopy and XRD results, we can argue that there is a phase change occurs from ferroelectric to paraelectic, after 1.0 hour X-ray irradiation. These observations give us important information, i.e

- Idea about the X-ray irradiations effect on P(VDF-TrFE) copolymer films
- Optimization the X-ray irradiation time

We have seen from FTIR and XRD analysis, P(VDF-TrFE) copolymer films shows a phase change after 1.0 hrs X-ray irradiation. Therefore we have elucidated the effect which is observable in X-ray photo electron spectroscopy (XPS) study. It is important to note that the phase change observation is arduous to say by XPS observation. Since our goal is to study the undistorted P(VDF-TrFE) surface.

Figure 2.31 (a) and (b) shows the C1s and F1s peak of pristine P(VDF-TrFE) copolymer film (100 nm thickness). Since the peak has overlapping components, the curve has been deconvoluted into best-fitting Gaussian components which have been indicated in the figure. The fact that the C1s photoelectron peak from each type of carbon is so distinctly different in binding energy makes XPS an excellent tool for studying these materials [89-93]. Figure 2.31 (a) shows three major well-separated components and a small tail. The highest binding energy component (291.5 eV) is from the $-\underline{C}F_2-$ component and the other major lowest binding energy peak (287.0 eV) is from the $-\underline{C}H_2-$ species [89-91]. And in between these two major component, the C1s spectra shows a well resolved small component at 289.3 eV arises due to $-\underline{C}FH-$ species [89]. The low energy tail with this peak (285.5 eV) might be corresponds to the hydrocarbon contamination [89]. Furthermore the C1s spectrum (figure 2.31 a) consists of three partially resolved peaks at 291.5, 289.3, and 287.0 eV with area ratios 46: 17: 35, corresponding to the $-\underline{C}F_2-$, $-\underline{C}FH-$, and $-\underline{C}H_2-$ carbons, respectively. These peaks area ratio

value is quite consentient with theoretical calculated value for 70:30 mole % ratio mixtures VDF and TrFE copolymer (–$\underline{C}F_2$–, –$\underline{C}FH$–, and –$\underline{C}H_2$– ratio: 9:3:7).

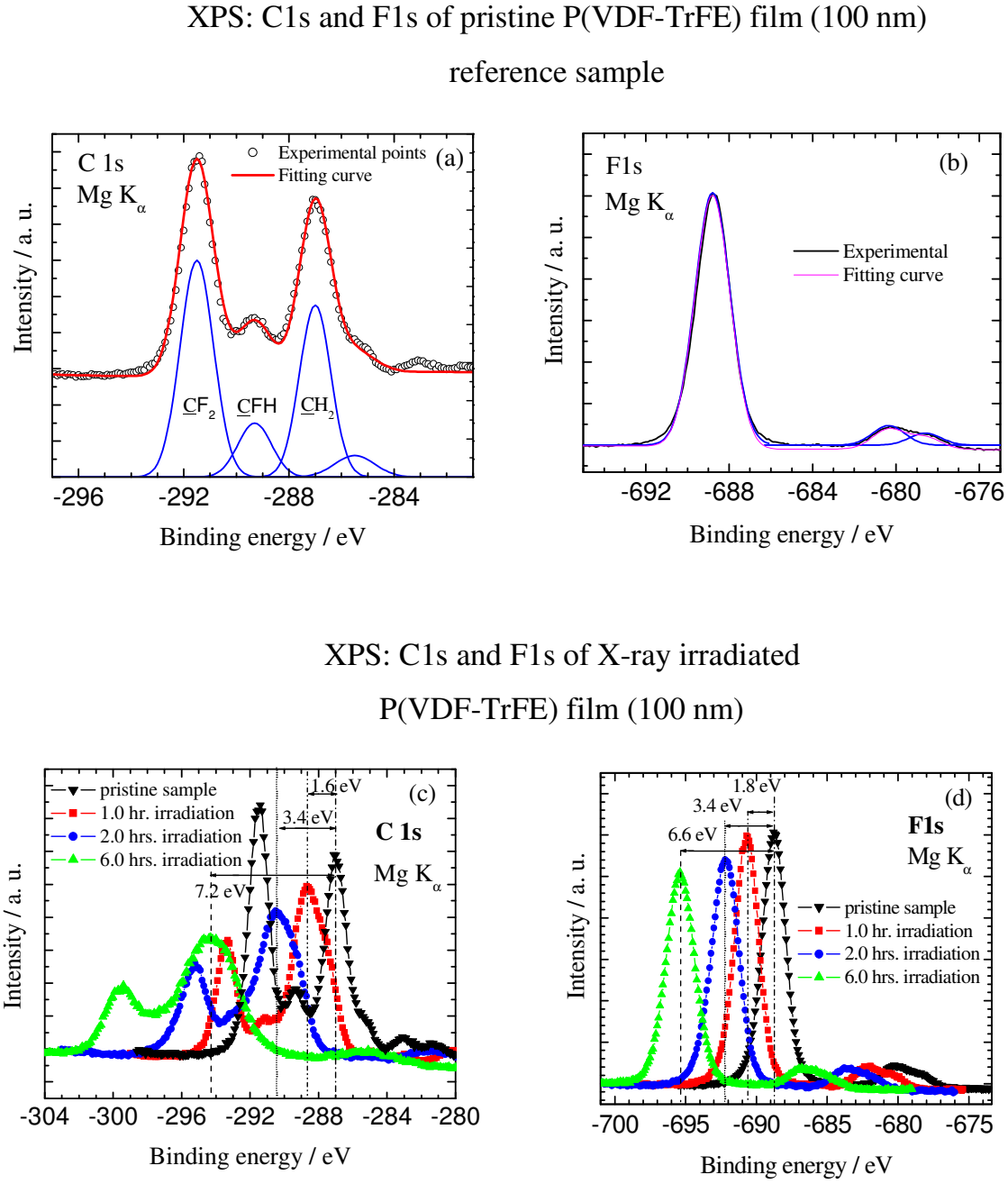

Figure 2.31. *XPS (a) C1s core level spectra of pristine sample of P(VDF-TRFE) film (cure fitting shown), (b) F1s core level spectra of pristine sample of P(VDF-TrFE) film(curve fitting shown) (c) C1s core level spectrum of X-ray irradiated samples for different duration; (d) F1s core level spectra spectrum of X-ray irradiated sample for different duration.*

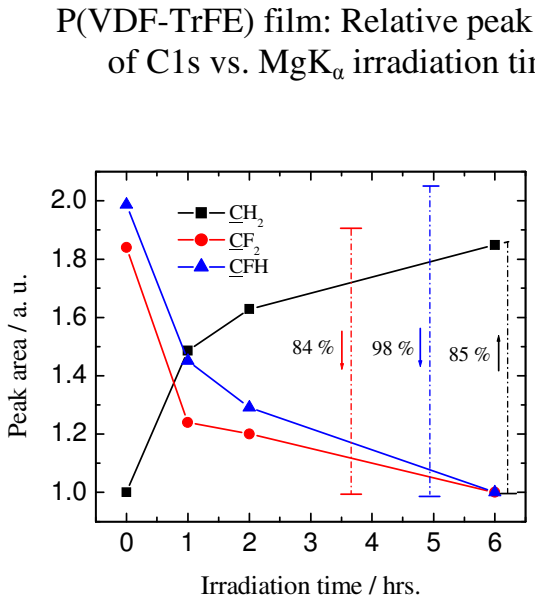

Figure 2.32. *The change of peak area (from figure 2.31c: C1s XPS result) due to different contributions of carbon component of P(VDF-TrFE) copolymer vs. X-ray irradiation time.*

In the figure 2.31 (b), the F1s core level XPS spectra is shown for pristine samples of P(VDF-TrFE) copolymer films. The F1s line at 688.8 eV has a line width of 1.9 eV. The peak position assignment is reproducible with reported results [89, 91, 92].

Figure 2.31 (c) and (d) illustrate the effect of X-ray irradiation represented by C1s and F1s core level spectrum respectively. A higher binding energy shift is observed with respect to increasing X-ray irradiation duration starting from 1.0 hour. From the theoretical calculation the peak area contribution of CF_2 and CH_2 of P(VDF-TrFE 70:30) copolymer should be 1.28 which is excellent agreement (1. 31) with our pristine film. In contrast the ratio of peak area from CF_2 and CH_2 is significantly changing after 1.0 hour irradiation (0.59) and after 6.0 hours irradiation it reduce to 0.38. Thus the change of peak area between CF_2 and CH_2 fall dramatically (about 93 %). This is one of the huge impacts by irradiation and it is benefited that XPS is very extensive tool for such quantities analysis. From figure 2.31 (d), we have seen that the change of line width of F1s line is not so significant with irradiation. On the other hand, we found from C1s spectra (see figure 2.32), there is significant change of three different existing carbon species ($-\underline{C}F_2-$, $-\underline{C}HF-$, $-\underline{C}H_2-$) with respect to irradiation, especially after 1.0 hour. With the irradiation duration, the $-\underline{C}H_2-$ species is increasing whereas $-\underline{C}HF-$ and $-\underline{C}F_2-$ is decreasing significantly which is shown in figure 2.32.

2.12. Experimental setup for external electric field

Our aim is to investigate ferroelectric dipoles orientation, especially for ultrathin (down to 10 nm thickness) spin coated P(VDF-TrFE) copolymer films.

The schematic for the application of external dc electric field is shown in figure 2.33. The electric field is locally imposed on the copolymer ultrathin film through two conducting tips as illustrate in aforesaid figure. The layer structure for the sample is schematic in figure 2.33, with different color. The top layer (pink color) is the copolymer spin coated film; the underneath layer, shown by blue color is a layer of PMMA (thickness ~700 nm) on the aluminum evaporated Si(100) wafer. The aluminum deposited Si wafer act as a bottom electrode for ultrathin copolymer films and we introduce PMMA layer to prevent leakage current during application of the electric field [94]. We used another aluminum coated Si wafer externally as a top electrode.

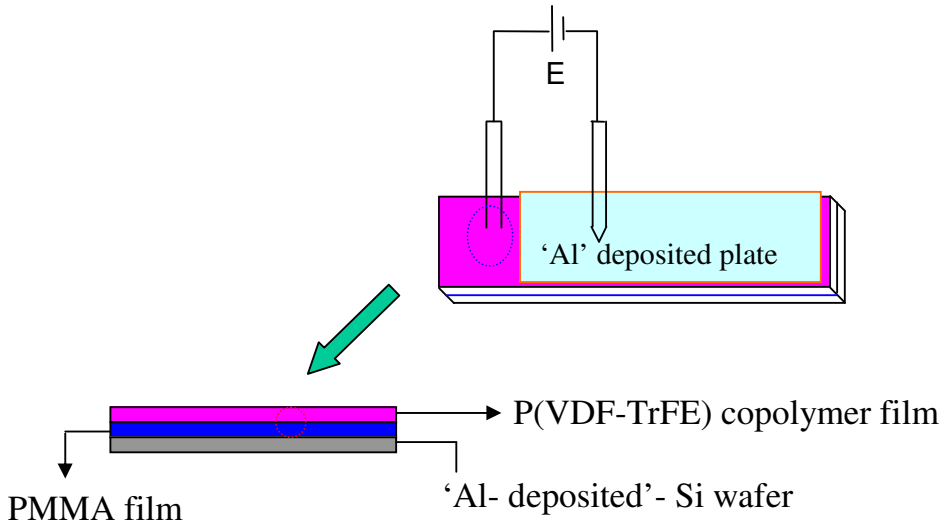

***Figure 2.33**. Schematic of the arrangement set-up for application of electric field in the ultrathin P(VDF-TrFE) copolymer film. Aluminum deposited Si-wafers are used as top and bottom electrodes. A non-conducting PMMA layer is used as buffer to prevent leakage current.*

References

1. V. P. Tolstoy, I. Chernyshova, and V. A. Skryshevsky, "Handbook of Infrared Spectroscopy of Ultrathin Films", *ISBN: 978-0-471-35404-8*.
2. R. J. Bell, "Introductory Fourier Transform Spectroscopy", *New York, Academic Press, 1972*.
3. R. M. Silverstein, G. C. Bassler, and T. C. Morrill, "Spectroscopic Identification of Organic Compounds", *4th Edition, New York, John Wiley & Sons, 1981*.
4. G. T. Davis, J. E. McKinney, M. G. Broadhurst, and S. C. Roth, "Electric-field-induced phase changes in poly(vinylidene fluoride)", *J. Appl. Phys. 49 (1978) 4998*.
5. K. Müller, D. Mandal, and D. Schmeißer, "XPS and NEXAFS of P(VDF-TrFE) films on different Substrates", *Thin Solid Films*, *communicated.*
6. Ed. H. S. Nalwa, "Handbook of Thin Film Materials", Academic *Press, 2002. ISBN 0-12-512911-4.*
7. Ed. Buddy Ratner and Vladimir V. Tsukruk, "Scanning Probe Microscopy of Polymers", American *Chemical Society: Washington, DC. 1998*.
8. D. Bonnel "Scanning Probe Microscopy and Spectroscopy: Theory, Techniques, and Applications", *2nd Ed., New York: Wiley, 2001*.
9. S. Morita, R. Wiesendanger, and E. Meyer, "Noncontact Atomic Force Microscopy", *Berlin, Springer, 2002*.
10. H. Hertz, "On an effect of ultraviolet light upon electric discharge", D. Sitzungsber, Berl. Akad. d. Wiss. *1877*.
11. P. D. Innes, "On the velocity of the Cathode Particle Emitted by Various Metals under the Influence of Rontgen Rays, and Its Bearing on the Theory of Atomic Disintegration", *Proc. R. Soc. A 79 (1907) 442.*
12. C. Nordling, E. Sokolowski, and K. Siegbahn, "Precision Methods for Obtaining Absolute values of Atomic Binding Energies", *Physical Review 105 (1957) 1676.*
13. E. Sokolowski, C. Nordling, and K. Siegbahn, "Chemical Shift Effect in Inner Electronic Levels of Cu Due to Oxidation", *Physical Review 110 (1958) 776.*
14. A. Fahlman, K. Hamrin, J. Hedman, R. Nordberg, C. Nordling, and K. Siegbahn, "Electron Spectroscopy and Chemical Binding", *Nature 210 (1966) 4.*
15. S. Hagstrom, C. Nordling, and K. Siegbahn, "Electron Spectroscopy for Chemical Analysis", *Phys. Lett. 9 (1964) 235.*

16. K. Siegbahn, "Philosophical Transactions of the Royal Society of London Series A-Mathematical and Physical Sciences", *268 (1970) 33*.
17. D. Briggs and M. P. Seah, Ed.,"Practical surface analysis", *Vol. 1, John Wiley & Sons Ltd.,1990*.
18. S. Hüfner, "Photoelectron spectroscopy: principles and applications", *2nd ed., Springer-Verlag, 1996*.
19. K. Siegbahn, C. Nordling, G. Johansson, J. Hedman, P. F. Heden, K. Hamrin, U.Gelius, T. Bergmark, L. O. Werme, R. Manne, and Y. Baer, "ESCA applied to free molecules", *North-Holland Publishing Company, 1969*.
20. Ed. J. Chastain, "Handbook of X-ray photoelectron spectroscopy", *Perkin-Elmer Corporation, 1992*.
21. D. A. Shirley, "Chemical Shift Effect in Inner Electronic Levels of Cu Due to Oxidation High-Resolution X-Ray Photoemission Spectrum of the Valence Bands of Gold", *Phys. Rev. B 5 (1972) 4709.*
22. S. Tougard, B. Jørgensen, Surf. Sci. 143 (1984) 482.
23. S. Tougard, "Formalism for quantitative surface analysis by electron spectroscopy", *J. Vac. Sci. Tech. A 8 (1990) 2197.*
24. J. Stöhr, "NEXAFS spectroscopy", *Springer Series in Surface Science. Springer Verlag, Berlin, Germany, 1992*.
25. M. O. Krause,"Atomic radiative and radiationless yields for K and L shells", *J. Phys. Chem. Ref. Data* 8 (1979) 307.
26. G. Appel, A. Y. Yfantis, W. Göpel, and D. Schmeißer, "Highly conductive polypyrrole films on non-conducting substrates", *Synth. Met. 67 (1996) 227*.
27. G. Appel, O. Böhme, and D. Schmeißer, "NEXAFS- Spectroscopy of differently doped polypyrroles", *BESSY annual report, 1997, ISSN 0179-4159*.
28. H. Naarmann, D. Schmeißer, A. Bartl, L. Dunsch, and W. Göpel, "Electronic and magnetic properties of polypyrrole films depending on their 1-dimensional and 2-dimensional microstructures", *Synthetic Metals 93 (1998) 43*.
29. R. P. Mikalo, P. Hoffmann, Th. Heller, and D. Schmeißer, "Lateral doping inhomogeneities as revealed by μ-NEXAFS and μ-PES", *Solid State Phenomena 63 (1998) 317.*
30. R.P. Mikalo, G. Appel, P. Hoffmann, and D. Schmeißer, "Determination of the vacuum level in NEXAFS-spectra by selected-yield-NEXAFS", *BESSY annual report, 1998*, *ISSN 0179-4159.*

31. G. Appel, O. Böhme, R.P. Mikalo, and D. Schmeißer, "The polaron and bipolaron contributions to the electronic structure of polypyrrole films", *Chem. Phys. Lett. 313 (1999) 411*.
32. E. Zschech, H. Stegmann, P. Hoffmann, D. Schmeißer, and P. Potapov, H.-J. Engelmann, D. Chumakov, H. Geisler, "Chemical Bonding, Permittivity and Elastic Properties in Locally Modified Organosilicate Glass", *MRS Proceedings 914 (2006) F11-03*.
33. O. Seifarth, R. Krenek, I. Tokarev, Y. Burkov, A. Sidorenko, S. Minko, M. Stamm, and D. Schmeißer, "Metallic Nickel nanorod arrays embedded into ordered block copolymer templates", *Thin Solid Films 515 (2007) 6552*.
34. F.A. Cotton, "Chemical Applications of Group Theory", *Wiley-Interscience, NY*, *USA, 2nd ed., 1971*.
35. J.N. Murrel, S.F. Kettle, and J.M. Tedder, "The Chemical Bond" *Wiley, Chichester UK, 2nd ed., 1985.*
36. D. A. Outka, J. Stöhr, R. J. Madix, H. H. Rotermund, and B. Hermsmeier, J. Solomon,"NEXAFS studies of complex alcohols and carboxylic acids on the Si(111)(7×7) surface", *Surf. Sci. 185 (1987) 53*.
37. Y. Wada and R. Hayakawa, "Piezoelectricity and Pyroelectricity of Polymers", *Jpn. J. Appl. Phys. 15 (1976) 2041*.
38. M. Tamura, S. Hagiwara, S. Matsumoto, and N. Ono, "Some aspects of piezoelectricity and pyroelectricity in uniaxially stretched poly(vinylidene fluoride)", *J. Appl. Phys. 48 (1977) 513*.
39. V. Schmidt, "Electron Spectroscopy of Atoms using synchrotron radition", *volume 6 of Cambridge monographs on atomic, molecular and chemical physics. Cambridge University Press, Cambridge, UK, 1997.*
40. C. Kittel, "Introduction to Solid State Physics", *Wiley, NY USA, 7th ed.,1996*.
41. D.R. Batchelor, R. Follath, and D. Schmeißer, "Commissioning results of the BTUC-PGM beamline", *Nucl. Instrum. Methods Phys. Res., Sect. A 470 (2001) 467.*
42. O. Seifarth, "Properties of Chromium, Cobalt and Nickel Nanoparticle embedded into ordered Block Copolymers and Conducting Polymers", *PhD thesis, BTU Cottbus, 1996*.
43. X. Weng, P. Rez, and O.F. Sankey, "Carbon K-shell near-edge structure: Multiple scattering and band-theory calculations", *Phys. Rev. B 40 (1989) 4175*.

44. R. A. Rosenberg, P. J. Love, and V. Rehn, "Polarization-dependent C(K) near-edge x-ray-absorption fine strcture of graphite", *Phys. Rev. B 33 (1986) 4034*.
45. D. Arvanitis, U Döbler, L. Wenzel, K. Baberschke, and J. Stöhr, "Position of the σ-shape and π resonances of C_2H_2, C_2H_4 and C_2H_6 on Cu(100) at 60 K: A NEXAFS study", *Surf. Sci. 178 (1986) 686.*
46. C. T. Chen, Y. Ma, and F. Sette, "K-Shell photoabsorption of the N_2 molecule", *Phys. Rev. A 40 (1989) 6737.*
47. D. A. Outka, J. Stöhr, R. J. Madix, H. H. Rotermund, B. Hermsmeier, and J. Solomon, "NEXAFS studies of complex alcohols and carboxylic acids on the Si(111)(7×7) surface", *Surf. Sci. 185 (1987) 53*.
48. W. Kern, "Handbook of Semiconductor Cleaning Technology", *Noyes Publishing, Park Ridge, NJ, 1993*.
49. W. W. Flack, D. S. Soong, A. T. Bell, and D. W. Hess, "A mathematical model for spin coating of polymer resists", *J. Appl. Phys. 56 (1984) 1199.*
50. S. A. Jenekhe, "Effects of solvent mass transfer on flow of polymer solutions on a flat rotating disk" *Ind. Eng. Chem. Fundam. 23, 425 (1984).*
51. X. Q. Chen, H. Yamada, T. Horiuchi, K. Matsushige, S. Watanabe, M. Kawai, and P. S. Weiss, "Surface potential of ferroelectric thin films investigated by scanning probe microscopy", *J. Vac. Sci. Technol. B 17 (1999) 1930.*
52. K. Kimura, K. Kobayashi, H. Yamada, T. Horiuchi, K. Ishida, and K. Matsushige, "Orientation control of ferroelectric polymer molecules using contact-mode AFM", *Eur. Poly. J. 40 (2004) 933.*
53. T. Fukuma, K. Kobayashi, T. Horiuchi, H. Yamada, and K. Matsushige, "Strcture and local electrical properties of ferroelectric polymer thin film in thermal process investigated by dynamic-mode atomic force microscopy", *Thin Solid films 397 (2001) 133*.
54. Polymer 17 (1994) 3612.
55. K. Tashiro, K. Takano, M. Kobayashi, Y. Chatani, and H. Tadokoro, Polymer 22 (1981) 1312.
56. K. Tashiro, K. Takano, M. Kobayashi, Y. Chatani, and H. Tadokoro, "Structural Study on Ferroelectric Phase Transition of Vinylidene Fluoride-Trifluoroethylene Copolymers (III) Dependence of Transitional Behavior on VDF Molar Content", *Ferroelectrics 57 (1984) 297.*

57. K. J. Kim, G. B. Gim, C. L. Vanlencia, and J. F. Rabolt, J. Polymer Sci. B: Polymer Phys. 32 (1994) 2435.
58. K. Tashiro, R. Tanaka, K. Ushitora, and M. Kobayashi, "Annealing effect ferroelectric phase transition behavior of vinylidene fluoride-trifluoroethylene copolymers: An interpretation based on the concept of domain and trans-gauche conformational disorder", *Ferroelectrics 171 (1995) 145*.
59. K. Tashiro and M. Kobayashi, "Structural phase transition in ferroelectric fluorine polymers: X-ray diffraction and infrared/Raman spectroscopic study", *Phase Transitions 18 (1989) 213*.
60. C. Y. Liang and S. Kirimm, "Infrared Spectra of High Polymers. III. Polytetrafluoroethylene and Polychlorotrifluoroethylene*", J. Chem. Phys. 25 (1956) 563*.
61. R. E. Moynihan, "The Molecular Structure of Perfluorocarbon Polymers. Infrared Studies on Polytetrafluoroethylene", *J. Am. Chem. Soc. 81 (1956) 1045*.
62. R. G. Brown, "Vibrational Spectra of Polytetrafluoroethylene: Effects of Temperature and Pressure", *J. Chem. Phys. 40 (1964) 2900*.
63. M. J. Hannon, F. J. Boerio, and J. L. Koenig, "Vibrational Analysis of Polytetrafluoroethylene", *J. Chem. Phys. 50 (1969) 2829*.
64. G. Masetti, F. Cabassi, G. Morelli, and G. Zerbi, "Conformational Order and Disorder in Poly(tetrafluoroethylene) from the Infrared Spectrum", *Macromolecules 6 (1973) 700*.
65. K. Tashiro and M. Kobayashi, "Vibrational spectroscopic study of the ferroelectric phase transition in vinylidene fluoride-trifluoroethylene copolymers: 1. Temperature dependence of the Raman spectra", *Polymer 29 (1988) 426*.
66. J. A. Day, E. L. V. Lewis, and G. R. Davis, "X-ray structural study of oriented vinylidene fluoride/trifluoroethylene copolymers", *Polymer 33 (1992) 1571*.
67. K. Tashiro, K. Takano, M. Kobayashi, Y. Chatani, and H. Tadokoro, "Structure and ferroelectric phase transition of vinylidene fluoride-trifluoroethylene copolymers: 2. VDF 55% copolymer", *Polymer 25 (1984) 195*.
68. G. T. Davis, T. Furukawa, A. J. Lovinger, and M. G. Broadhurst, "Structural and dielectric investigation on the nature of the transition in a copolymer of vinylidene fluoride and trifluoroethylene (52/48 mol %)", *Macromolecules 15 (1982) 329*.

69. K. Tashiro, Y. Itoh, M. Kobayashi, and H. Tadokoro, "Polarized Raman spectra and LO-TO splitting of poly(vinylidene fluoride) crystal form I", *Macromolecules 18 (1985) 2600*.
70. L. Lauchlan and J. F. Rabolt, "Polarized Raman measurements of structural anisotropy in uniaxially oriented poly(vinylidene fluoride) (form I)", *Macromolecules 19 (1986) 1049*.
71. M. Kobayashi, K. Tashiro, and H. Tadokoro, "Molecular Vibrations of Three Crystal Forms of Poly(vinylidene fluoride)", *Macromolecules 8 (1975) 158*.
72. J. S. Green, J. P. Rabe, and J. F. Rabolt, "Studies of chain conformation above the Curie point in a vinylidene fluoride/trifluoroethylene random copolymer", *Macromolecules 19 (1986) 1725*.
73. K. J. Kim and G. B. Kim, "Curie transition and piezoelectricity of the blends of a ferroelectric VDF/TrFE copolymer and PMMA", *J. Appl. Polym. Sci. 47 (1993) 1781*.
74. T. Kajiyama, N. Khuwattanasil, A. Takahara, "Electric field induced structural change for poly(vinylidene fluoride-co-trifluoroethylene) ultrathin films studied by scanning Maxwell stress microscope", *J. Vac. Sci. Technol. B 16 (1998) 121*.
75. K. Henkel, B. Seime, I. Paloumpa, K. Müller, and D. Schmeißer, "Buffer layer investigation of MFIS stacks for organic nonvolatile memory applications", *Thin Solid Films, submitted.*
76. T. Furukawa, "Ferroelectric Properties of Vinylidene Fluoride Copolymers", *Phase Transitions 18 (1989) 143*.
77. Q. M. Zhang, V. Bharti, and X. Zhao, "Giant Electrostriction and Relaxor Ferroelectric Behavior in Electron-Irradiated Poly(vinylidene fluoride-trifluoroethylene) Copolymer", *Science 280 (1998) 2101*.
78. F. Macchi, B. Daudin, and J. F. Legrand, "Electron Irradiation Induced Strctural Modifications in Ferroelectric P(VDF-TRFE) copolymers", *Nucl. Instr. And Meth. B 46 (1990) 324*.
79. V. Bharati, G. Shanthi, H. Xu, Q. M. Zhang, and K. Liang, "Evolution of transitional behavior and structural electron-riiadiated poly(vinylidene fluoride-trifluoethylene) copolymer films", *Mat. Lett. 47 (2001) 107*.
80. F. Macchi, B. Daudin, J. Hillairet, J. Lauzier, J. B. Ngoma, J. Y. Cavalla, and J. F. Legrand,"Micromechanical Properties of Electron Irradiated PVDF-TrFE Copolymers", *Nucl. Instr. And Meth. B 46 (1990) 334*.

81. B. Xu, C. N. Borca, S. Ducharme, A. V. Sorokin, P. A. Dowben, V. M. Fridkin, S. P. Palto, N. N. Petukhova, and S. G. Yudin, "Aluminium doping of poly(vinylidene fluoride with trifluoroethylene) copolymer", *J. Appl. Phys. 114 (2001) 1866*.
82. B. Xu, C. N. Borca, P. A. Dowben, A. V. Sorokin, S. P. Palto, N. N. Petukhova, and S. G. Yudin, "Comparison of aluminum and sodium doped poly(vinylidene fluoride-trifluoroethylene) copolymers by X-ray photoemission spectroscopy", *Appl. Phys. Lett.78(2001)488*.
83. A. V. Bune, V. M. Fridkin, S. Ducharme, L. M. Blinov, S. P. Palto, A. V. Sorokin, S. G. Yudin, and A. Zlatkin, "Two dimensional ferroelectricity", *Nature 391 (1998) 874*.
84. G. T. Davis, J. E. McKinney, M. G. Broadhurst, and S. C. Roth, "Electric-field-induced phase changes in poly(vinylidene fluoride), *J. Appl. Phys. 49 (1978) 4998*.
85. M. V. Fernandez, A. Suzuki, and A. Chiba, "Study of Annealing Effects on the Structure of Vinylidene Fluoride-Trifluoroethylene Copolymers using WAXS and SAXS", *Macromolecules 20 (1987) 1806*.
86. K. Koga and H. Ohigashi, "Piezoelectricity and related properties of vinylidene fluoride and trifluoroethylene copolymers", *J. Appl. Phys. 59 (1986) 2142*.
87. F. Fang, M. Z. Zhang, and J. F. Huang, "Deformation and Fracture Behaviour of poly(vinylidene fluoride-trifluorethylene) Ferroelectric Copolymer Films under Uniaxial Tension", *J. Poly. Sc. Part B: Poly. Phy. 43 (12005) 3255*.
88. A. J. Lovinger, G. T. Davis, T. Furukawa, and M. G. Broadhurst, "Crystalline Forms in a Copolymer of Vinylidene Fluoride and trifluorethylene (52/48 mol %)", *Macromolecules 15 (1982) 323*.
89. D. T. Clark, W. J. feast, D. Kilcast, and W. K. R. Musgrave, "Applications of ESCA to Polymer Chemistry. III. Structures and Bonding in Homopolymers of Ethylene and the Fluoroethylenes and Determination of the Compositions of Fluoro Copolymers", J. Polymer Sci.11 (1973) 389.
90. T. S. Chen and S. Mukhopadhyay, "Metallization of electronic polymers: A comparative study of polyvinylidene fluoride, polytetrafluoroethylene, and polyethylene", *J. Appl. Phys. 78 (1995) 5422*.
91. B. Xu, C. N. Borca, S. Ducharme, A. V. Sorokin, P. A. Dowben, V. M. Fridkin, S. P. Palto, N. N. Petukhova, and S. G. Yudin, "Aluminum doping of poly(vinylidene fluoride with trifluroethylene) copolymer", *J. Chem. Phys. 114 (2001) 1866*.

92. B. Xu, J. Choi, C. N. Borca, P. A. Dowben, and A. V. Sorokin, "Comparison of aluminum and sodium doped poly(vinylidene fluoride-trifluoroethylene) copolymers by X-ray photoemission spectroscopy*", Appl. Phys. Lett. 78 (2001) 448*.
93. D. T. Clark, D. Kilcast, W. J. Feast, and W. K. R. Mugsrave, *J. Polym. Sci. A 10 (1972) 1637*.
94. K. Müller, I. Paloumpa, K. Henkel, and D. Schmeisser, "A polymer high-K dielectric insulator for organic field-effect transistors", *J. Appl. Phys. 98 (2004) 056104*.

Chapter 3. Aluminum and PEDOT: PSS interaction with P(VDF-TrFE)

In this chapter, we focus on the properties of the ferroelectric copolymer P(VDF-TrFE) layer in the contest of scaling of layer thickness. We have to find out the reason for the threshold thickness for aluminum electrode, in contrast we also discuss the advantage of the organic electrode PEDOT:PSS.

3.1. Introduction

Copolymer films P(VDF-TrFE), used as a nonvolatile memory element has became a great deal of interest in research area, motivated by the aspect of industrial application [1-11]. Since the coercive field (E_c) of P(VDF-TrFE) copolymers is extremely large (over 40 MV/m for >200 nm thickness of the copolymer [3]), it is necessary to fabricate them into very thin films (below 100 nm) for low operation voltages. Based on the reported effects of thin film fabrication of P(VDF-TrFE) copolymers by Kimura and Ohigashi [17], many studies have focused on low operating voltage applications [4-16].

In this investigations, we concentrate on the properties of the ferroelectric copolymer P(VDF-TrFE) layer in the contest of scaling of layer thickness. A number of studies dealing with this issue followed [6, 17-22]. A study regarding the thickness scaling of P(VDF-TrFE) copolymer films reported an increase in both coercive field and switching time with decreasing layer thickness [17]. An overview of the remanent polarization (*Pr*) values verses ferroelectric layer thickness is shown in figure 3.1. It is also noted that the polarization also depends on the molar ratio of VDF and TrFE of the copolymer used [6].

In figure 3.1, the decline of curves 1-3 below 100 nm has been attributed to a reduction of crystallinity, ascertain by X-ray diffraction results [19, 20, 22]. As P(VDF-TrFE) films are semicrystalline and the ferroelectricity arises from the crystalline phase. Curves 3-5 indicate a downward shift of this apparent critical thickness from 100 to 70 nm. Using an annealing temperature lower than 140^{o}C showing less decline of the remanent polarization, e.g., 30% P_r decline at 40 nm instead of 50% at 60 nm [22]. This observation is explained by an improved crystallization due to a reduction of the crystal lamellar size. In contrast of these results, curves 6 and 7 showed even less decline, e.g., only 10% at 50 nm [18, 21].

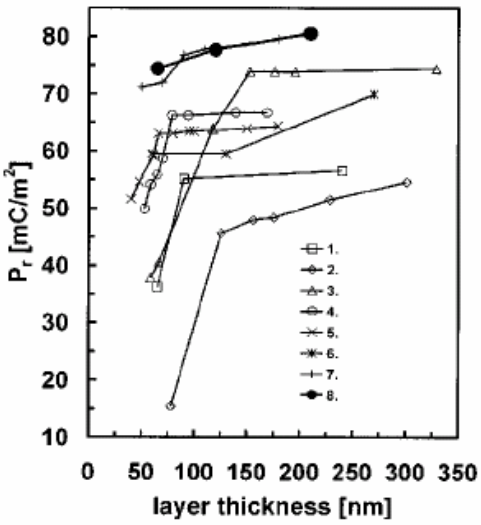

Figure 3.1. *Summary of the remanent polarization of spin coated P(VDF-TrFE) capacitors as a function of the ferroelectric layer thickness[6]. The lines indicate as a guide to the eye. [1. ref. 19; 2. ref. 20; 3. ref. 20 (140^{o}C); 4. ref. 20 (128^{o}C); 5. ref. 20 (120^{o}C); 6. ref. 21; 7. ref. 18; 8. ref. 6].*

The small decline is most likely due to different measurement procedure rather other parameters [6]. Curves 6 is obtained with unusually high fields exceeding 300 MV/m. Curve 7 is measured using common field strengths of about 100 MV/m but with field application times exceeding seconds. As the switching time depends exponentially on the applied field, these results are mutually consistent and suggested that it is mainly the switching time that is affected by the reducing layer thickness. It has been demonstrated by taking into consideration of retainment of the P_r in bulk material in sub-100-nm thin films and also the preservation of the switching time [6].

In figure 3.1, curve 1-7 are obtained on capacitors that had transition metal or aluminum bottom electrode [18-22].
By introducing a polymeric (PEDOT:PSS) bottom electrode it has been found that almost unaffected P_r, E_c and switching time (t_s) behavior down to lowest 65 nm P(VDF-TrFE) layer thickness [6]. This enables switching of 65 mC/m^2 with 5.2 V (80 MV/m) while the switching current peaks at 80 μs (the full switching event is completed within 400 μs) [18].

Since we need thinner (below 100 nm) films, it is an important question, what happen at the interface of the ferroelectric device. From literature it is well know from several works [6, 18-21] that we have threshold for the remanent polarization for films below 100 nm of thickness, if we use aluminum as electrode. Therefore, we have to find out the reason for the threshold

thickness for aluminum electrode, in contrast we also investigate the advantage the use of the organic electrode PEDOT:PSS.

3.2. XPS results

Figure 3.2 (A) shows the XPS spectrum around the C1s region of a 100 nm P(VDF-TrFE) copolymer sample. Here, we could identify three typical chemical states of peaks, at binding energies of 287.0 eV, 289.3 eV and 291.5 eV. In addition to three main peaks one low energy small window arises around 285.5 eV of binding energy, corresponds to the hydrocarbon contamination [23]. For an assignment of the peaks, we first must point out, that all peaks are chemical shifted to higher binding energies due to the presence of fluorine [23-25]. For the binding energies, we should have the following assignments, from lower to higher binding energies: The first peak at 287.0 eV has to be attributed to the (H-C-H) group, the peak at 289.3 eV should be the feature for the (H-C-F) group and the peak with highest binding energies at 291.5 eV has to be assigned to the (F-C-F) group.

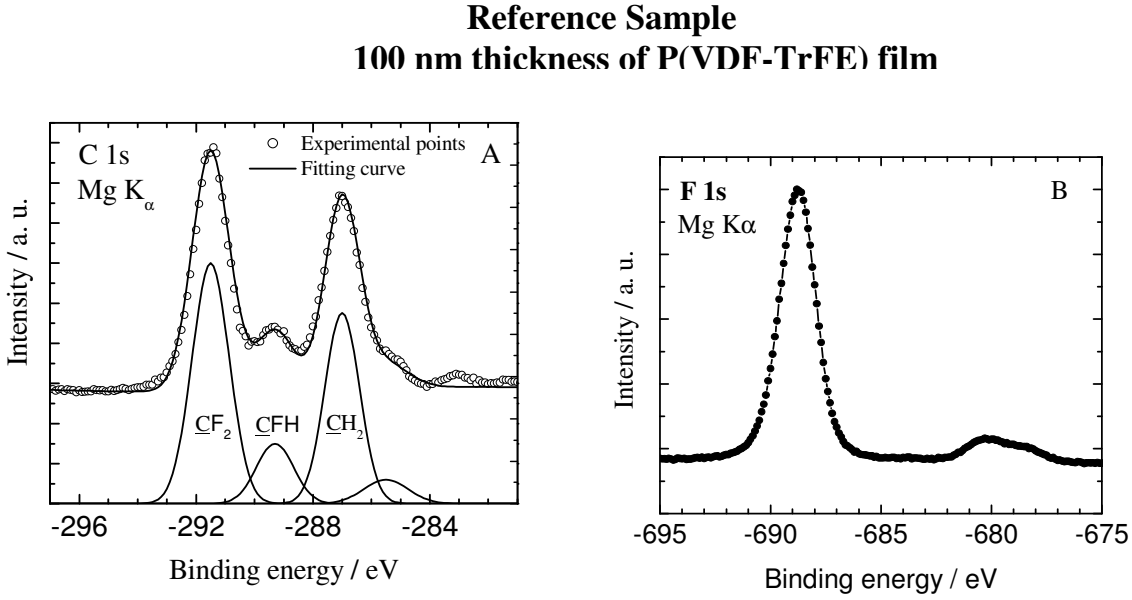

***Figure 3.2**. XPS C1s (A) and F1s (B) spectra of P(VDF-TrFE) copolymer film (100 nm film thickness). The C1s spectra has to be taken as reference to monitor changes induced by interaction with the electrodes (Al or PEDOT:PSS). A Gaussian fit of the three main peaks is also shown.*

The peak intensities reflects the copolymeric ratio of VDF:TrFE 70:30. Figure 3.2B shows the XPS spectrum around F1s region of the same sample. The F1s line at 688.8 eV has a line width of 1.9 eV. The peak assignment is quite consistent with previous reported results [24-26]. The individual peak assignment and quantitative analysis has been discussed in previous section of the thesis.

Top electrode Structure

Thermally evaporated Al on P(VDF-TrFE)

Now, we show the XPS spectrum of a P(VDF-TrFE) copolymer film after deposition of a thin layer (around 1nm) of thermal evaporated aluminum (figure 3.3A), as top-electrode. Compared to the spectrum of the pure P(VDF-TrFE) copolymer film (figure 3.2 A), we find the following modifications:

- The relative intensity between CH_2 and CF_2 peaks is modified towards lower fluorine content
- Small shift of CH_2 and CFH, and
- A new peak at lower binding energy (~285 eV).

This is a clear indication for a surface reaction.

Figure 3.3 (B) shows the XPS spectrum of the F1s region. With reference to the copolymer film without aluminum deposition, as shown, we reveal a slight asymmetry, indicating a surface reaction of the aluminum with fluorine.

The Al2p spectrum (figure 3.3 C) gives a confirmation for the formation of a thin AlF_3 layer [27]. The main peak arises of binding energy 72.5 eV, is characteristic of bulk aluminum 2p core level. Here, we have a second small peak with a very high binding energy of 76.8 eV. This is due to the presence of fluorine. An oxidized surface of aluminum would have binding energies of around 75.4 eV [28].

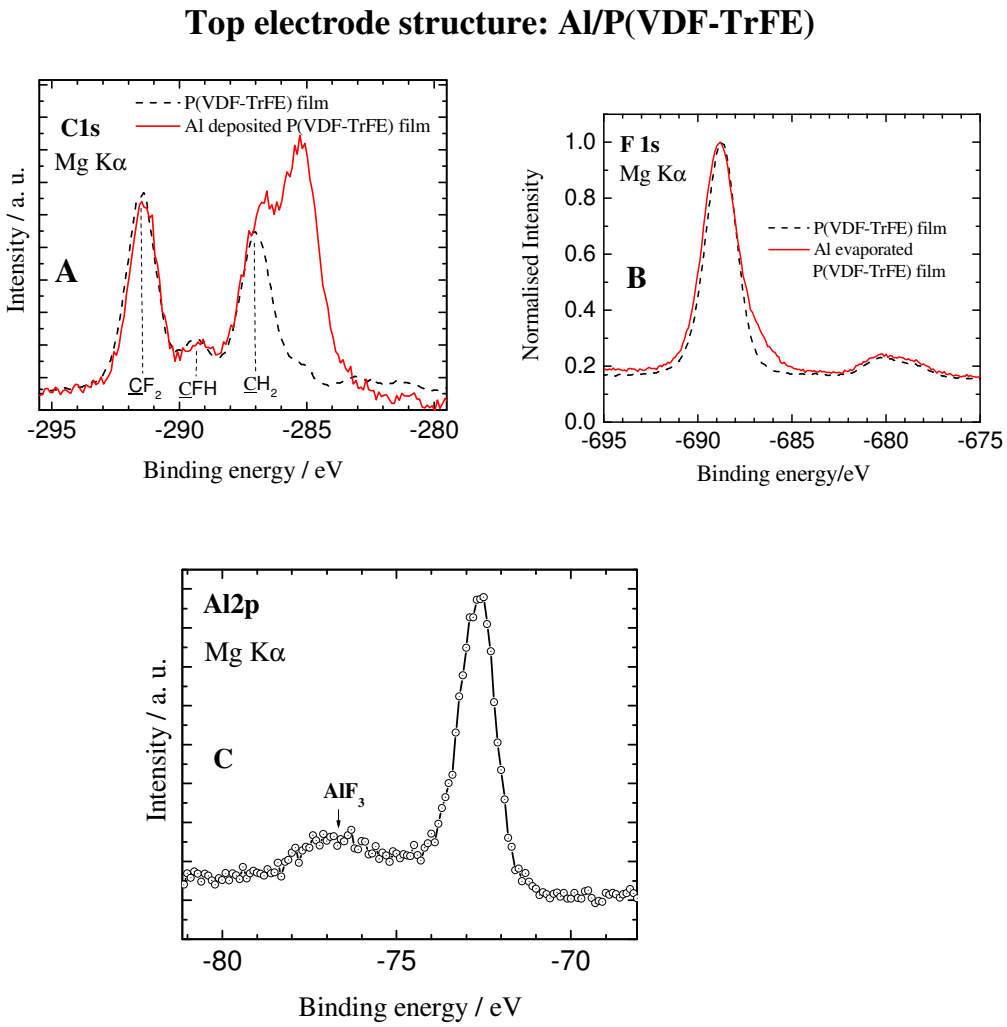

Figure 3.3. *(A) C1s XPS spectrum of a P(VDF-TrFE) film, after thermal evaporation of Aluminum (red solid line), compared to spectrum of the reference sample (black dashed line). The spectrum after deposition of Al is normalized with reference to the CF_2 peak of the pure copolymer film. (B) XPS spectrum of the F1s level after evaporation of Aluminum (red solid line), compared to spectrum of the pure copolymer film (black dotted line). The spectrum is normalized with reference to the F1s peak of the bulk film. (C) Al2p XPS spectrum of copolymer film, after evaporation of Aluminum.*

Bottom electrode Structure

P(VDF-TrFE) on thermally evaporated Al

The next question we address: is there any surface reaction in the reversed case of a bottom electrode of aluminum? Therefore, we measure two times: a set of samples with aluminum as bottom electrode, without any annealing, just after spin coating, then we anneal the samples at 135°C for 2 hours and measure again. The related XPS spectra for the C1s and the Al2p level are given in figure 3.4. Obvious is an additional peak for the C1s level, even for the sample without any annealing procedure. If we compare the C1s XPS results of these two geometries (namely, aluminum on top and at bottom), we find a similar behavior: the relative intensity between the CH_2 and CF_2 peak is modified and a new peak occurs at binding energies near the CH_2 feature. This means: when we talk about a surface reaction for an evaporated electrode, in top geometry, we have to talk about a surface reaction in the bottom electrode geometry, also. An interface layer is obviously built up even at room temperature. For elevated temperatures, as example the common annealing procedure (135°C, 2h), we have to expect an increased amount of this additional C1s feature. This is exactly the case: the relative intensity of the additional peak is increased after tempering (figure 3.4 A). The concentration for spin coating of this sample is 0.1 w% P(VDF-TrFE) in 2-butanone. For a set of samples with 0.3 and 0.5 w% P(VDF-TrFE), we find the same behavior, but the relative intensity of the additional C1s feature is lowered proportional to concentration, indicating a layered structuring. The F1s and the O1s levels are also analyzed for the same set of samples; here no relevant modification is visible, before and after annealing.

The Al2p spectrum is also shown (figure 3.4 B). Here, we found a formation of an oxidized layer, as revealed by a peak at a binding energy of 75.4 eV. This oxidation is takes place due to the experimental procedure: In this case after aluminum evaporation in *in-situ* environment, we have transfer the samples into our glove box for spin coating of P(VDF-TrFE) films. Hence the oxidation easily takes place in air with aluminum deposited layer.

In summary, for the bottom geometry structure, we have an obviously degenerated copolymer at the interface not only even at room temperature, but also, even though we have an oxidized surface of aluminum.

Bottom electrode structure: P(VDF-TrFE)/Al

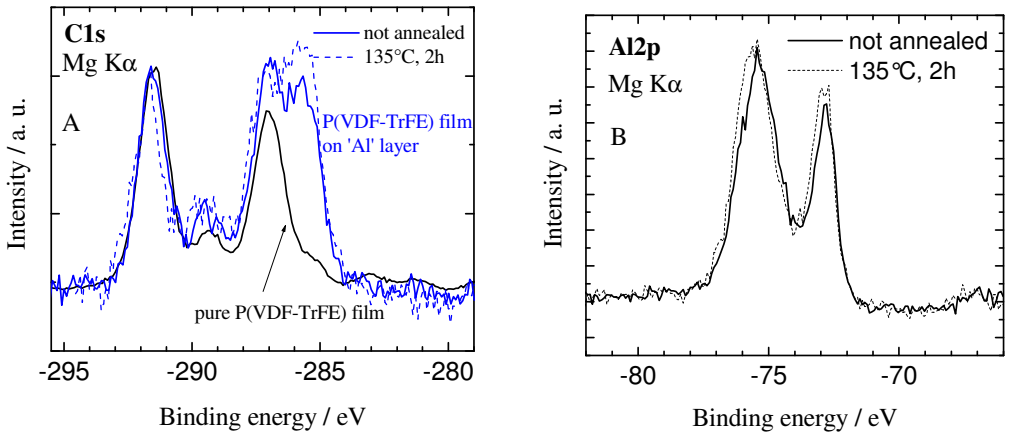

Figure 3.4. *(A) C1s XPS spectra of a P(VDF-TRFE) film, spin coated onto a Al/Si substrate (bottom electrode structure). Straight line: just after spin coating. Dashed line: after thermal annealing at 135°C, for 2 hours. The concentration for spin coating is 0.1 w% P(VDF-TrFE) in 2-butanone. Spectra are corrected for 0.4eV and normalized with reference to the bulk film, also shown; (B) Al2p XPS spectra of a P(VDF-TrFE) film, spin coated onto a Al/Si substrate (bottom electrode structure).*

P(VDF-TrFE)/PEDOT:PSS interface

Thin films of P(VDF-TrFE) are spin coated on PEDOT:PSS, as described in experimental section (chapter 2). In figure 3.5 (A), we show the C1s spectra of four samples with thin films of P(VDF-TrFE), spin coated in different concentrations in 2-butanone (0.x weight %), compared to a pure PEDOT:PSS spectrum (no.1). As revealed from figure 3.5 (A), no additional structure near the CH_2 feature occurs.

Like aluminum, a possible interface reaction should have an influence on the relative intensities, also (for example CF_2 and CH_2 of P(VDF-TrFE), here an analysis of peak attenuation is helpful. As we read out, also in Figure 3.5 (A), the intensity of the PEDOT:PSS (PEDOT, written for simplicity) -related signal at 284.8 eV is attenuated proportional to P(VDF-TrFE) concentration in the 2-butanone solution. The relative intensity of this PEDOT-signal is plotted in figure 3.5 (B). Here we extract a linear dependence and from that, we can conclude, that no interface reaction with a modification of intensities occurs. For a concentration of 0.6 w%,

the straight line intersects with the x-axis. In this case, the thickness of the P(VDF-TrFE) film is larger than the information depth of photoelectrons.

Therefore, If we use PEDOT:PSS as the electrode, we have found clearly no interface modification and an ideal sandwich layer. From the spectra of S2p, F1s and O1, this is also confirmed.

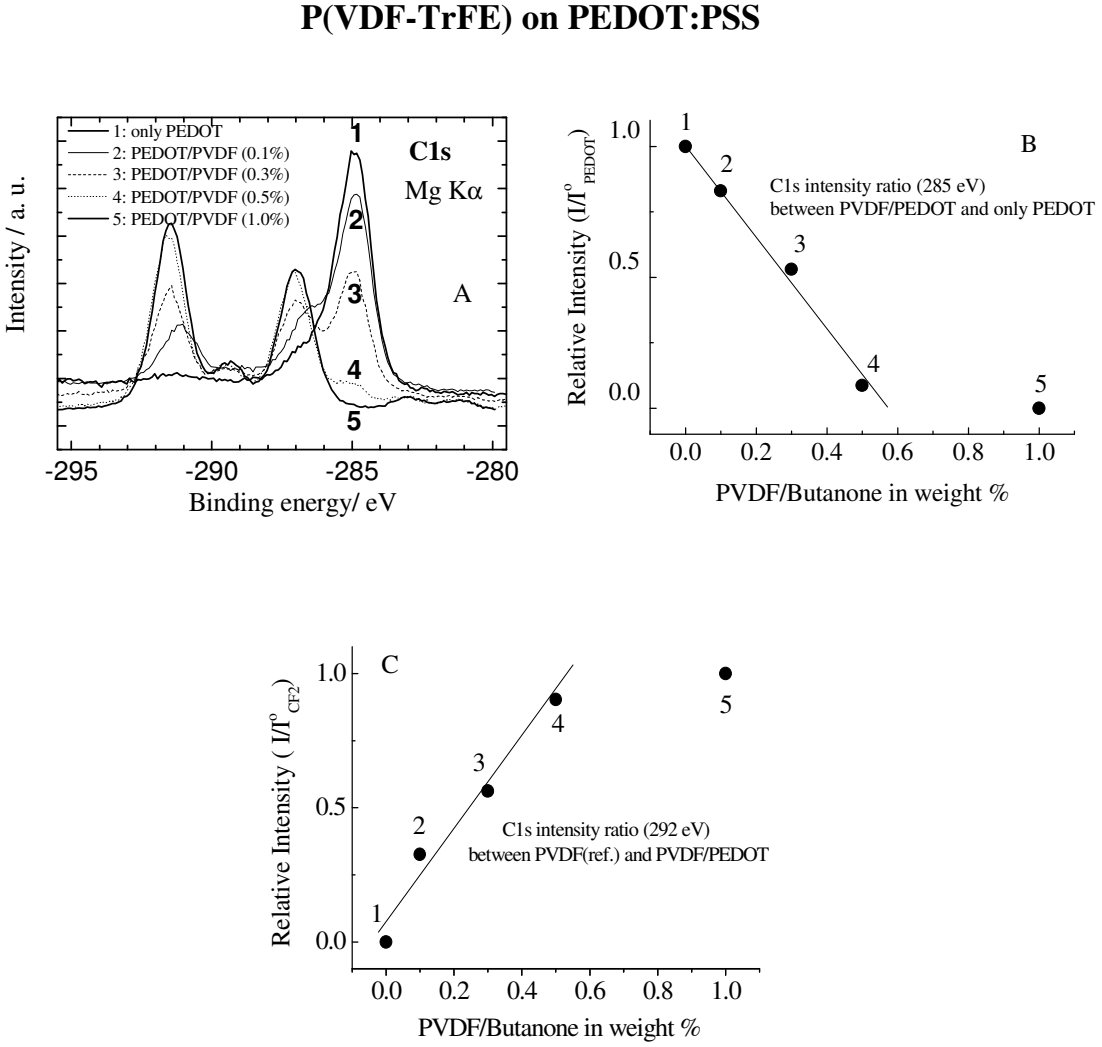

Figure 3.5. *(A) C1s spectra of samples with thin films of P(VDF/TrFE), spin coated in different concentrations in 2-Buthanone (0.x weight %); (B) Relative intensities of the PEDOT:PSS-attributed C1s feature, versus P(VDF-TrFE) concentration in 2-buthanone solution, as* I/I^{0}_{PEDOT}*. (C) Relative intensities of the* CF_2 *attributed for the P(VDF-TrFE) films versus P(VDF-TrFE) concentration in 2-butanone solution, as* $I/I^{0}_{(CF2)}$*. The line is only drawn as guide for the eyes.*

Layer thickness of P(VDF-TrFE)ultra thin films

From the XRS results, we tried to the determine of the overlayer thickness ($d_{P(VDF)}$) of P(VDF-TrFE) copolymer layer on PEDOT:PSS/Si substrates. We used a value of 1 nm as mean free path of photoelectron [30]. The over layer thickness of the P(VDF-TrFE) is expressed by,

$$d_{P(VDF)} = \lambda \ln\left[1 + \alpha \frac{I_{(CF)_2}}{I_{PEDOT}}\right]$$

Where $\alpha = \frac{I_0^{PEDOT}}{I_0^{(CF)_2}} \approx 1.9$, calculated by dividing spectrum number 5 by spectrum number 1 in figure 3.5 A. From the figure 3.5 B and C, we can substitute the rest of the two parameters I_{PEDOT} and $I_{(CF2)}$.

We receive the following values: 0.35 nm for 0.1 w%, 0.80 nm for 0.3 w% and 2.5 nm for 0.5 w%. Also the film thickness corresponds linearly to the P(VDF-TrFE) concentration in 2-butanone.

3.3. Discussions

As revealed by XPS measurements under radiation damage free conditions, we show a clear indication for a surface reaction of P(VDF-TrFE) with Al-electrodes, not only for evaporated Al, but also at room temperature, for the metal as bottom electrode. The new peak at lower binding energy (~285eV), the relative intensity between CH_2 and CF_2 peaks is modified towards lower fluorine content and small binding energy shift of CH_2 and CFH (see figure 3.3A) confirms that the surface reaction takes place of P(VDF-TrFE) with evaporated Al . Furthermore, if we look on Al2p spectra (see figure 3.3C), then we find the layer formation of AlF_3. In sharp contrast, for PEDOT:PSS, the XPS measurements indicates a layer by layer structure of PEDOT:PSS/P(VDF-TrFE) without any interface modification. This could be the reason for lower relaxation times, higher switching frequencies and in consequence, a better field dependence of the ferroelectric polarization, if we choose PEDOT:PSS as material for the electrode.

References

1. M. Date, T. Furukawa, T. Yamaguchi, A.Kojima, and I. Shibata, "Opto-ferroelectric memories using vinylidene fluoride and trifluoroethylene copolymers", *IEEE Trans. Electr. Insul. EI-24 (1989) 537.*
2. Q. Zhang, V. Barthi, and X. Zhao, "Giant Electrostriction and Relaxor Ferroelectric Behavior in Electron-Irradiated Poly(vinylidene fluoride-trifluoroethylene) Copolymer", *Science 280 (1998)2101*.
3. J. Glatz-Reichenbach, F. Epple, and K. Dransfeld, "The ferroelectric switching time in thin VDF-TrFR copolymer films", *Ferroelectrics 127 (1992) 13*.
4. T. J. Reece, S. Ducharme, A. V. Sorokin, and M. Poulsen, "Nonvolatile memory element based on a ferroelectric polymer Langmuir-Blodgett film", *Appl. Phys. Lett. 82 (2003) 142*.
5. K. Narayanana, Unni and R. de Bettignies, 'A nonvolatile memory element based on an organic field-effect transistor", *Appl. Phys. Lett. 85 (2004) 1823*.
6. R. C. G. Naber, P. W. M. Blom, A. W. Marsman, and D. M. De Leeuw, "Low voltage switching of a spin cast ferroelectric polymer", *Appl. Phys. Lett. 85 (2004) 2032*.
7. K. Müller, I. Paloumpa, K. Henkel, and D. Schmeisser, "A polymer high-k dielectric insulator for organic field-effect transistors", *J. Appl. Phys. 98 (2005) 056104*.
8. R. C. G. Naber, B. De Boer, P. W. M. Blom, and D. M. De Leeuw, "Low-voltage polymer field-effect transistors for nonvolatile memories", *Appl. Phys. Lett. 87 (2005) 203509*.
9. K. Müller, I. Paloumpa, K. Henkel, and D. Schmeiβer, "Organic thin film transistors with polymer high-k dielectric insulator", *Mat. Sci. Engg. C 26 (2006) 1028*.
10. R. C. G. Naber, P. W. M. Blom, G. H. Gelinck, A. W. Marsman, and D. M. De Leeuw, "An Organic field-Effect Transistor with Programmable Polarity", *Adv. Mater. 17 (2005) 2692*.
11. K. Müller, D. Mandal, and D. Schmeiβer, "No interfacial layer for PEDOT electrodes on PVDF: Characterization of reactions at the interface P(VDF/TrFE)/Al and P(VDF/TrFE)/PEDOT:PSS", *MRS Proc. 997 (2007) I6-02*.

12. R. C. G. Naber, M. Mulder, B. De Boer, P. W. M. Blom, and D. M. De Leeuw, "High charge density and mobility in poly(3-hexylthiophene) using a polarizable gate dielectric", *Organic Electronics 7 (2006) 132*.
13. K. Müller, K. Henkel, I. Paloumpa, and D. Schmeiβer, "Organic field effect transistors with ferroelectric hysteresis" , *Thin Solid Films 515 (2007) 7683*.
14. R.C.G. Naber, J. Massolt, M. Spijkman, K. Asadi, P.W.M. Blom, and D.M. de Leeuw, "Origin of the drain current bistability in polymer ferroelectric field-effect transistors", *Appl. Phys. Lett. 90 (2007) 113509.*
15. K. Müller, Y. Burkov, D. Mandal, K. Henkel, I. Paloumpa, A. Goryachko, and D. Schmeiβer, "Microscopic and spectroscopic characterization of interfaces and dielectric layers for OFET devices", *Phys. Stat. Sol. A 205 (2008) 600.*
16. T. T. Wang, J. M. Herbert, and A. M. Glass, "The Applications of Ferroelectrics Polymers", Blackie, Glasgow, 1988.
17. K. Kimura and H. Ohigashi "Polarization Behavior in Vinylidene Fluoride-Trifluoroethylene Copolymer Thin Films", *Jpn. J. Appl. Phys. 25 (1986) 383.*
18. Y. Tajitsu, "Effects of Thickness on Ferroelectricity in Vinylidene Fluoride and Trifluoroethylene Copolymers", *Jpn. J. Appl. Phys. 34 (1995) 5418.*
19. K. Urayama, M. Tsuji, and D. Neher, " Layer-Thinning Effects on Ferroelectricity and the Ferroelectric-to-Paraelectric Phase Transition of Vinylidene Fluoride-Trifluoroethylene Copolymer Layers", *Macromolecules 33 (2000) 8269.*
20. Q. M. Zhang, H. Xu, F. Fang, Z.-Y. Cheng, and Q. M. Zhang, "Critical thickness of crystallization and discontinuous change in ferroelectric behavior with thickness in ferroelexctric polymer thin films", *J. Appl. Phys. 89 (2001) 2613.*
21. T. Furukawa, S. Sakai, and Y. Takahashi, "Thickness Dependence of Ferroelectric Properties in Copolymers of Vinlidene Fluride and Trifluoroethylene", *Mater. Res. Soc. Symp. Proc. 698 (2002) EE 2.6.*
22. F. Xia, B. Razavi, H. Xu, Z.-Y. Cheng, and Q. M. Zhang, "Dependence of threshold thickness of crystallization and film morphology on film processing conditions in poly(vinylidene fluoride-trifluoroethylene) copolymer thin films", *J. Appl. Phys. 92 (2002) 3111.*
23. G. Beadmton and D. Briggs, "High resoluation XPS of Organic Polymers. The Scienta ESCA300 database", *Wiley, Chichester (1992).*
24. D. T. Clark, W. J. feast, D. Kilcast, and W. K. R. Musgrave, "Applications of ESCA to Polymer Chemistry. III. Structures and Bonding in Homopolymers of Ethylene and

the Fluoroethylenes and Determination of the Compositions of Fluoro Copolymers", *J. Polymer Sci. 11 (1973) 389.*

25. T. S. Chen and S. Mukhopadhyay, "Metallization of electronic polymers: A comparative study of polyvinylidene fluoride, polytetrafluoroethylene, and polyethylene", *J. Appl. Phys. 78 (1995) 5422.*
26. B. Xu, C. N. Borca, S. Ducharme, A. V. Sorokin, P. A. Dowben, V. M. Fridkin, S. P. Palto, N. N. Petukhova, and S. G. Yudin, "Aluminum doping of poly(vinylidene fluoride with trifluroethylene) copolymer", *J. Chem.. Phys. 114 (2001) 1866*.
27. G. E. McGuire, G. K. Schweitzer, and T. A. Carlson, "Study of Core Electron Binding Energies in Some Group IIIa, Vb, and VIb Compounds", *Inorg. Chem. 12 (1973) 2451*.
28. J. F. Moulder, W. F. Stickle, P. E. Sobol, and K. D. Bomben, "Handbook of X-ray Photoelectron Spectroscopy*", Perkin-Elmer Corporation ISBN:0-9627026-2-5 (1992).*
29. C. Wagner, W. Riggs, L. Davies, J. Moulder, G. Mullenberg (Editor), "Handbook of X-Ray Photoelectron Spectroscopy", *Perkin Elmer Corporation, Physical Electronics Division, Minnesota, 1978.*
30. C. Powal, "Attenuation lengths of low-energy electrons in solids", *Sur. Sci. 44 (1974) 29.*

Chapter 4. Summary of the electrical characterizations of the thin films

In this chapter, we will discuss about the electrical characterizations of the P(VDF-TrFE) copolymer thin films which are useful for the non-volatile memory applications.

4.1. Introduction

In terms of a low cost approach for electronics, based on organic devices, the introduction of organic non volatile memories is of great importance. P(VDF-TrFE) copolymer is the material with a very hopeful perspective, in this part we will give a summary on our electrical measurements with P(VDF-TrFE). By capacitance voltage measurements, we confirm the ferroelectric behavior of the polymer by measurements at elevated temperatures (Curie-Point), we found a threshold for remanent poalrization for films below 100 nm, if we use aluminum electrodes, but with inert electrodes, a downscaling of a low coercitive field was possible down to ten nm. This is very important, because due to the high coercitive field of the copolymer (> 50 MV/m), we need ultrathin films for low operation voltages. Prerequisite for memory applications is a high retention time, this was also confirmed, as described later in detail.

4.2. Results and discussion of electrical characterizations

For the measurements of the ferroelectric hysteresis of P(VDF-TrFE) copolymer via the flat-band shift, we used capacitors with oxidized p-type (doping concentration ~10^{15} cm^{-3}) silicon substrate (10-235 nm SiO_2) to prevent large amounts of leakage current. The copolymer film preparation procedure is described in thin film preparation section. We used films of thickness from 100 nm to 1µm. The structures are prepared in 'top electrode geometry', with thermal evaporated aluminum and for ultrathin films below 100 nm, we use Indium as contact electrode, patterned via a shadow mask (see figure 4.1).

The measurements of capacitance versus voltage (CV) are carried out with an Agilent 4284A LCR meter at a frequency of 1 MHz with a 25 mV (RMS value) test signal level while sweeping the DC bias with rates from 12.5 mV/s to 50 mV/s. The sample was hold in a sample holder under dark condition. Measurements are mostly performed at room temperature, at higher temperatures the sample holder is kept in a common drying oven.

All measurements were started in accumulation and finished there too, after driving the voltage in the investigated range to inversion and back (e. g. -10 V to 10 V and backwards to -10 V; we identify this '± '10 V loop'). Due to the polarization of the ferroelectric copolymer layer, the CV curves show a hysteresis loop [1, 2], which depends on the maximum voltage in the CV mode (see figure 4.2, right panel).

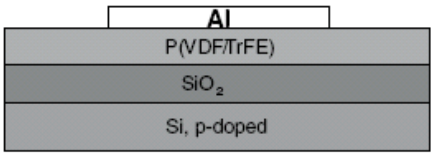

Figure 4.1. *The schematic of the top electrode geometry structure.*

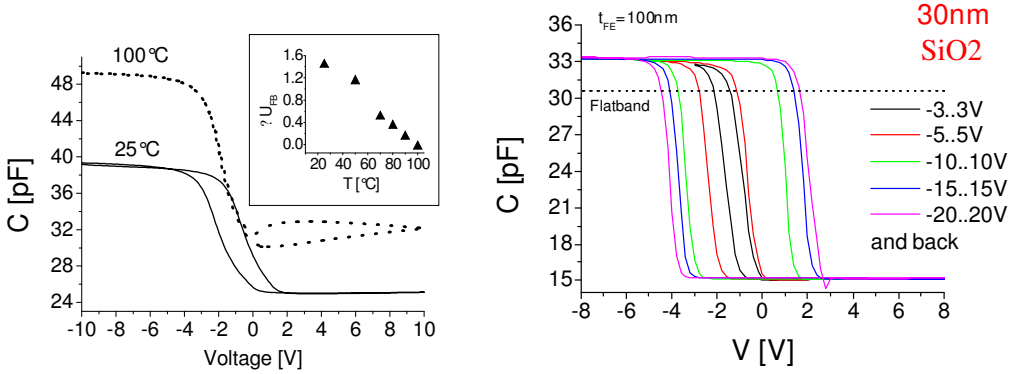

Figure 4.2. *Left panel: Capacitance-voltage characteristic of a 100 nm SiO_2/110 nm P(VDF-TrFE) sample at room temperature and at 100°C. The inset shows the flatband shifts dependent on temperature. Right panel: capacitance-voltage characteristic of 100 nm P(VDF-TrFE)/30 nm SiO_2/Si sample at room temperature. Different voltage (±3, ±5, ±10, ±15, ±20 V) loop are shown.*

In figure 4.2 (left panel), a typical CV characteristic of a Si/100 nm SiO_2/110 nm P(VDF-TrFE) capacitor is shown. The CV plot shows sections of the ± 10 V loop measurement at room temperature (RT) and at 100°C. The inset shows the flatband shift ΔV_{FB} (memory window) versus temperature. The calculation of ΔV_{FB} value is according to as described in the literature [3]. In the right panel of figure 4.2, CV characteristics of Si/30 nm SiO_2/100 nm P(VDF-TrFE) capacitor at different voltage loops are shown. We note in the RT line a clear hysteresis for the measurement loop. The hysteresis of the CV line indicates the presence of polarization charges and a ferroelectric behavior of the P(VDF-TrFE) copolymer, resulting in a shift of the CV line along the voltage axis (flatband voltage shift), as is known for fixed charges in the insulator for MIS devices [4]. The shift of the flatband voltage is a result of ferroelectric polarization of the copolymer. This is conformed by CV measurements at elevated temperature. The reported Curie temperature of P(VDF-TrFE) is in the region of 100°C [5]. Figure 4.2 also summarized these investigations. We note the disappearance of the hysteresis at 100°C. Furthermore, in the CV data we find an increased permittivity value at 100°C by 80%, signified by a higher capacitance in accumulation (see figure 4.2, left panel). This is in agreement with observation in literature, the permittivity is increasing up to the Curie point [4, 6].

We calculate a permittivity value of P(VDF-TrFE) of 6.7 ± 0.9 at room temperature and at a frequency of 1 MHz, which is in the same range as in other works [7, 8]. This value is used for a calculation of the charge density, which is proportional to the ferroelectric polarization. The flatband voltage shift (ΔV_{FB}) is also needed to calculate this 'fixed' charge (N_{fix}) using

$$N_{fix} = \frac{\Delta V_{FB} \varepsilon_0 \varepsilon_{PVDF}}{q t_{PVDF}}$$

Where ε_0 is the permittivity of vacuum, ε_{PVDF} is the relative permittivity value for P(VDF-TrFE), t_{PVDF} is the thickness of P(VDF-TrFE) and q is the elementary charge.

We also study the flatband shift, e.g. the polarization, as a function of copolymer film thickness. For the measurements, a relatively thick SiO_2 buffer layer of 235 nm was used and the result revel a clear thickness dependence of the ferroelectric polarization. We calculated

ΔE_{PVDF} as the voltage drop only over the P(VDF-TrFE) layer. For accumulation, negative voltages, the voltage is divided into two parts: $U_1 = U_{1PVDF} + U_{1SiO_2}$. For depletion, we have to calculate an additional voltage drop over the depletion layer, according to $U_2 = U_{2PVDF} + U_{2Sio_2} + U_{2D}$. The field, applied only at the P(VDF-TrFE) layer, is calculated as filed amplitude $(U_{2PVDF} - U_{1PVDF})/t_{PVDF} = \Delta E_{PVDF}$, with a layer thickness t_{PVDF}.

Figure 4.3(a) shows the calculated N_{fix} values versus the total field amplitude ΔE_{PVDF}. We find an almost linear dependence of the 'fixed' charges versus the electric field strength applied. For the remanent polarization, which is proportional to the amount of the 'fixed' charges, saturation at relatively high field strength is to be expected. For our samples, even at high applied fields, no saturation occurs. However, we should refer to the fact that here the sum of the electric field in both branches of the polarization loop is shown, so it might be plausible that the field is not yet hight enough for saturation. Indeed, it is found that by reducing buffer layer thickness (see figure 4.3b) or using high-*k* material the saturation occurs [7].

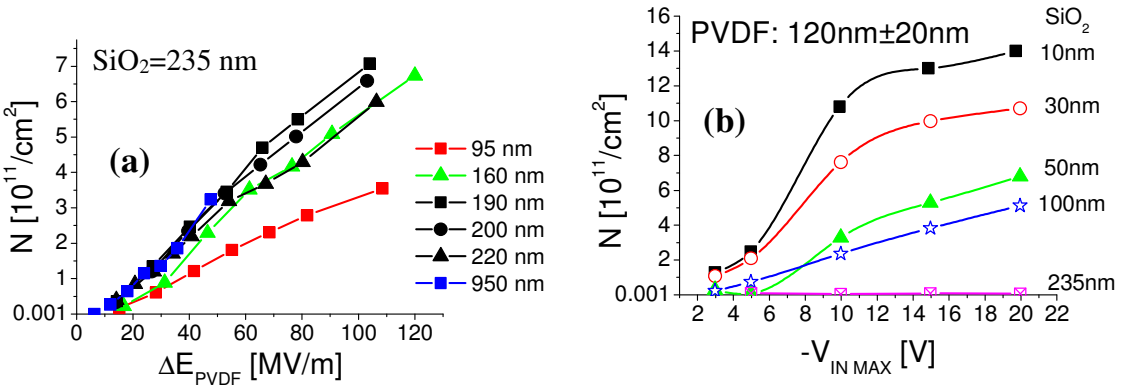

Figure 4.3. *(a) Calculated 'fixed' charges versus the electric field change of the ferroelectric layer inside one CV loop for SiO_2/P(VDF-TrFE) stacks with different thickness of the ferroelectric layer. Thickness of the buffer layer is 235 nm and thickness of the P(VDF-TrFE) is as indicated. (b) Calculated 'fixed' charges versus input voltage of the CV curve for SiO_2/P(VDF-TrFE) stacks with different thickness of the buffer layer where ferroelectric layer is 120 nm.*

Retention investigations are performed using capacitance-time measurements at a fixed bias voltage after applying a programming pulses. For the definition of the fixed bias value, a ±5V capacitance-voltage loop is performed before. The result of this measurement is plotted in figure 4a. It shows, that after applying of a negative voltage pulse the CV curve is moving to right along the voltage-axis, while after applying of a positive pulse the CV curve moves to left.

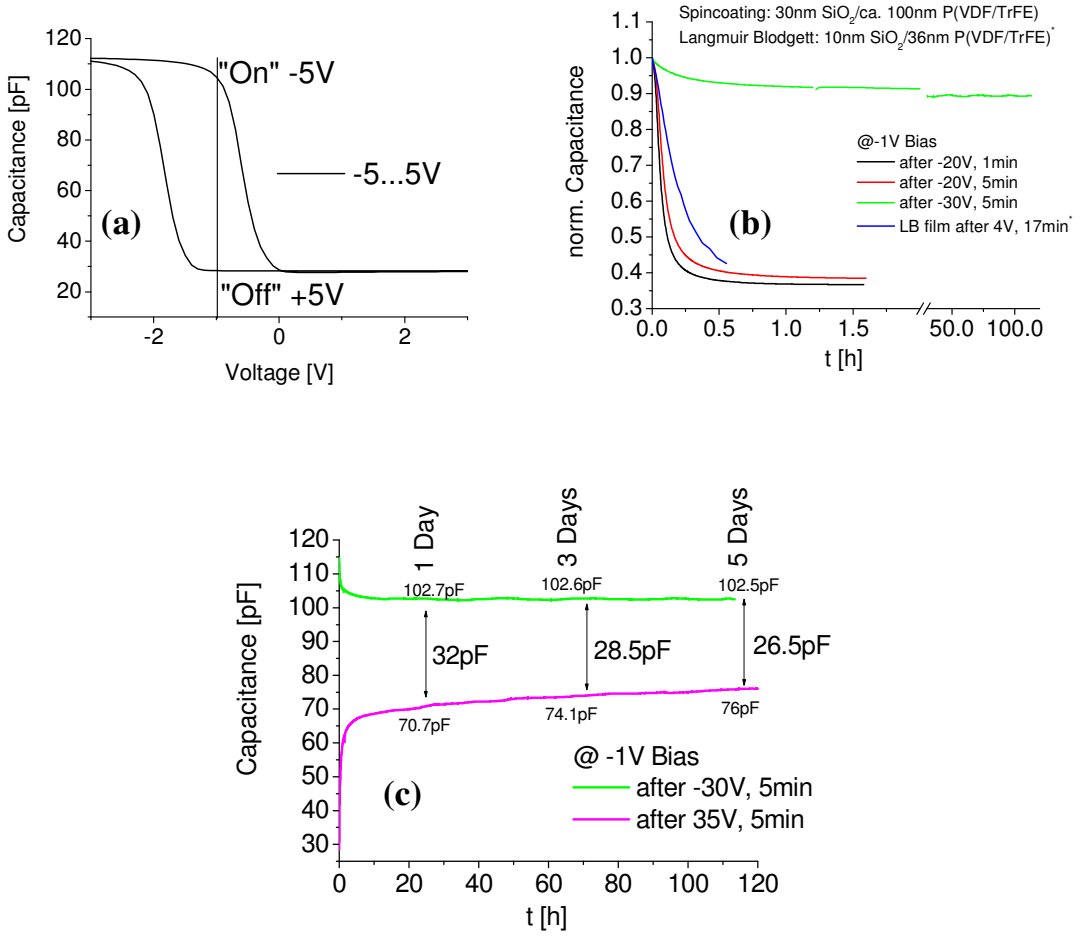

Figure 4.4. *(a) capacitance-voltage characteristic of a 30 nm SiO_2/100 nm P(VDF-TrFE) sample for a voltage loop of ± 5 Volt, (b) data retention measurement obtained after applying different negative programming pulses as mentioned in the legend, comparison to a value taken from literature [11] data retention after applying either a negative or a positive programming pulse, (c)retention of the high capacitance state and low capacitance state.*

Thus, at a voltage of –1 V two different states of the capacitance can be distinguished, which can be defined as high capacitance state (HCT) or low capacitance state (LTC) or in terms of a memory as "1" and "0" or "On" and "Off". Therefore further capacitance-time measurements are performed at this fixed bias voltage value. Figure 4.4(b) summarizes measurements after applying negative pulses of different height and duration. A comparison to a LB film taken from literature [11] is shown too (blue curve). After applying –30 V for 5 minutes a sufficient retention of the HCT is found (green curve). This state is found to be stable up to the investigated time of 18 days. In figure 4.4 c the retention of both the HCT and the LCT is reported. In the very beginning of the measurement both states are changing there value quickly, but after approximately 5 hours the difference between the two states is much more stable, but still decreasing. Here especially the LCT is increasing its value. This might be supported by the applied fixed value of the bias of negative sign which is opposite of that of the necessary programming pulse of this state.

We also recognize a significant reduction of polarization for the P(VDF-TrFE) thickness below 100 nm, while between 200 nm and 950 nm the dependence is very similar. Generally it has been postulate that the corrective filed increases with decreasing of its thickness [9]. It must be pointed out here that a critical thickness is found for electrodes made of aluminium, not for polymer electrode PEDOT:PSS [10]. We have already shown in the chapter 3, the reactive interactions occurs between P(VDF-TrFE) and aluminium, not for P(VDF-TrFE)/PEDOT:PSS interface. This become even more important when the thickness of P(VDF-TrFE) film is further down-scaled.

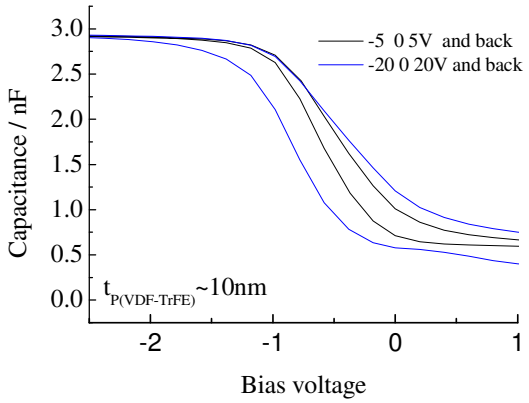

Figure 4.5. *CV measurements of a 10 nm thick P(VDF-TrFE) film on a Si/SiO2(30nm) substrate, indium is used as top electrode.*

All electrical characterizations described here are the important steps for making non volatile memory devices based on the P(VDF-TrFE) copolymer.

References

1. S. L. Miller and P. J. McWhorter, "Physics of the ferroelectric nonvolatile memory field effect transistor", *J. Appl. Phys. 72 (1992) 5999*.
2. K. Müller, I. Paloumpa, K. Henkel, and D. Schmeiβer, "Organic thin film transistors with polymer high-k dielectric insulator", *Mater. Sci. Eng. C 26 (2006) 1028*.
3. K. Müller, K. Henkel, I. Paloumpa, and D. Schmeiβer, "Organic field effect transistors with ferroelectric hysteresis", *Thin Solid Films 515 (2007) 7683*.
4. E. H. Nicollian and J. R. Brews, "MOS Physics and Technology", *Wiley, New York, 1982*.
5. T. Furukawa, "Ferroelectric Properties of Vinylidene Fluoride Copolymers", *Phase Transit. 18 (1989) 143*.
6. Y. Tajitsu, "Effects of thickness of ferroelectricity in vinylidene fluoride and trifluoroethylene copolymers", *Jpn. J. Appl. Phys. 34 (1995) 5418*.
7. K. Henkel, B. Seime, I. Paloumpa, K. Müller, D. Schmeißer, "Buffer layer investigation of MFIS stacks for organic nonvolatile memory applications", *Thin Solid Films, submitted.*
8. K. Kimura and H. Ohigashi, Generation of very high-frequency ultrasonic waves using thin films of vinylidene fluoride-trifluoroethylene copolymer, J. Appl. Phys. 61 (1987) 4749.
9. M. Dwber, P. Chandra, P. B. Littlewood, and J. F. Scott, "Depolarization corrections to the coercive field in thin-film ferroelectrics", *J. Phys.: Condens. Matter 15 (2003) L 393*.
10. R. Naber, P. Bolm, A, Marsman, and D. de Leeuw, "Low voltage switching of a spin cast ferroelectric polymer", *Appl. Phys. Lett. 85 (2004) 2032*.
11. A. Gerber, H. Kohlstedt, M. Fitsilis, R. Waser, T. J. Reece, S. Ducharmeb, E. Rije, "Low-voltage operation of metal-ferroelectric-insulator-semiconductor diodes incorporating a ferroelectric polyvinylidene fluoride copolymer Langmuir-Blodgett film", *J. Appl. Phys. 100 (2006) 024110*.

Chapter 5. Orientation of the ferroelectric dipoles

In this chapter we will discuss the dipole orientation effect by the help of polarization dependent tool Near Edge X-ray Absorption Fine Structure (NEXAFS) Spectroscopy.

1st we focus on the decovoulation of the NEXAFS spectra and peak assignment for different resonances. Then we discuss the possible dipole orientation of different thickness of the P(VDF-TrFE) films on different substrates, namely Si (100) and PEDOT:PSS/Si(100).

Finally, we discuss the effect of the electric field on P(VDF-TrFE) films revel from NEXAFS spectrum. Furthermore we have calculated the polarization charge for different thickness (down to 10 nm) of P(VDF-TrFE) films.

5.1. Introduction

The most promising property of P(VDF-TrFE) copolymer its ferroelectricity, which is eventually useful for the application as non-volatile memory element [1]. The evidence of the ferrolectricity arises due the presence of the component of trifluoroethylene (TrFE) with PVDF [2], which do exhibits a clear ferroelectric-paraelectric phase transition. The P(VDF-TrFE) crystallize into various crystal forms depending on their molar content rations of VDF (x) and TrFE (1-x), and on crystallization conditions [3-5]. Under ordinary pressure, the α crystal form consisting of *TGTG* chains is stable for the VDF homopolymer (PVDF), while the β phase crystal consisting of *all-trans* chains becomes more stable on introducing TrFE sequences into VDF chains [6]. The β phase crystal is well known to be ferroelectric from its D-E hysteresis loops [7, 8], polarization switching [9], temperature behavior of the dielectric constant [7, 10, 11], and anomalous X-ray dispersion [12]. Addition of the larger and less molar ratio of TrFE ruined the transition temperature by reducing the average dipole moment of the chains, expanding the lattice, and introducing defects.

As stated earlier, we choose the composition of 70% VDF and 30 % TrFE molar ratio, because it has the most distinct ferroelectric properties and can be made mostly crystalline without stretching treatments.
In this investigation we concentrate on the dipole orientation effect by the help of polarization dependent tool Near Edge X-ray Absorption Fine Structure (NEXAFS) Spectroscopy.

- 1st we focus on the decovoulation of the NEXAFS spectra and peak assignment for different resonances.
- Then we discuss the possible dipole orientation of different thickness of the P(VDF-TrFE) films on different substrates, namely Si (100) and PEDOT:PSS/Si(100).
- Finally, we discuss the effect of the electric field on P(VDF-TrFE) films revel from NEXAFS spectrum. Furthermore we have calculated the polarization charge for different thickness (150 nm to 10 nm) of P(VDF-TrFE) films.

5.2. Peak assignment of NEXAFS spectra

We have employed polarized Near edge X-ray absorption fine structure (NEXAFS) spectroscopy to explore the molecular structure and the dipole orientation of P(VDF-TrFE) copolymer spin coated films in different environments, such as different substrate effects, thickness dependence, applied electric field dependence. The preparation of thin films and theoretical aspects of NEXAFS spectroscopy has been discussed in chapter 2 of the thesis.

In the part of "NEXAFS spectroscopy" (in chapter 2), we have presented spectra those appraised near the Carbon *K*-edge and Fluorine *K*-edge to show the necessity of the grandness of the analysis. First of all, it is worthful to discuss the assignment of different peaks due the molecular transitions. Furthermore, the deconvolution by peak fitting also plays a significant role for the analysis. The assignment of the spectral structure of NEXAFS for large and complex molecules, the building block approach is very useful and has been widely used [13]. For ordered films of the organic molecules, the polarization dependence of NEXAFS spectra provides the symmetry of the π^* and σ^* unoccupied states. It is important to note that for our peak assignment, fluorine containing materials such as poly(terafluoroethylene) (PTFE), poly(vinylidene fluoride) (PVDF), perflurinated oligo(p-phenylene) (PF8P), fluorine-thiophene copolymer, and fluorinated comb polymers are investigated as a reference [15-23].

Figure 5.1, shows the deconvolution of a C *K*-edge NEXAFS spectrum in the photon energy range from 275 eV to 325 eV for a 100 nm thickness of P(VDF-TrFE) copolymer spin coated film on a Si(100) wafer. From the deconvolution of the curve, we can isolate the transition from C1s to different unoccupied molecular levels. The transition bands from the C1s level are assigned as listed in the bottom table in figure 5.1. The lower energy peak arises at 287.2 and 289 eV were assigned to transitions from the C1s to the σ^*(C-H) unoccupied level [13, 14]. The peaks at 292.6 and 294 eV can be assigned to the transitions from C1s to the σ^*(C-F) and σ^*(C-C) orbital respectively [12-24]. The rest of the peaks are only identifiable after the curve fitting procedure (see. figure. 5.1). Here we do not observed the sharp π^* resonance (around 285.1 eV), as the P(VDF-TrFE) copolymer does not contain unsaturated C-C bonds. From the spectra we can also learn that we don't have beam damage for our copolymer thin film, as mentioned that the absence of π^* resonance peak. In the figure 5.1, the σ^*(C-C) resonances are fitted by a Lorentzian profile. The rest of the peaks are fitted with asymmetric Gaussian, because of the increase in width of resonances with increasing energy. This can be simply attributed to lifetime broadening. That is, the higher the energy of the final state, the

shorter its lifetime and hence the broader the peaks [25, 26]. In addition to peaks, NEXAFS contain one or sometime more step-like features referred as continuum steps. These steps are the results of the excitation of the core electron to a continuum or quasi-continuum of final states, e.g. to the smooth density of states [13].

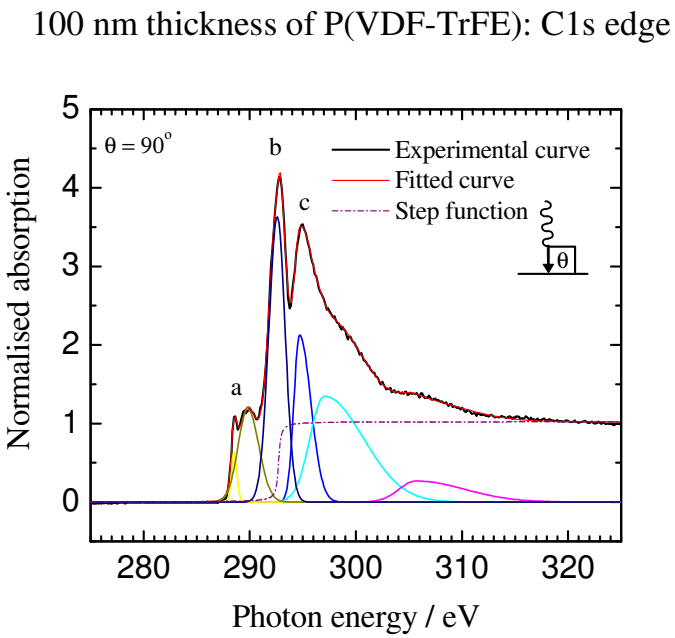

Peaks	**Photon energy**	**Transition level from C1s**
a	287.2 & 289 eV	σ^*(C-H)
b	292.6 eV	σ^*(C-F)
c	294 eV	σ^*(C-C)

Figure. 5.1. *Deconvolution of the C K-edge total electron yield NEXAFS spectra for the 2.5 % P(VDF-TrFE) copolymer film (thickness ~ 100 nm) on Si(100) and their peak assignments in the bottom.*

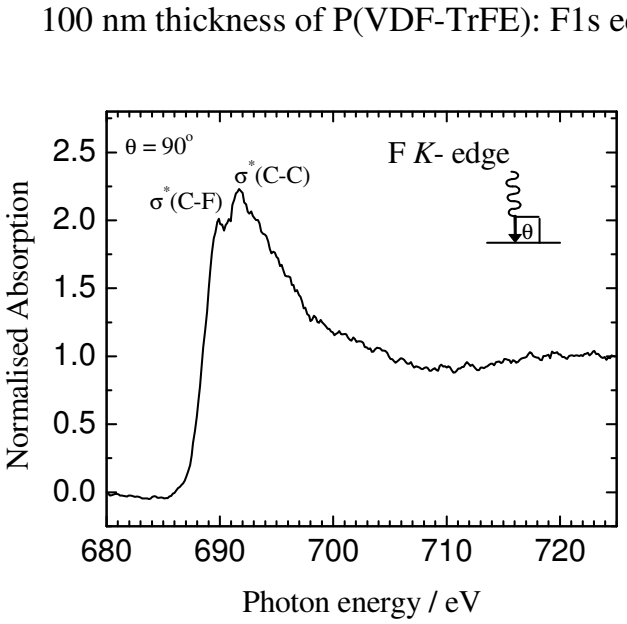

Figure. 5.2. *F K-edge total electron yield NEXAFS spectra for the 2.5 % P(VDF-TrFE) copolymer film (thickness ~ 100 nm) on Si(100).*

Figure 5.2 shows the F *K*-edge NEXAFS spectrum of the same copolymer film as a continuation of the previous measurement at the C *K*- edge. The two prominent peaks arise in the photon energy at 689.7 and 691.5 eV. In compatible with literature results, the peak assignment is done. The peaks at photon energy at 689.7 eV and 691.5 eV are ascribed to the transition from F1s to σ^*(C–F) and to σ^*(C–C), respectively [16, 27-29].

As part of our investigation, we have attempted angular dependence C *K*-edge NEXAFS spectroscopy for study of the influence of CF_2 dipole of different thickness of P(VDF-TrFE) copolymer film on the organic substrate, PEDOT:PSS. The deconvoluation of the NEXAFS plays very significant role, especially for this kind of study. For example, here we show the lower coverage of P(VDF-TrFE) film (thickness ~0.35 nm) on the substrate PEDOT:PSS/Si(100). The building block of the layer structure and the chemical structure of PEDOT:PSS is illustrated in figure 5.3 (right side panel). We have employed the total electron mode NEXAFS measurement and for such case, the escape depth of photoelectrons is about 5 nm [28]. Therefore, the unoccupied level transition from the PEDOT:PSS layer is obvious,

especially for the lowest coverage of the P(VDF-TrFE) copolymer layer. In figure 5.4, the deconvolution of the C K-edge total electron yield NEXAFS spectra is shown for the 0.35 nm thickness of P(VDF-TrFE) copolymer film on the PEDOT:PSS/Si(100) substrate. The details of the thin film procedure have been discussed in the experimental section (chapter 2) of the thesis. The very sharp peak at a photon energy of 285.1 eV can be assigned to the transition from the C1s orbital to the π^* orbital [13]. This contribution is strictly arises from the double bond environment (C=C π^* resonances) of the PEDOT:PSS structure. The rest of the individual peaks are only identifiable by a curve fitting procedure (see. figure 5.4). Likewise, a peak near 287.2 eV and 288.9 eV can be assigned to transitions from the C1s orbital to the σ^*(C-H) and σ^*(C-S) unoccupied orbital respectively [13, 14]. The peak at 292.4 eV arises from the copolymer film and the peak is assigned for the transition from the C1s orbital to the σ^*(C-F) unoccupied orbital. The higher photon energy peaks (above 294.8 eV) are mostly due to C1s to σ^*(C-C) orbital transitions [13]. In the curve fitting procedure, the C=C π^* resonance fits to a Gaussian profile which match the height of the experimental peaks. The Gaussian function matched well because of the limitation of the instrumental resolution, while the Lorentzian fit is poor because the base is too broad [13].

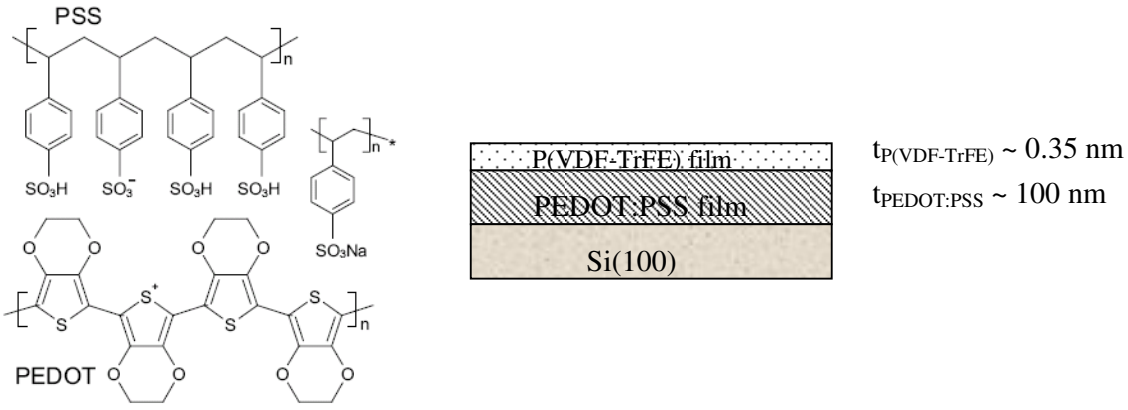

Figure 5.3. *The chemical structure of the polymer system PEDOT:PSS, composed of the two components PEDOT and PSS (left panel); The layer structure of the sample for NEXAFS measurement (right panel).*

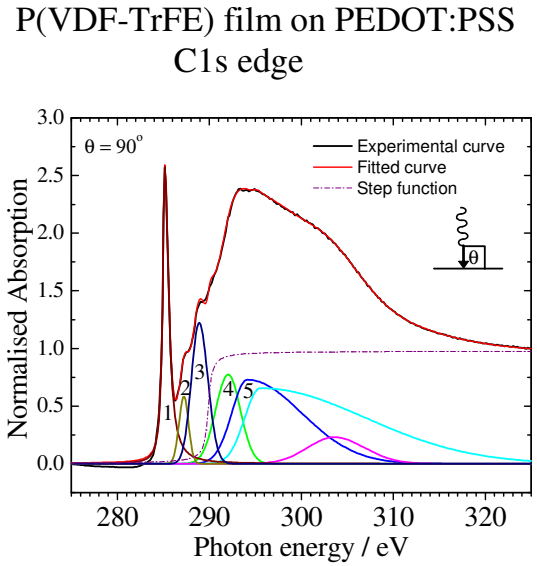

Peaks	Photon energy	Transition level from C1s
1	285.1 eV	π^*
2	287.2 eV	σ^*(C-H)
3	288.9 eV	σ^*(C-S)
4	292.4 eV	σ^*(C-F)
5	294.8 eV	σ^*(C-C)

Figure. 5.4. *Deconvolution of the C K-edge total electron yield NEXAFS spectra for the 0.1 % P(VDF-TrFE) copolymer film (thickness ~ 0.35 nm) on PDOT:PSS/Si(100) (left panel) and their peak assignments (right panel).*

5.3. Dipole Orientation Evaluation by Angular Dependent NEXAFS

Introduction

The mechanism of dipole orientation in P(VDF-TrFE) copolymer films still remains as the central issue of our current investigations on ferroelectricity of copolymer films. Although the orientation of dipoles in polar β-form crystals has often been proposed, the published results related to such orientation has not been conclusive [29-32]. Hence, we attempted a powerful technique angular dependence NEAXFS to understand the degree of average dipole orientation existing in the copolymer films. Investigations of anisotropy's are performed with a P(VDF-TrFE) copolymer film on a Si(100) wafer and PEDOT:PSS/Si(100) as substrate. The spin coating and annealing procedure steps is described in the thin film preparations section of this thesis. We have conformed that the good compatibility between the P(VDF-TrFE 70:30) copolymer and the 2-butanone solvents aids the formation of a monophase. Our XPS results revel that there is no interfacial reaction when P(VDF-TrFE) copolymer is spin coated on PEDOT:PSS films.

In the previous section we have discussed the peak assignments and curve convoulation of the C *K*- edge NEXAFS spectrum for a P(VDF-TrFE) copolymer film on Si(100) and also on a PEDOT:PSS/Si(100) substrate (see figure 5.1 and 5.4). Measurements of angular dependence NEXAFS are performed with a set of samples (Sample A to E) with different layer thickness (see figure 5.6). The layer thicknesses are estimated from XPS results, as described in the chapter 3.

The C *K*-edge NEXAFS spectra of the spin coated films were measured as a function of the $\vec{E}$ (electric) vector orientation relative to the surface normal in 20° intervals from 10° to 90°. The geometry of the sample (surface normal) and the incident photon beam ($\vec{E}$) is illustrated in figure 5.5, where the angle θ is defined as the incident photon angle.

Figure 5.5. *The relation of the $\vec{E}$ vector orientation relative to the surface normal $\vec{n}$ of the sample. The incidence photon angle θ (angle between $\vec{E}$ and $\vec{n}$) is also shown.*

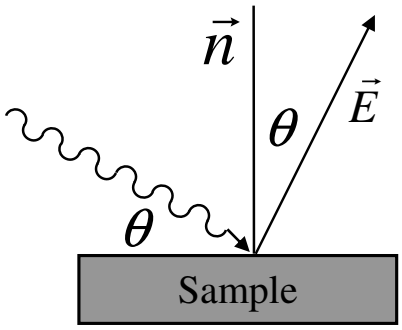

As discussed in earlier in chapter 2, the dipole selection rules related to K-shell NEXAFS resonance intensities are quite simple: the resonance intensity associated with the specific molecular orbital final state is largest if the $\vec{E}$ vector points in the direction of that molecular orbital, i.e., lies in the nodal plane of the orbital. The σ^* resonance is most pronounced and the π^* resonance is smallest when the $\vec{E}$ vector is parallel to the surface. It would be more convenient if we look back on the angular dependent NEXAFS spectra (see figure 2.10) of oriented molecules CO on Mo(110) and C_2H_4 on Ag(100) is described in chapter 2. In contrast, the polarization dependence of molecules discussed here will give clear comparison with the orientation of the C-H, the C-F and the C-C bond for the P(VDF-TrFE) copolymer for different ultra-thin film thickness with different substrates, i.e. an organic substrate PEDOT:PSS

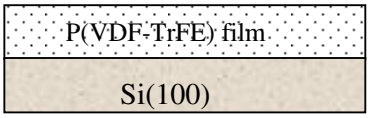

Sample A: $t_{P(VDF\text{-}TRFE)}$ ~ 100 nm

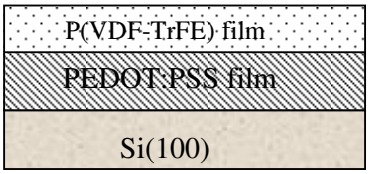

Sample B : $t_{P(VDF\text{-}TRFE)}$ ~ 30 nm, $t_{PEDOT:PSS}$ ~100 nm

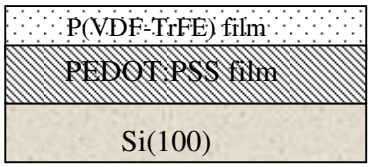

Sample C : $t_{P(VDF\text{-}TRFE)}$ ~ 0.8 nm, $t_{PEDOT:PSS}$ ~100 nm

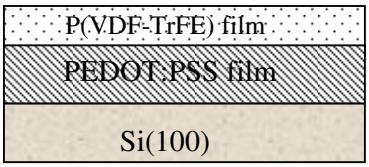

Sample D : $t_{P(VDF\text{-}TRFE)}$ ~ 2.5 nm, $t_{PEDOT:PSS}$ ~100 nm

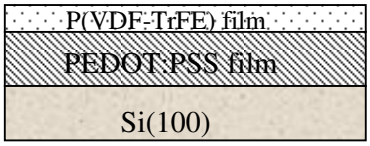

Sample E: $t_{P(VDF\text{-}TRFE)}$ ~ 0.35 nm, $t_{PEDOT:PSS}$ ~100 nm

Figure 5.6. *Building block of layer structure of ultrathin copolymer film on Si(100) and PEDOT:PSS/Si(100) substrate.*

and an inorganic substrate Si(100). In our spin coated copolymer films are semicrystalline copolymers that have morphology of crystallites in an amorphous matrix, had also shown from FTIR and XRD studies. The morphology of this copolymer is that of a long macromolecular in a *trans* conformation as presented in figure 5.8, where the unit cell contains VDF

(–CH_2–CF_2–) and trifluoroethylene TrFE (–CF_2–CFH–). It may be noted that the macromolecular character of these molecules is particularly advantageous because it suppresses complicated fluctuation [33]. The difference in electronegativity between fluorine and hydrogen atoms results in dipole moments (see the figure 5.9), the direction of the dipoles is shown in figure 5.8.

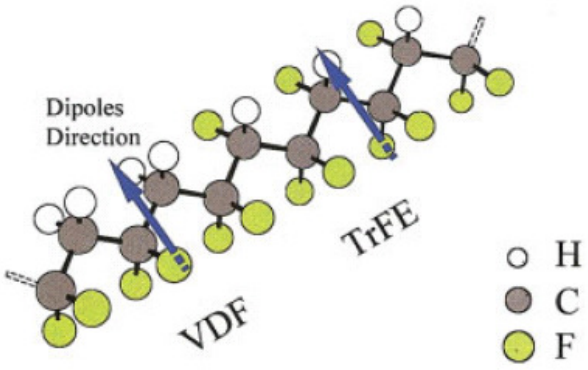

Figure 5.8. *Schematic depiction of the molecule chain trans conformation in* the *P(VDF-TrFE) copolymer. The arrow indicates the dipole direction resulting from the difference in electro negativity between fluorine and hydrogen atoms.*

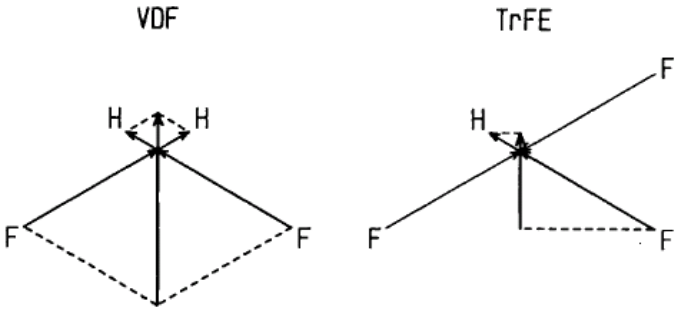

Figure 5.9. *Dipole moment of VDF and TrFE units [adopted from ref. 34].*

5.4. Results and discussion

The angular dependence of the C *K*-edge NEXAFS spectrum is shown in figure 5.10 (a) for sample A. The sample geometry with respect to the photon beam is illustrated in figure 5.5. The spectra are scaled to the same edge jump by matching their intensities at 280 eV and 325

eV of photon energies, clearly show the pronounced angular dependence of the three principal resonances. In particular, we have plotted the relative intensities for C1s to the σ^*(C-F) and σ^*(C-H) resonances versus the incident photon angles (θ) in figure 5.10 (b), (c) respectively.

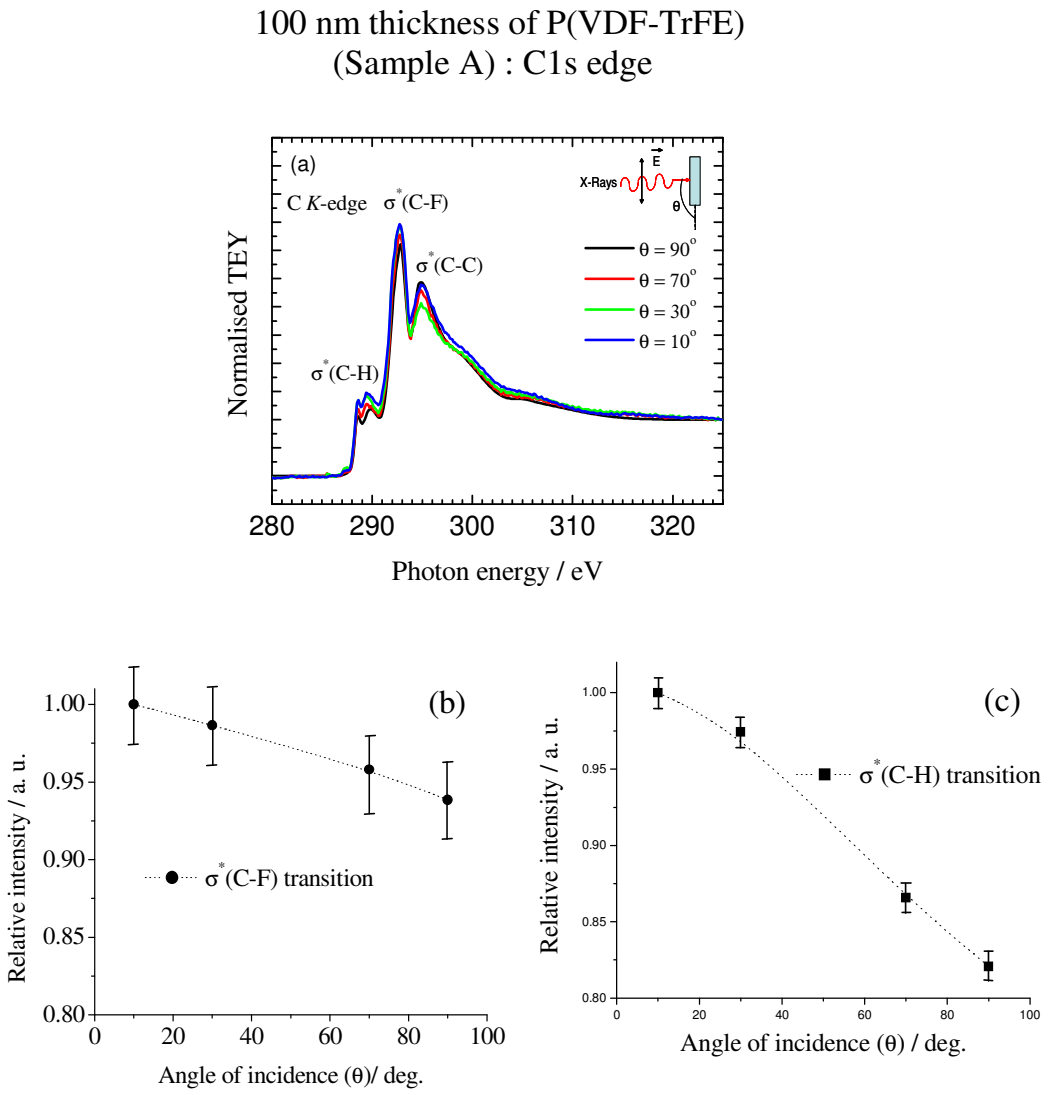

Figure 5.10. *(a) The angular dependence of the total electron yield at the C K-edge. NEXAFS spectra of 2.5 % P(VDF-TrFE) copolymer film (thickness ~ 100 nm) on Si(100)(Sample A, see fig.5); The plot of the relative intensities for (b) C1s to σ^*(C-F) resonance and (c) C1s to σ^*(C-H) resonance versus the angle of incidence photon (θ), The intensity is normalized to the peak intensity at an incident photon angle of θ = 10°.*

Thus the σ^*(C-F), σ^*(C-H) resonances showing higher intensity for the lowest grazing angle ($\theta = 10^o$) with respect to higher grazing angles and also for normal incidence ($\theta = 90^o$). On the other hand for the σ^*(C-C) resonance the intensity at normal incidence is highest with respect to the rest of the grazing photon incidence (see figure 5.10 a). Therefore we may say that for sample A, probably the average main C–C backbone chain of the copolymer is oriented parallel to the substrate. Although, it is important to mention that the spin coated copolymer film contains the polarized *all-trans* β- crystalline phase along with a surrounding amorphous region. Thus we can't make the conclusion that the backbone chain of the copolymer is completely aligned parallel to the substrate. Furthermore, from the behavior of the σ^*(C-F), σ^*(C-H) resonances for sample A, there is a highest probability for an average dipole alignment perpendicular to the substrate. This is quite salubrious to use the term 'dipole alignment' instead of 'CF_2 dipoles' for sample A as both σ^*(C-F), σ^*(C-H) resonances contributing from the copolymer film (see figure 5.8).

On the other hand, the rest of the samples (sample B to E), we have to look for the most important 'CF_2' dipoles orientation, as due to ultra thin thickness of the copolymer film on PEDOT:PSS films, there is a probability that the rest of σ^*(C-H), σ^*(C-C) resonance attribute to C-H and C-C antibonding molecular orbitals from PEDOT:PSS films as well. Furthermore, for supporting data we have also looked for the F *K*-edge NEXAFS spectra for sample A, shown in figure 5.11 (a) and the corresponding F1s to σ^*(C-F) resonance which is illustrated in figure 5.11 (b). Eventually, we found that the average orientation of the'CF_2' dipoles are aligned the perpendicular to the substrate.

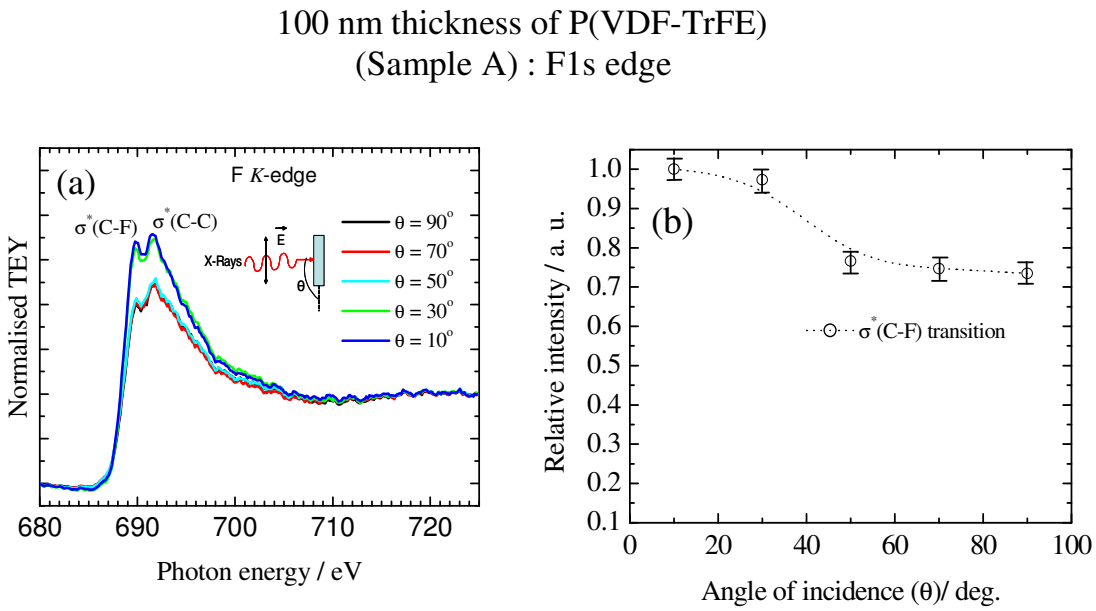

Figure 5.11. *(a) The angular dependence of* the *total electron yield F K-edge NEXAFS spectra of 2.5 % P(VDF-TrFE) copolymer film (thickness ~ 100 nm) on Si(100) (Sample A, see fig. 5.6); (b) The plot of Angle of incidence photon versus relative intensity for F1s to σ*(C-F) resonance. The intensity is normalized to the peak intensity at incident photon angle θ = 10°.*

The figure 5.12 (a), shows that the angular dependence C *K*-edge NEXAFS spectrum for sample B, the sharp resonance at 285.1 eV arises due to C1s to π^* resonances which is contribution from C=C double bond of PEDOT:PSS films.

The apparent overall structure of the C *K*-edge NEXAFS spectrum of sample B is very similar in comparison to figure 5.10 (a) which is for sample A. As expected the sharp π^* resonance peak arises at a lower photon energy (285.1 eV). The resonances contribution of C1s to σ^*(C-F) at different incidence photon angles (θ = 10°, 30°, 50°, 70° and 90°) are shown in figure 5.10 (b). Thus the values shows that such resonance is dominated for lower grazing angle (θ = 10°) whereas the rest of the resonances are lower value. The dotted curve indicates that the resonance at higher incidence photon angle is always lower than for the consecutive lower incidence photon angle. Furthermore, if we look to the C1s to σ^*(C-C) resonances (see figure 5.10a), the average tendency of the σ^*(C-C) resonances is higher at normal incidence. There might be the possibility of σ^*(C-C) resonances attributing from PEDOT:PSS films as well. Therefore, we will not consider the dependence of σ^*(C-C) resonances of the rest of the sam-

ple (sample C and E), as here the copolymer layers thickness are significantly low (i.e. 2.5 nm and 0.8 nm).

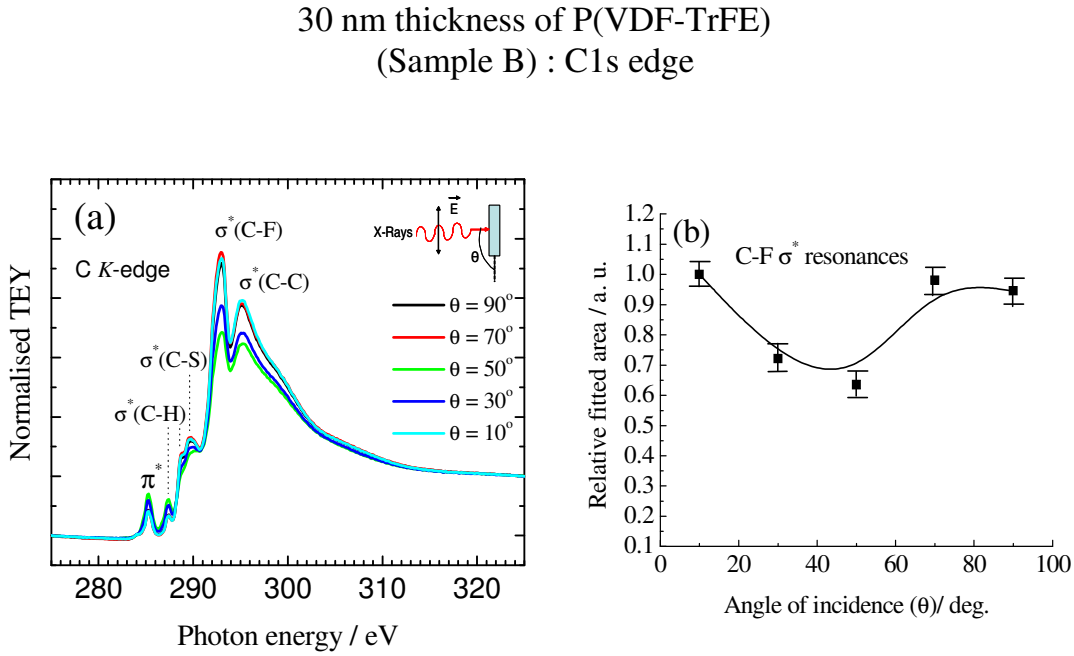

Figure 5.12 *. (a) The angular dependence of the total electron yield C K-edge NEXAFS spectra of a 1.0 % P(VDF-TrFE) copolymer film (thickness ~ 30 nm) on PEDOT:PSS/Si(100)(Sample B, see fig.5); The data of relative intensities for (b) C1s to* σ^**(C-F) resonance versus the angle of incidence photon (θ) is shown. The intensity is normalized to the peak intensity at an incident photon angle of* $\theta = 10^o$.

The C *K*-edge NEXAFS spectrum for an ultra thin copolymer film (thickness ~ 2.5 nm) of sample D is shown in figure 5.13 (a). In comparison with figure 5.12 (a) which is for sample B, the π^* resonance peak is more sharp indicating the prominent resonance to less attenuated photo electrons coming from the PEDOT:PSS films. The contribution for C1s to σ^*(C-F) resonances (taken from the curve deconvolution of the spectra of 5.13a) is shown in figure 5.13 (b). The curve shows the tendency of the resonance at normal incidence is lower than the rest of the grazing incidence. This result is also support that the average orientations of the CF_2 dipoles are tendency to standing up with respect to the substrate. In figure 5.14 (b), for

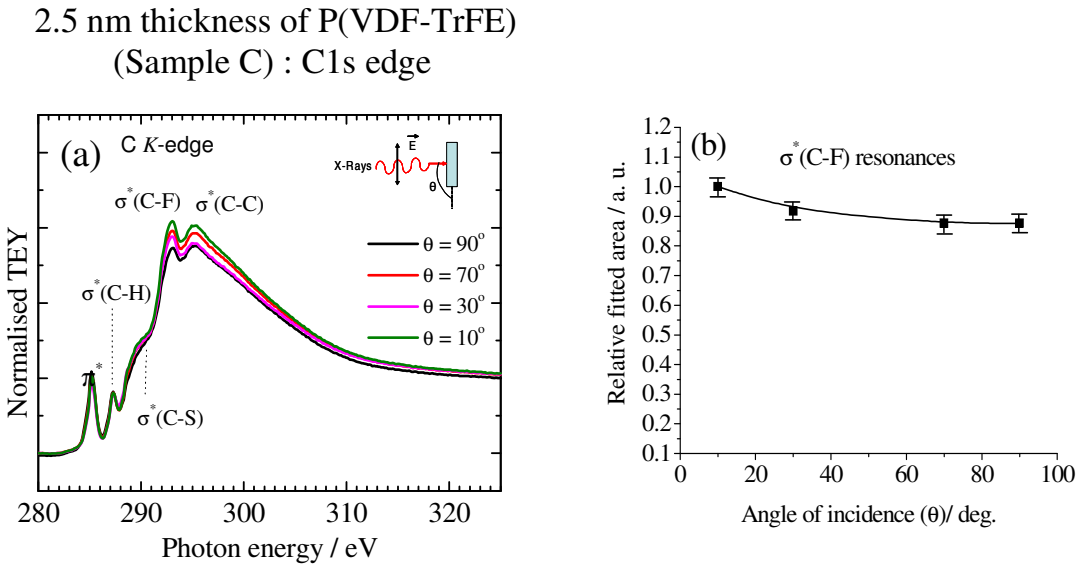

Figure 5.13 *. (a) The angular dependence total electron yield for C K-edge NEXAFS spectra of a 0.5 % P(VDF-TrFE) copolymer film (thickness~ 2.5 nm) on PEDOT:PSS/Si(100)(Sample C, see fig.5); The data of relative intensities for (b) C1s to* σ^**(C-F) resonance versus the angle of incidence photon (θ) is shown. The intensity is normalized to the peak intensity at an incident photon angle* $\theta = 10^o$.

sample D (copolymer film thickness ~ 0.8 nm), σ^*(C-F) resonances shows that the resonance intensity is lower at normal incidence and gradually increases for lower incidence. This also evidence of the average CF_2 dipoles standing up orientation on the substrate. We did not showed the σ^*(C-C) and the σ^*(C-H) resonance plot separately as there are definite contributions comes from PEDOT:PSS films in addition to copolymer films. Therefore, it is difficult to make stick conclusions for such a film in terms of dipole orientation.

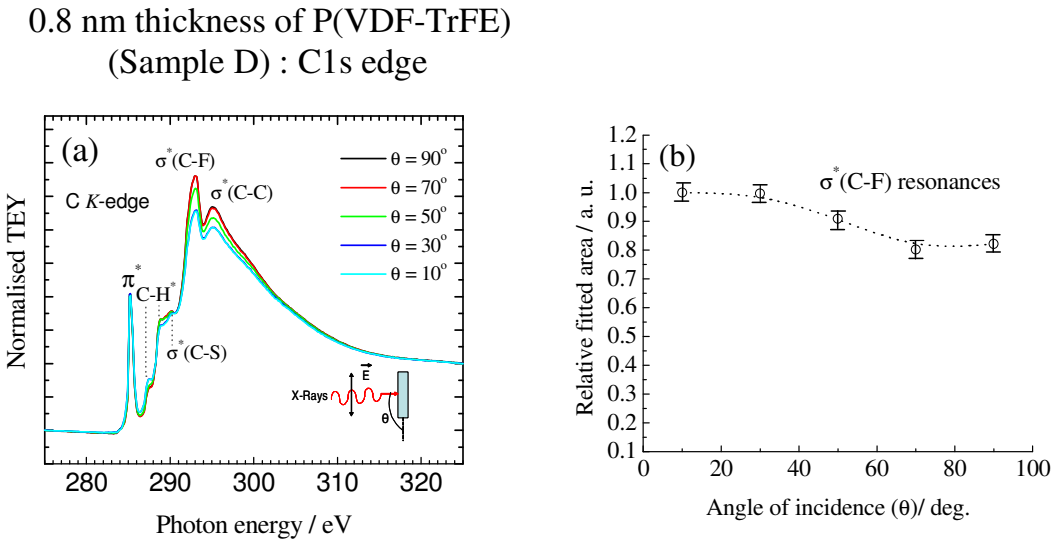

Figure 5.14. *(a) The angular dependent total electron yield of C K-edge NEXAFS spectra of a 0.3 % P(VDF-TrFE) copolymer film (thickness~ 0.8 nm) on PEDOT:PSS/Si(100) (Sample D, see fig.5); The data of* the *relative intensity for (b) C1s to* σ^**(C-F) resonance versus the angle of incidence photon (θ) is shown. The intensity is normalized to the peak intensity at an incident photon angle* $\theta = 10^o$.

The angular dependence of the C *K*-edge NEXAFS spectrum for the lowest coverage of a copolymer ultra thin film (thickness ~ 0.35 nm) on PEDOT:PSS/Si(100) is shown in figure 5.15 (a). The corresponding building block of the layer structure of the sample is illustrated in figure 5.6. The obvious sharp π^* resonances showing that the contribution of less attenuated excited PEDOT:PSS photoelectrons, as there is no existence of C=C double bonds in the co-polymer film. Here it is important to mention that we have confirmed that we don't have beam damage due to synchrotron photon beam. Therefore, there is almost less chance of such π^* resonances attributing from the beam degraded of copolymer film. This is also revel from the C *K*-edge NEXAFS spectrum of a 100 nm thick copolymer film, shown in figure 5.10 (a). There is no such sharp contribution of the π^* resonance at lower photon energy (285.1 eV). The details of peak assignments and the curve deconvoulation of the C *K*-edge NEXAFS spectrum of sample E is discussed in previous section. Here also we find that the resonance contribution for C1s to σ^*(C- F) resonances is relative higher for grazing incidence of the photon with respect to normal incidence (see figure 5.15 b). This fact also attributed that for lowest coverage of copolymer films also have the average degree of dipole CF_2 orientations. In

figure 5.15 (b), we also show that ideal case of the CF_2 dipole orientation ($\cos^2\theta$ dependence) to compare our results. A curve fitting, according to $I=0.2\ \cos^2(\theta)+0.8$, is also shown and gives a good agreement.

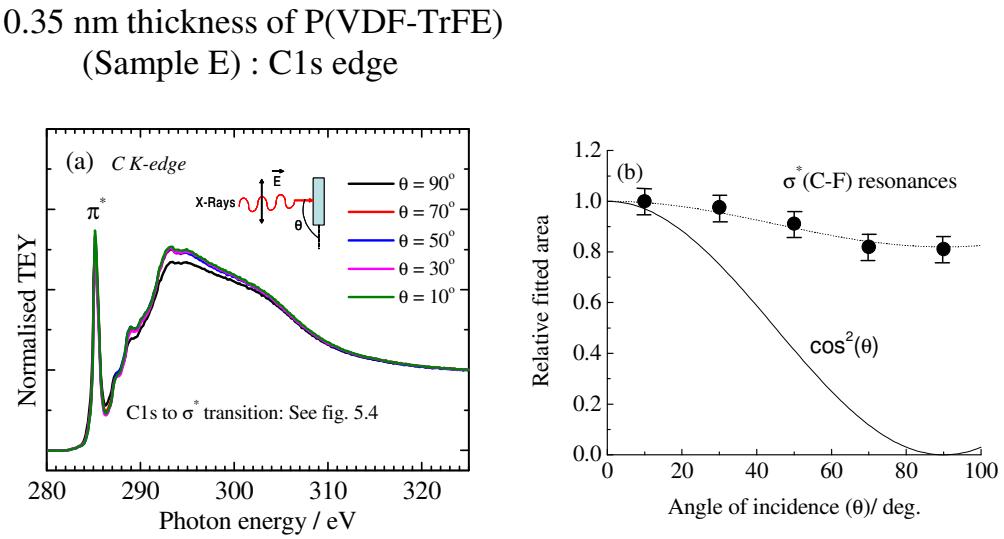

Figure 5.15. *(a) The angular dependence total electron yield C K-edge NEXAFS spectra of 0.1% P(VDF-TrFE) copolymer film (thickness~0.35 nm) on PEDOT:PSS/Si(100)(Sample E, see fig.5);The data of relative intensities for (b) C1s to σ^*(C-F) resonance versus the angle of incidence photon (θ) is shown ,The intensity is normalized to the peak intensity at incident photon angle $\theta = 10^o$. The $\cos^2\theta$ line presents the modulation of resonances for an idealized alignment of CF_2 dipoles (100% perpendicular to the surface of the substrate).*

The $\cos^2(\theta)$ dependence is an approximation, of course: we have to take into account following statements: First, the incident beam is not an idealized point, we have an rectangular area. Second, we need a further rotation θ inside the plane of the surface of the sample (rotation perpendicular to θ), because an alignment of dipoles perpendicular to the surface is an idealization. We have $I=I(\theta, \Phi)$ and quantitative estimations, for example the relative amount of aligned dipoles, are only possible, when $I(\theta, \Phi)$ under variation of the angle Φ is maximized. Here, further investigations are might be most conclusive.

Nevertheless, the measurements show a clear average degree of alignment of dipoles. This is an additional confirmation for a well ordered copolymer without any degradation, as in the case of aluminum as substrate or electrode. It seems, that ferroelectric ordering occurs even for ultrathin and spin coated films, if we use an inert substrate like PEDOT:PSS.

5.5. Electric Field Induced Polarization

Introduction

The ferroelectric memory performance strongly depends on the orientation of the ferroelectric dipoles. The pursuit of nonvolatile random-access memory devices and nanoscale electronic devices has provided impetus to study of ferroelectric thin films [35-38]. Ferrolectricity is difficult, generally, to maintain when the size of the ferroelectric material is greatly reduced [39]. Furthermore, the ferroelectric co-polymer P(VDF-TrFE), provide to fabricate high-quality ultrathin crystalline ferroelectric films [40-42]. There has been numerous research work investigated to study the orientation of the ferroelectric dipoles and the effect of the electric field in PVDF and its copolymer P(VDF-TrFE) [39, 40, 44-47] but it is yet an open question to reach a conclusive guideline. However it is found that the orientation of dipoles effectively depends on the choice of the substrates [40, 44-46].

Here we employed a NEXAS on ultrathin films (scale down to 10 nm thickness) of P(VDF-TrFE) copolymer, were prepared on PMMA/Al/Si(100) substrate by spin coating method. The details steps of the spin coating procedure for this stacking layer structure and annealing procedure is described in 'chapter2' of this thesis. The layer structure for the sample is schematic in figure 5.16, with different color. The top layer (pink color) is the copolymer spin coated film; the underneath layer, shown by blue color is a layer of PMMA (thickness ~700 nm) on the aluminum evaporated Si(100) wafer.

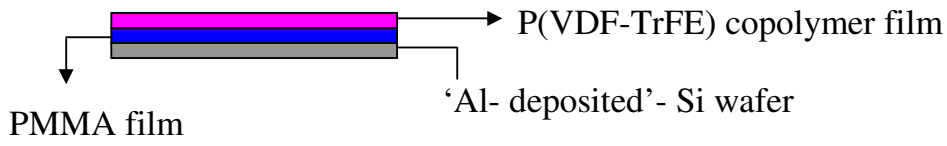

***Figure 5.16**. The layer structure of the sample.*

Our aim is to investigate the effect of the ferroelectric dipoles, especially for ultrathin spin coated films. In our layer structure of the samples, the aluminum deposited Si wafer act as a bottom electrode for ultrathin copolymer films and we introduce PMMA layer to prevent leakage current during application of the electric field [43]. We used another aluminum coated

Si wafer externally as a top electrode. The experimental detail for the application of external dc electric field is described in the chapter 2.

5.6. Results

Relating to P(VDF-TrFE) copolymer layer thickness, we have deal with relative thick (thickness 100 nm and 80 nm) and one extremely thin (thickness ~10 nm) film. 1st of all, we have measured the angular dependence F *K*-edge NEXAFS spectrum in total electron mode for all samples. Here we avoid the C *K*-edge NEXAFS spectrum, utilizing the merit of the fluorine edge NEXAFS spectrum. The spectrum of all samples is measured as a function of the $\vec{E}$ (electric) vector orientation relative to the surface normal in 20^o intervals from 10^o to 90^o. The definition of incidence photon angle θ is the same as described in figure 5.5. The F *K*- edge NEXAFS spectra are shown in figure 5.17 (left panel), before the application of the applied field. Afterwards, we have applied an electric field for each sample. Here we apply a dc voltage 30 volt between top and bottom electrodes for 30 minutes duration. Thereafter, the sample is transferred into a UHV chamber with a base pressure of 7.0×10^{-8} mbar for the NEXAFS measurement. The same treatment is done for all three samples. Here it is important to note that the sample transfer time between the ends of the application of the electric field into main measuring UHV chamber takes about 15 minutes. In the figure 5.17 (right panel), the F *K*-edge NEXAFS spectrum in total electron mode after the application of the electric field is shown. All spectra are normalized to the same edge jump by matching their intensities at 680 eV and 725 eV of photon energies.

To analyze the degree of orientation of the CF_2 dipole, we have to consider the resonance intensity of the F1s to σ^*(C-F) antibonding orbital, revel by the most pounced peak in figure 5.17. The plot of the σ^*(C-F) resonances versus different incidence angles for each sample (without electric field and after application of electric field) is shown in figure 5.18. The specification for more clarity of presentation is described in the corresponding figure caption. With analogy as described in previous section, we also observed the resonance intensity fluctuations with respect to incidence photon angle. Here we used different substrates, i.e PMMA/Al/Si(100). But the interesting thing is that the resonance intensity is varying with incidence photon angle and most importantly the behavior of resonance is changing after and before the nearly magic angle ($\theta = 50^o$). As the magic angle consider as critical angle for the molecular orientation with respect to incidence photon [13]. The 80 nm and 10 nm thickness

of the copolymer films also shows the effect of dipolar orientation reveled by the average resonance intensity follows the same trades, shown by red and blue solid symbols in figure 5.18. The intensity at grazing angles (θ = 10^o and 30^o) is higher in this case, indicating the possibility of average CF_2 dipoles orientation is perpendicular with respect to substrates. On the other hand, after application of the electric field, we found the σ^*(C-F) resonance intensity also changing with respect to different photon angle incidence and most interestingly in reverse way (see the figure 5.18). The all resonances for three different thicknesses of the copolymer films are shown with hollow symbols in figure 5.18. Therefore the results indicate the effect of the electric field demand that the ferroelectric dipole orientation, even in a scale down to ultrathin films. As we applied the negative voltage at the top electrode, therefore there is highly chance the electro positive hydrogen atoms attract by the top electrode and on the other hand the positive voltage at the bottom electrode attracts the electro negative fluorine atoms. Therefore, the electric field induces the dipoles to polarize into certain direction in some extent with parallel to the electric field. Although the percentage of the average dipole orientations of the spin coated films is probably depends on the percentage of crystallinity in the semicrystalline films and the strength of the electric field. The figure 5.18, shows the change of intensity of σ^*(C-F) resonance with respect to incidence photon angle, which is most prominent for 10 nm thickness of the copolymer films. Therefore, as a part of our analysis we concluded that the effect might be coming from the strength of the electric field. As described, we applied the external electric field (30 Volt for 30 minutes) to polarize the dipoles for three different thickness (100 nm, 80 nm and 10 nm) of the P(VDF-TrFE) copolymer films. Therefore, we employed further experiment to ensure the ferroelectric dipole alignments with lower applied voltage (15 Volt for 30 minutes) for 10 nm thickness of ultra thin P(VDF-TrFE) copolymer films. Here in addition to total electron mode of F *K*-edge NEXAFS measurement, we also measure in another mode namely, total fluorescent yield (TFY) mode. As TFY mode gives more surface information depth (about 200 nm). Although the TEY mode is efficient enough to analyze such observation, the TFY mode should be better to verify if the there is any contribution coming from the bulk of the sample. In figure 5.19, we showed the angular dependence of the TEY mode F *K*-edge NEXAFS spectrum for 10 nm film thickness of the copolymer. The left side panel and right side panel of the figure 5.19, shows the spectrum without the application of the electric field and after the application of the electric filed respectively. The corresponding TFY mode F *K*-edge NEXAFS spectrum are shown in figure 5.20 where the left side panel described the spectrum for without application of the electric field while the right side panel described the spectrum taken after

the application of the electric field. We found there is sharp resonance observed in TFY mode but the relative angular dependence resonance are littlie more prominent in TEY (see figure 5.19 and 5.20).

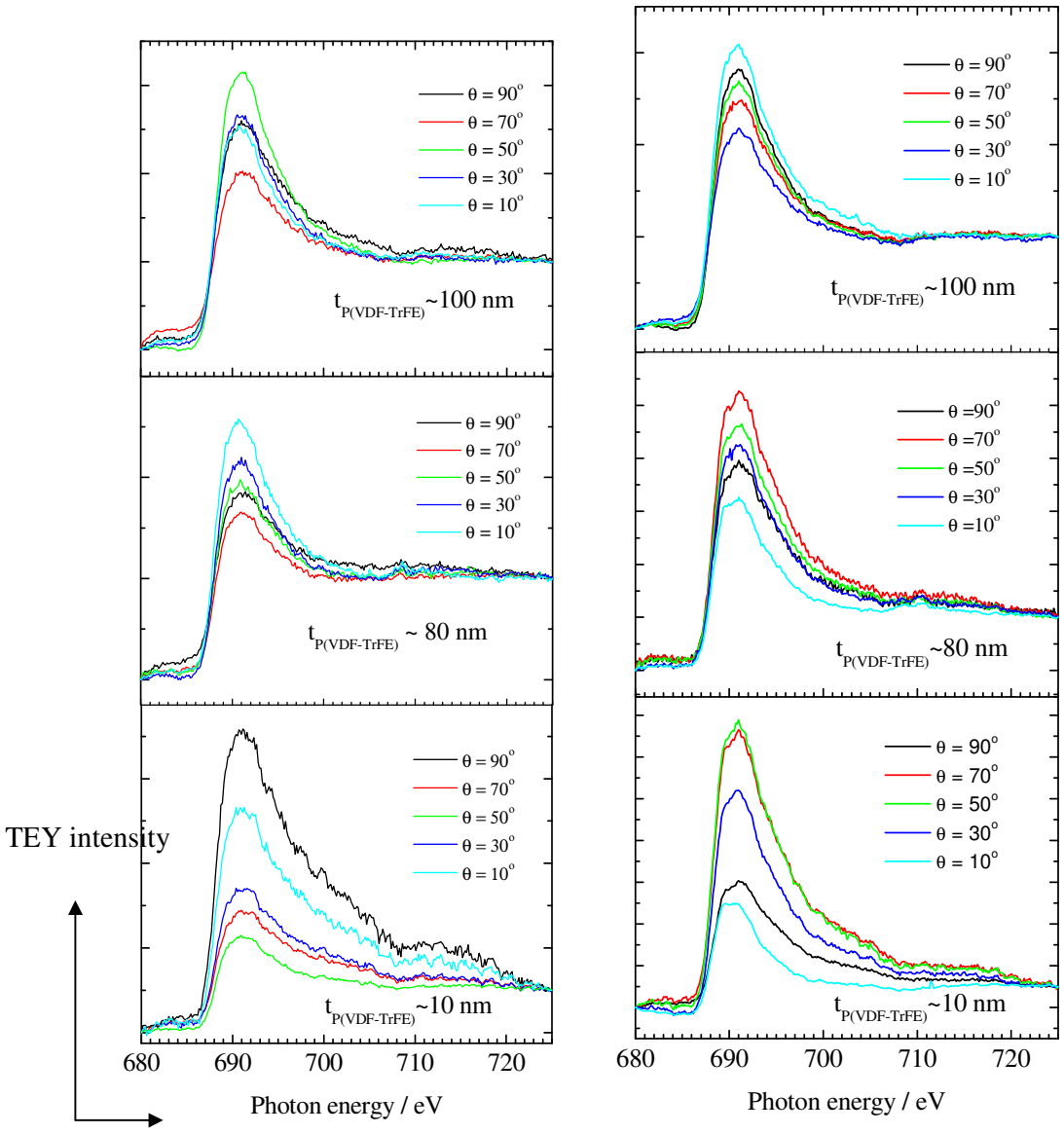

Figure 5.17. The angular dependence of the total electron yield F K-edge NEXAFS spectrum for ultra-thin copolymer films (thickness values are mentioned in the inset). All spectrums shown in left side panel are taken before the application of the electric field and in right side panel are taken after the application of the electric field (applied voltage: 30 Volt for 30 minutes).

To analyze the effect of dipole orientation with the electric field, we have plotted the relative σ^*(C-F) resonance intensity (taken from figure 5.19 and 5.20) versus the angle of incidence photon angle, which is shown in figure 5.21. In both cases, TEY and TFY, we found the same kind of behavior of σ^*(C-F) resonance, indicating that the resonance does not effect from the bulk of the sample. This case, we also found the effect of the electric field even for lower applied voltage (15 Volt) down to half of the previous measurements. Those results are shown in figure 5.18.

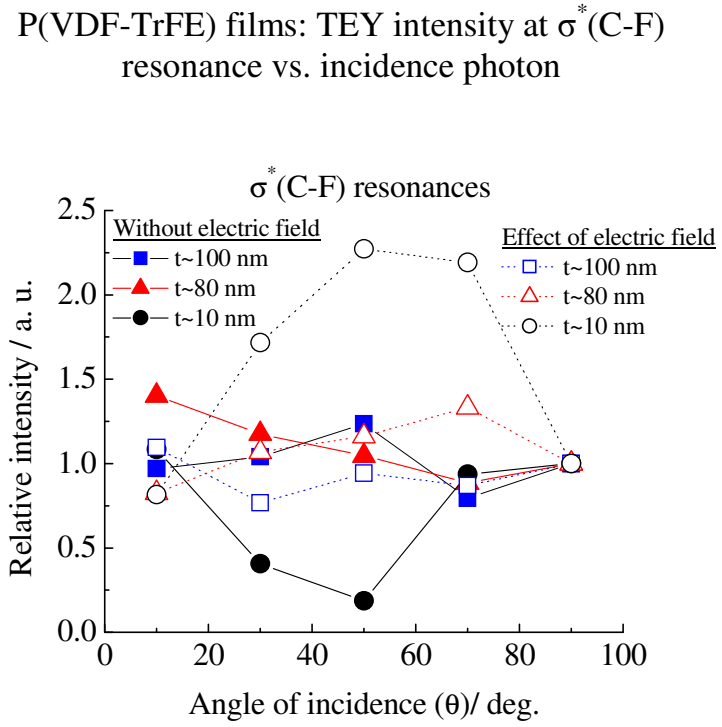

***Figure. 5.18**. The plot of relative TEY intensity of σ^*(C-F) resonances for mentioned thickness of P(VDF-TrFE) copolymer films versus angle of incidence (θ) photon. All aforesaid resonance intensity (from figure 5.17) are normalized to the peak intensity at incident photon angle $\theta = 90^o$. The solid symbols indicate the results are taken without application of the electric field and hollow symbols indicate the results are taken after the application of the electric field (applied voltage: 30 Volt). The same color code indicates the results are for the same sample.*

Therefore, we may conclude that we have observed the dipole orientation for ultrathin film thickness of 10 nm and the effect of electric field. To ensure the ferroelectric property in such ultrathin spin coated film we also employed supporting additional measurement through ferroelectric hysteresis measurement and found the hysteresis loop even if for 10 nm thickness of the copolymer films.

5.7. Further results of ultra thin film (10 nm thickness)

Here we apply lower external electric field (15 Volt for 30 minutes) for the polarized the ferroelectric dipoles. The electric field over the copolymer, calculated with respect to the resulting voltage divider, is 0.46 MV/cm, we use a relative dielectric constant of 3.0 for PMMA and 6.7 for P(VDF-TrFE). This value is well below the calculated field for the "intrinsic" switching mechanism.

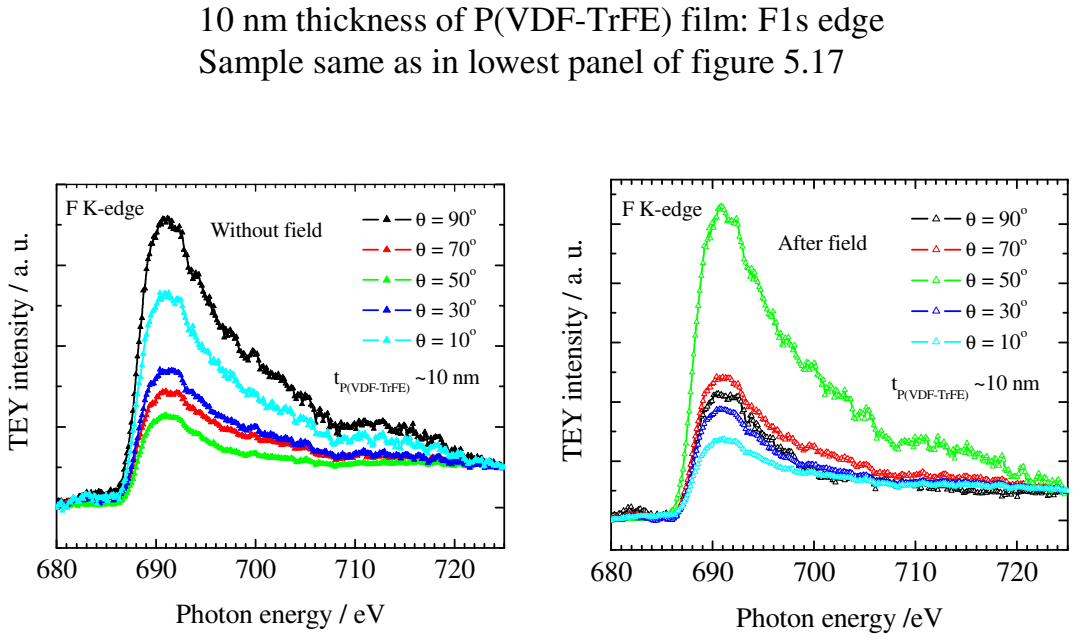

Figure 5.19. *The angular dependence of the total electron yield F K-edge NEXAFS spectrum for 10 nm thickness of ultra-thin P(VDF-TrFE) copolymer. Spectrum shown in left side panel are taken before the application of the electric field and in right side panel are taken after the application of the electric field (applied voltage: 15 Volt for 30 minutes).*

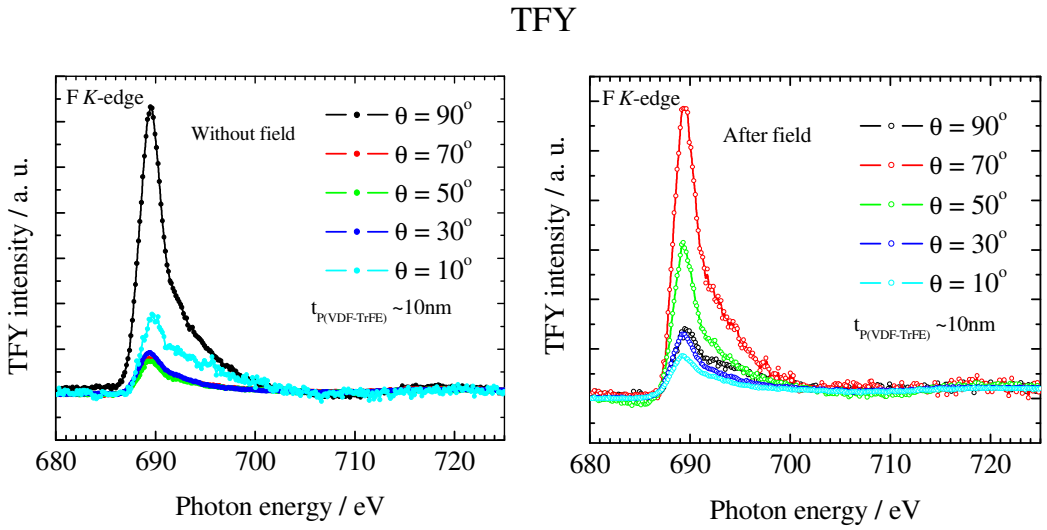

Figure 5.20. *The angular dependence of the total fluorescent yield F K-edge NEXAFS spectrum for 10 nm thickness of ultra-thin P(VDF-TrFE)copolymer. Spectrum shown in left side panel are taken before the application of the electric field and in right side panel are taken after the application of the electric field (applied voltage: 15 Volt for 30 minutes).*

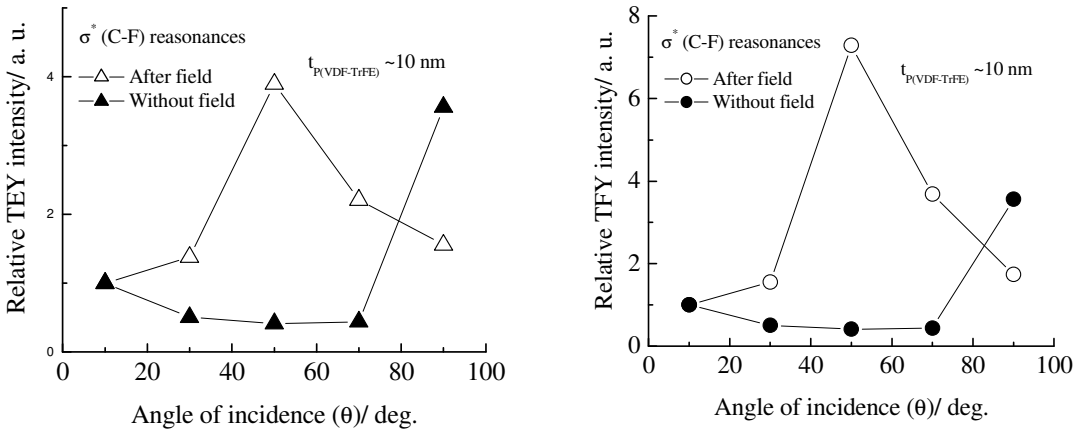

Figure 5.21. *The plot of relative TEY intensity of σ^*(C-F) resonances 10nm thickness of P(VDF-TrFE) copolymer films versus angle of incidence (θ) photon. All aforesaid resonance intensity (from figure 5.19, left side panel and from 5.20, right side panel) are normalized to the peak intensity at incident photon angle $\theta = 10^o$. The solid symbols indicate the results are taken without application of the electric field and hollow symbols indicate the results are taken after the application of the electric field (applied voltage: 15 Volt for 30 minutes).*

5.8. Discussion

In this discussion, we address the two following questions:

First: Is there a fundamental threshold for ferroelectric functionality for ultrathin films under the condition of an adapted polarization procedure?

Second: What is the quantity of the polarization with respect to thicker spincoated copolymer films ($\geq$ 100nm), definitely switching in an extrinsic mechanism?

In figure 5.22, two F1s NEXAFS spectra with two different angle of incidence (θ) are drawn. The external electric field (15 V, 30 min) is already applied. We show the total fluorescence yield (TFY) with higher information depth than for the total electron yield (200 nm). A schematic of the beam geometry is drawn as inset. The field vector $E_{//}$ corresponds to an angle θ of 50°, and $E_{\perp}$ corresponds to θ =10°. The linear dichroism, expressed as $P = (I_{E//} - I_{E\perp})/(I_{E//} + I_{E\perp})$ in percent, is also shown in figure 5.22, below. A very strong linear dichroism of almost 80% is observed.

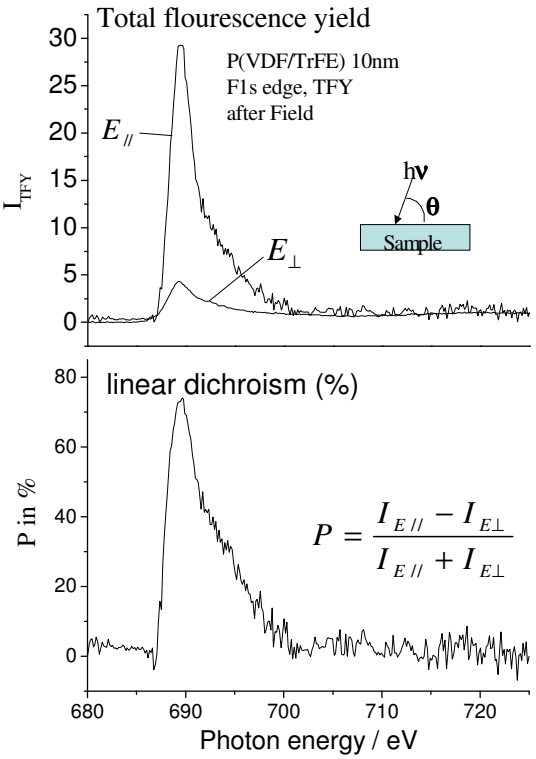

***Figure 5.22**. Linear dichroism of a polarized P(VDF/TrFE) film (10nm, 2 butanone, field: 15V, 30min). Above: F1s NEXAFS intensities versus photon energy for two different angle of incidence. The field vector $E_{//}$ corresponds to θ=50°, $E_{\perp}$ corresponds to θ=10°. A schematic of the beam geometry is drawn as inset. Below: ratio of linear dichroism in %, also versus photon energy.*

In both cases, before and after application of the external field, a strong linear dichroism is found. For the pristine film, the linear dichroism is weaker and additionally carries another sign than after application of the field. The dipole moments of the pristine film are obviously ordered in another direction, with a smaller net ferroelectric moment inside the plane of beam direction and its field vector $\vec{E}$. After application of the external electric field, the linear dichroism is almost doubled, with a maximum of intensity at θ=50°. This clearly indicates a switching process of the C-F dipoles, respectively a remanent polarization of the copolymer.

The effect of the dipole alignment on the linear dichroism is summarized in figure 5.23. Here, a comparison of the two series of NEXAFS spectra of the pristine and the polarized film is given for TFY. We plot the maximum of the σ*(C-F) resonance I_{Θ}^{Max} with reference to the corresponding value $I^{Max}{}_{E\perp}$ for the field vector $E_{\perp}$, respectively the maximum intensity at θ=10°, as $P(\theta) = (I_{\Theta}^{Max} - I^{Max}{}_{E\perp})/(I_{\Theta}^{Max} + I^{Max}{}_{E\perp})$.

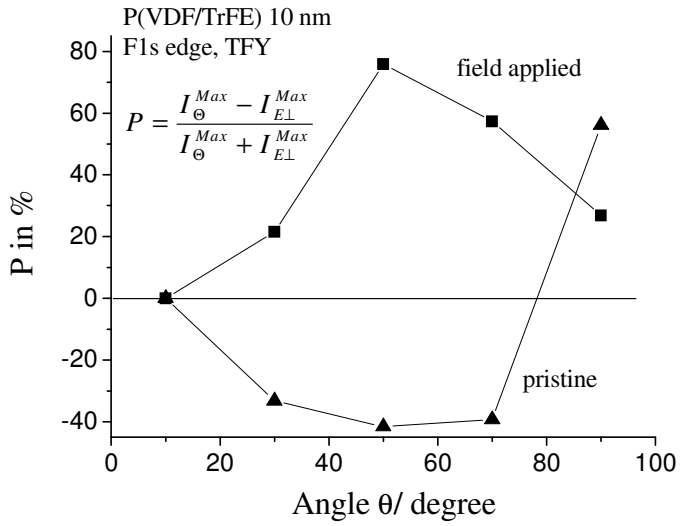

***Figure 5.23**. Linear dichroism as a function of incident beam direction θ, before (pristine) and after application of 15 V (0.46 MV/cm), 30 min. Derived from TFY. The maximum of the σ*(C-F) resonance (I_{Θ}^{Max}) is plotted with reference to the maximum of the resonance for θ=10° ($I^{Max}{}_{E\perp}$), as* $P(\theta) = (I_{\Theta}^{Max} - I^{Max}{}_{E\perp}) / (I_{\Theta}^{Max} + I^{Max}{}_{E\perp})$.

Here, we have to conclude, that even for an ultrathin film, for a field well below the value necessary for a collective intrinsic switching, a ferroelectic alignment occurs, obviously due to an extrinsic switching process. This is also observed for the C-F bonds in the C1s NEXAFS data. The analysis is more complicated due to an overlap with the C-H and the C-C signals.

The extrinsic switching of ultrathin films is confirmed by our electrical characterization. Now, we come to the quantity of the polarization, performed by an analysis of the flatband shift of a capacitance voltage (CV) characteristics. The measurement is carried out with copolymer films in different thickness, with a minimum thickness of (9.7±3) nm, measured directly by AFM.

In figure 5.24 (top), we show the CV measurement with a p-Si/SiO2 substrate, and the thinnest copolymer film. Indium is used as top electrode. The CV measurement is started in accumulation of the p-silicon substrate, at negative gate bias. After driving the bias voltage into the range of inversion, with positive voltages and backwards to accumulation, a "gate bias window" is completed. The figure shows two voltage windows: the ±5V and the ±15V

window. Here we realize a clear hysteresis for the measurement loop. This hysteresis (as flat band voltage shift) of the CV line indicates the presence of polarization charges and hence, a ferroelectric alignment [46, 47]. A reference measurement of a p-Si/SiO2/In stack without P(VDF/TrFE) shows no flatband shift.

A direct extraction of the coercive field from CV measurements is difficult [48], but an estimation of the polarization charge is possible with a calculation of "fixed" surface charges (N_{fix}), according to

$$N_{fix} = \frac{\Delta V_{FB}\, \varepsilon_0 \varepsilon_{PVDF}}{q t_{PVDF}} \qquad 5.1$$

here, ΔV_{FB} is the flat band voltage shift, measured by the CV characteristics, ε_0 is the permittivity value of vacuum, ε_{PVDF} is the relative permittivity value for P(VDF/TrFE), we use 6.7, t_{PVDF} the thickness of P(VDF/TrFE), and q is the elementary charge.

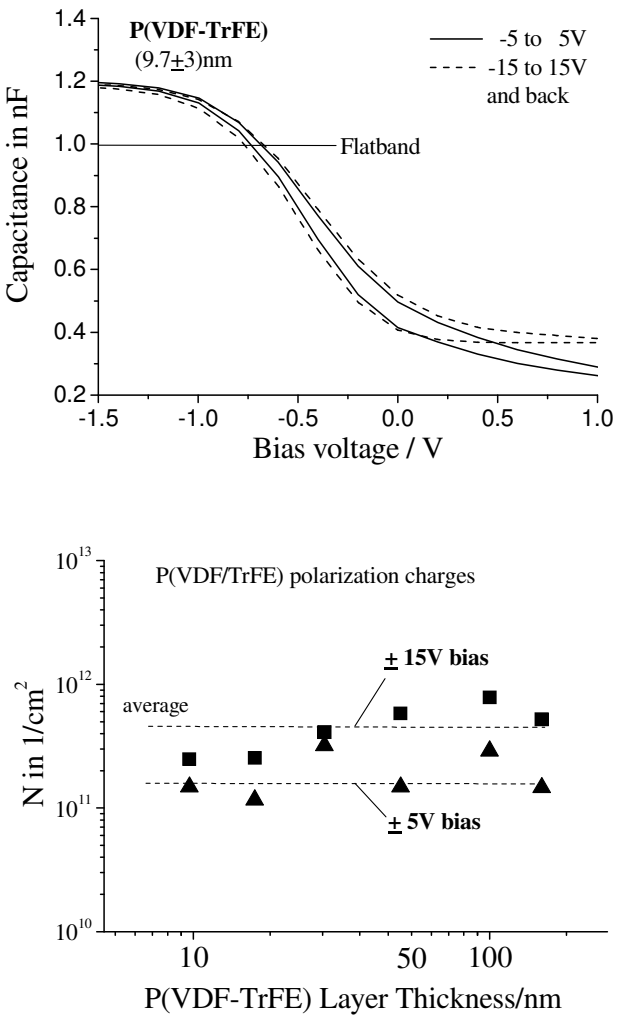

Figure 5.24. Top: CV measurements of a 10nm thick P(VDF-TrFE) film on a Si/SiO2(30nm) substrate, indium is used as top electrode, solvent is AZ-EBR. Flatband capacitance is calculated from electrode area and doping density of the Si-substrate.

Down: Surface charge N_{Fix}, calculated from equation 5.1, versus film thickness. Data are received from two different bias windows: for ±5V and ±15V. (Solvent: for 10 and 16 nm: AZ EBR, others: 2 Butanone)

This surface charge is a measure for the polarization charge. In earlier investigations of thicker films with a minimum thickness of 95 nm and Al top electrodes, we found exactly the above mentioned reduction of ferroelectric functionality, as a drop of the fixed surface charge N_{fix} at a thickness around 100 nm [49, 50]. So this value is really useful for a ferroelectric characterization of ultrathin (< 100 nm) and thin films.

The number of fixed surface charges per cm^2, calculated from equation 5.1, is plotted in figure 5.24 (down). We present the results for different copolymer film thickness, from around 10nm to a maximum value of 150 nm. The values for 150 nm film thickness represents the extrinsic switching behavior of a bulk film.

From the diagram, we are able to extract the following two main observations:

- First, we observe a flatband shift also for our ultrathin films in a thickness of 10 nm.
- Second, no decline of polarization is found for ultrathin films below 100 nm, the number of surface charges at a certain voltage window is more or less constant and independent of film thickness.

The first observation confirms the NEXAFS measurement before and after an application of the electric field. Even for ultrathin films of the copolymer a **linear dichroism** effect was found, which has to be attributed to a ferroelectric alignment. Further, our interpretation of the NEXAFS data is confirmed. The second observation leads to the conclusion, that the low voltage switching behavior, the so called "extrinsic" switching mechanism, is at least scalable down to a thickness of 10 nm. Here it has to be pointed out, that we have to calculate the field over the copolymer with the voltage divider SiO_2/P(VDF-TrFE), in accumulation. For -15V, the field strength is between 2 to 0.7 MV/cm for 10 nm and 150 nm, more than the coercive field E_c for extrinsic switching (0.5 MV/cm). For this field strength, the value N_{fix}, respectively the polarization charge has to be saturated, as confirmed by own measurements. Assuming a constant value for E_c with extrinsic switching, then N_{fix} has to be independent of film thickness, as observed. For –5V, the field is stronger than E_c up to 30 nm copolymer thickness. Additionally, the polarization seems to be independent of pinhole density.

Prerequisite for this low voltage switching and for minimized operation voltages is an adapted system of electrodes. Interactions at the interfaces during the preparation should be avoided. A fundamental threshold for ferroelectric switching itself does not exist down to at least 10 nm thickness of a spin coated copolymer film.

This is a very promising observation for spin coated ultrathin films. Ultrathin spin coated organic films should be important for a low cost approach for low cost memory applications with low operation voltages.

References

1. O. Auciello, J. F. Scott, and R. Ramesh, "The physics of ferroelectric memories", *Phys. Today 51 (1998) 22*.
2. T. Yagi, M. Tatemoto, and J. Sako, "Transition Behavior and Dielectric Properties in Trifluoroethyleneand Vinylidene Fluoride Copolymers" *Polymer J., 12 (1980) 209*.
3. K. Tashiro, K. Takano, M. Kobayashi, Y. Chatani, and H. Tadokoro, "Structural study on ferroelectric phase transition of vinylidene fluoride-trifluoroethylene copolymers (III) dependence of transitional behavior on VDF molar contant", *Ferroelectrics 57 (1984) 297*.
4. H. Ohigashi, Proc. 6th Int. Meeting on Ferroelectricity, Kobe 1985, *Jpn. J. Appl. Phys. 24 (1985) 23*.
5. J. B. Lando, and W. W. Doll, "The polymorphism of poly(vinylidene fluoride). I. the effect of head-to-head strcture", *J. Macromolecular science-Physics B 2 (1968) 205*.
6. B. L. Farmer, A. J. Hopfinger, and J. B. Lando, "Polymorphism of poly(vinylidene fluoride): potential energy calculations of the effects of head-to-head units on the chain conformation and packing of poly(vinylidene fluoride)", *J. Appl. Phys. 43 (1972) 4293.*
7. T. Furukawa, M. Date and E. Fukada, Y. Tajitsu, and A. Chiba, "Ferroelectric behavior in the copolymer of vinylidene fluoride and trifluoroethylene", *Jpn. J. Appl. Phys., 19 (1980) L109*.
8. G. T. Davis, M. G. Broadhurst, A. J. Lovinger, and T. Furukawa "Hysteresis in copolymers of vinylidene fluoride and trifluoroethylene", *Ferroelectrics 57 (1984) 73*.
9. T. Furukawa, M. Date, M Ohuchi, and A. Chiba, "Ferroelectric switching characteristics in a copolymer of vinylidene fluoride and trifluoroethylene", *J. Appl. Phys. 56 (1984) 1481*.
10. T. Furukawa, "Phenomenological aspect of a ferroelectric vinylidene fluoride/trifluoreethylene copolymer", *Ferroelectrics 57 (1984) 63.*
11. T. Furukawa, G. E. Johnson, H. E. Bair, Y. Tajitsu, A. Chiba, and E. Fukada,"Ferroelectric phase transition in a copolymer of vinylidene fluoride and trifluoroethylene", *Ferroelectronics 32 (1981) 61.*
12. Y. Takahashi, Y. Nakagawa, H. Miyaji, and K. Asai, *J. Polym. Sci., Part C, Polym. Lett. 25 (1987) 153*.
13. J. Stöhr, "NEXAFS Spectroscopy", *Springer-Verlag, 1996*.

14. W. L. Jolly, K. O. Bomben, and C. J. Eyermann, *At. Data Nucl. Data tables 31 (1984) 433*.
15. K. Seki, R. Matsumoto, E. Ito, T. Araki, T. Sakurai, D. Yoshimura, H. Ishii, Y. Ouchi, T. Miyamae, T. Narita, S. Nishimura, Y. Takata, T. Yokoyama, T. Ohta, S. Suganuma, F. Okino, and H. Touhara, Mol. Cryst. Liq. Cryst. 355 (2001) 247.
16. K. K. Okudaira, H. Yamane, K. Ito, M. Imamura, S. Hasegawa, and N. Ueno, Surf. Rev. Lett. 9 (2002) 335.
17. C. K. Tione, K. Tanaka, J. Maruyama, N. Ueno, M. Imamura, and N. Mastsubayashi, *J. Chem. Phys. 100 (1994) 5988.*
18. N. Ueno, K. Kamiya, Y. Harada, M. K.C. Tinone, T. Sekitani, and K. Tanaka, *Optoelectronics 11 (1996) 91*.
19. K. K. Okudaira, K. Ohara, H. Setoyama, T. Suzuki, Y. Sakamoto, M. Imamura, S. Hasegawa, K. Mase, and N. Ueno, *Nucl. Inst. Meth. Phys. Res. B 199 (2003) 265*.
20. K. Nagayama, R. Mitsumoto, T. Araki, Y. Ouchi, and K. Seki, "Polarized XANES studies on the mechanical rubbing effect of poly(tetrafluoroethylene) and its model compound", *Physica B 208/209 (1995) 419*.
21. R. P. Lisa, A. Hexemer, E. J. Kramer, S. Krishnan. P. M. Petroff, and D. A. Fischer, "Probing the Ordering of Semiconducting Fluorene-Thiophene Copolymer Surfaces on Rubbed Polyimide Substrates by Near-edge X-ray Absorption Fine Structure", *Macromolecules 39 (2006) 2225*.
22. A. Fujimori, T. Araki, H. Nakahara, E. Ito, M. Hara, H. Ishii, Y. Ouchi, and K. Seki, "Polarized Near Edge X-ray Absorption Fine Structure Spectroscopic Study on Organized Molecular Films of Fluorinated Comb Polymers with Various Chain Lengths", *Langmuir 18 (2002) 1437.*
23. A. Fujimori, T. Araki, H. Nakahara, E. Ito, M. Hara, N. Matsuie, H. Ishii, Y. Ouchi, and K. Seki, "Molecular Orientation in the Organized Molecular Films of Flurinated Cobm Polymers with Various Chain Lengths Studied by Soft X-ray Absorption Spectroscopy", *Bull. Chem. Soc. Jpn. 76 (2003) 663*.
24. A. Fujimori, H. Nakahara, E. Ito, M. Hara, K. Kanai, Y. Ouchi, and K. Seki, "Characteristic of molecular behavior and multilayer film strctures of comb polymers having different kinds of fluorocarbon side-chains", *J. Coll. Inter. Sci. 279 (2004) 184*.
25. J. L. Dehmer, D. Dill, and S. Wallace, *Phys. Rev. Lett. 43 (1979) 1005*.
26. F. Sette, J. Stöhr, and A. P. Hitchcock, *J. Chem. Phys. 81 (1984) 4906*.

27. K. Nagayama, T. Miyanae, R. Mitsumoto, H. Ishii, Y. Ouchi, and K. Seki, *J. Electron Spec. Relat. Phenom. 78 (1996) 407*.
28. D. G. Castner, K. B. Lewis Jr., D. A. Fischer, B. D. Ratner, and J. L. Gland, *Langmuir 9 (1993) 537*.
29. Y. Wada and R. Hayakawa, *Jpn. J. Appl. Phys. 15 (1976) 15*.
30. M. Tamura, S. Hagiwara, S. Matsumoto, and N. Ono, *J. Appl. Phys. 48 (1977) 513*.
31. R. G. Kepler and R. A. Anderson, *J. Appl. Phys. 49 (1978) 1232*.
32. T. Kajiyama, N. Khuwattanasil, and A. Takahara, *J. Vac. Sci. Tech. B 16 (1998) 121*.
33. H.-J. Sue, CK-Y Li, *Mater. Sci. 17 (1998) 853*.
34. T. Furukawa, "Ferroelectric Properties of Vinylidene Fluoride Copolymers", *Phase Trans. 18 (1989) 143*.
35. S. Mathews, R. Ramesh, T. Venkatesan, and J. Benedetto, *Science 276 (1997) 238*.
36. K. Müller, I. Paloumpa, K. Henkel, and D. Schmeiβer, "Organic thin film transistors with polymer high-k dielectric insulator", *Mat. Sci. Engg. C 26 (2006) 1028*.
37. R. C. G. Naber, P. W. M. Blom, A. W. Marsman, and D. M. De Leeuw, "Low voltage switching of a spin cast ferroelectric polymer", *Appl. Phys. Lett. 85 (2004) 2032*.
38. K. Müller, K. Henkel, I. Paloumpa, and D. Schmeiβer, "Organic field effect transistors with ferroelectric hysteresis", *Thin Solid Films 515 (2007) 7683*.
39. T. Tybell, C. H. Ahn, and J.-M. Triscone, *Appl. Phys. Lett. 75 (1999) 856*.
40. A. V. Bune, V. M. Fridkin, Stephene Ducharme, L. M. Blinov, S. P. Palto, A. V. Sorokin, S. G. Yudin, and A. Zlatkin, *Nature 391 (1998) 874*.
41. S. Palto, L. Blinov, A. Bune, E. Dubovik, V. M. Fridkin, N. Petuknova, K. verkhovskaya, and S. Yudin, *Ferolectric. Lett. 19 (1995) 65*.
42. S. Palto, L. Blinov, A. Bune, E. Dubovik, V. M. Fridkin, N. Petuknova, A. Sorokin, K. Verkhovskaya, S. Yudin, and A. Zlatkin, *Europhys. Lett. 34 (1996) 465*.
43. K. Müller, I. Paloumpa, K. Henkel, and D. Schmeisser, "A polymer high-K dielectric insulator for organic field-effect transistors", *J. Appl. Phys. 98 (2004) 056104*.
44. J. Choi, S.-J. Tang, P.T. Sprunger, P.A. Dowben, V. M. Fridkin, A. V. Sorokin, S. P. Palto, N. Petukhova, and S. G. Yudin, *J. Phys.: Condens. Matter 12 (2000) 4735*.
45. C.-G. Duan, W. N. Mei, W.-G. Yin, J. Liu, J. R. Hardy, S. Ducharme, and P. A. Dowben, *Phys. Rev. B 69 (2004) 235106*.
46. T. Reece, S. Ducharme, A. Sorokin, M. Poulsen, *Appl. Phys Lett. 82 (2003) 182*.
47. S. Lim, A. Rastogi, S. Desu, *J. Appl. Phys. 96 (2004) 5673*.
48. S.L. Miller, P.J. McWhorter, *J Appl Phys 72 (1992) 5999*.

49. K. Henkel, B. Seime, I. Paloumpa, K. Müller, D. Schmeißer, "Buffer layer investigation of MFIS stacks for organic nonvolatile memory applications", *Thin Solid Films 2008, submitted*.
50. K. Müller, Y. Burkov, D. Mandal, K. Henkel, I. Paloumpa, A. Goryachko, D. Schmeißer, "Microscopic and spectroscopic characterization of interfaces and dielectric layers for OFET devices", *Physica Status Solidi* ***5/3*** *(2008) 600*.

Chapter 6. Summary and outlook

We have successfully spin coated of different thickness P(VDF-TrFE) copolymer films. By this, we can able to make ultra thin copolymer films by controlling solution concentrations and spinning speeds. To measuring ultra thin films layer thickness we have employed a useful technique by the help of XPS results. Our FTIR and XRD results shows that our spin coated films are semicrystalline. We have improved the crystallinity by introducing the proper annealing environment. Our optimized best suitable annealing parameter is 135^{o} C for 2.0 hours. We have identified the ferroelectric β-phase for all thickness of the films independently by FTIR and XRD. By NC-AFM topographical studies we confirm that the well grown lamellar crystalline region appears while annealing. We have also found that the root mean surface roughness is improving significantly by annealing for all thickness of the copolymer films which good indication of the improvement of the crystallinity. We also show the effect of the annealing step by CV measurements, where we observed much more symmetric behavior in the flat-band voltage shift inside one CV loop after annealing, while the CV loops of non-annealed samples additionally shift due to a probable charge injection. Here we found that annealing lead to a higher polarization value.

We have optimized the X-ray irradiation time to investigate the XPS study by non disturbing condition. While optimization we notice that there might be phase change of the copolymer films from ferroelectric to paraelectric phase for longer time X-ray irradiation. This observation is conformed from FTIR and XRD results. Thus we can say that our XPS study has been done with proper care.

It is well known that the existence threshold for the remanent polarization for films below 100 nm of thickness, if we use aluminum as electrode. In this work we have find out the reason for the threshold thickness for aluminium electrode, incontrast we also investigate the advantage the use of the organic electrode PEDOT:PSS. We show a clear indication for a surface reaction of P(VDF-TrFE) with Al-electrodes, not only for evaporated Al, but also at room temperature, for the metal as bottom electrode. In sharp contrast, for PEDOT:PSS, the XPS measurements indicates a layer by layer structure of PEDOT:PSS/P(VDF-TrFE) without any interface modification. This could be the reason for lower relaxation times, higher switching

frequencies and in consequence, a better field dependence of the ferroelectric polarization, if we choose PEDOT:PSS as material for the electrode.

By capacitance voltage measurements, we confirm the ferroelectric behavior of the polymer by measurements at elevated temperatures (Curie-Point), we found a threshold for remanent poalrization for films blow 100nm, if we use aluminum electrodes, but with inert electrodes, a downscaling of a low coercitive field was possible down to ten nm. This is very important, because due to the high coercitive field of the copolymer (> 50MV/m), we need ultrathin films for low operation voltages. Prerequisite for memory applications is a **high retention time**, this was also confirmed.

We have investigated the **ferroelectric dipole orientation** of the P(VDF-TrFE) films by NEXAFS. By this we can able to identified the ferroelectric dipole orientation properties independently by with interaction with other layer. Thus the results confirm that the effect strictly arises from the ferroelectric film. As per our best of knowledge, this work could not done before.

By NEXAFS, we have also investigated that the effect of the electric field up to lowest thickness of 10 nm copolymer films. Here we also verified by the total fluorescent yield mode filed which can cover total film thickness. We have found significant effect of dipole orientation even for ultra thin (10 nm) spin coated film. To conforming the ferrolectricity, we have additionally employed the CV measurements.

The NEXAFS observations confirms that even for ultrathin films of the copolymer a **liner dichroism effect** was found, which has to be attributed to a ferroelectric alignment. The CV measurements leads to the conclusion, that the low voltage switching behavior, the so called “extrinsic” switching mechanism, is at least scalable down to a thickness of 10 nm (5 monolayers). This is a very promising observation for spin coated ultrathin films. Ultrathin spincoated organic films should be important for a low cost approach for low cost memory applications with low operation voltages.

List of abbreviations

PVDF	Polyvinylidene fluoride
TrFE	Trifluoroethylene
P(VDF-TrFE)	Poly (vinylidene–trifluorethylene)
FeFET	Ferroelectric field effect transistor
MFIS	Metal/ferroelectric/insulator/semiconductor
TeFE	Tetrafluoroethylene
PEDOT:PSS	Poly(3,4- ethylenedioxidythiophene):poly(styrenesulfonicacid)
FTIR	Fourier transformed infra-red spectroscopy
FWHM	Full width at half maxima
XRD	X-ray diffraction
AFM	Atomic Force Microscope
CV	Current-Voltage
XPS	X-ray Photoelectron Spexctroscopy
NEXAFS	Near edge X-ray Absorption Fine Structure
TEY	Total electron yield
TFY	Total fluorescent yield

List of Publications

1. K. Müller, Y. Burkov, D. Mandal, K. Henkel, I. Paloumpa, A. Goryachko, and D. Schmeißer, "Microscopic and spectroscopic characterization of interfaces and dielectric layers for OFET devices", *Physica Status Solidi A 205/3 (2008) 600*.

2. K. Müller, D. Mandal, and D. Schmeißer, "No Interfacial Layer for PEDOT Electrodes on PVDF: Characterization of Reactions at the Interface P(VDF/TrFE)/Al and P(VDF/TrFE)/PEDOT:PSS", *MRS Proceedings 997 (2007) I6-02*.

3. K. Henkel, D. Mandal, B. Seime, I. Paloumpa, I. Lazareva, K. Müller, P. Müller, and D. Schmeißer, "Electrical investigations on MFIS strctures consisting P(VDF/TrFE) as ferro-electric layer for non-volatile memory applications", *Proceedings of 15th Workshop on Dielectrics in Microelectronics (2008) 159*.

4. K. Müller, D. Mandal, K. Henkel, I. Paloumpa, and D. Schmeißer, "Ferroelectric properties of spin-coated ultra-thin (down to 10nm) P(VDF/TrFE) copolymer films", *Applied Physics Letters, 93 (2008) 112901*.

5. K. Henkel, I. Lazareva, D. Mandal, I. Paloumpa, K. Müller, Y. Koval, P. Müller, and D. Schmeißer, "Electrical investigations on MFIS structures using P(VDF/TrFE) as ferroelectric layer for organic nonvolatile memory applications", *Journal of Vacuum Science and Technology B, submitted (2008).*

6. D. Schmeißer, M. Tallarida, K. Henkel, K. Müller, D. Mandal, D. Chumakov, and E. Zschech," Characterization of oxidic and organic materials with synchrotron radiation based XPS and XAS", *Materials Science Poland, submitted (2008).*

7. K. Müller, D. Mandal, and D. Schmeißer, " XPS and NEXAFS of P(VDF-TrFE) films on different Substrates", EMRS spring meeting 2007, Symposium E, *Thin Solid Films, submitted* (2007).

8. D. Mandal, K. Müller, K. Henkel and D. Schmeißer, "Effect of X-ray irradiation on P(VDF-TrFE) copolymer thin film", *J. Poly. Sci. 2008 (in preparation).*

9. D. Mandal, K. Müller, K. Henkel, and D. Schmeißer, "Effect of external electric field for P(VDF-TrFE) films: a NEXAFS study", Applied Physics Letter, *2008 (in preparation).*

Conference/Meetings contributions

1. **"Study of reactions at the interface P(VDF-TrFE)/Al and P(VDF-TrFE)/PEDOT:PSS",** D. Mandal, K. Müller, O Seifarth, P Hoffman, K Henkel, and D. Schmeißer, Annual Meeting of the Deutsche Physikalische Gesellschaft and DPG (26-30 March, 2007; Regensburg, Germany).

2. **"Orientation of dipoles in the P(VDF-TrFE) co-polymer films"**, D. Mandal, K. Müller, and D. Schmeißer, The 15th International Conference on Vacuum Ultraviolet Radiation Physics (VUV) (July 29 - August 03, 2007; Berlin, Germany).

3. **"NEXAFS of P(VDF-TrFE)/PEDOT:PSS films on Si"**, K. Müller, D. Mandal, D. Schmeißer, O. Seifarth, P. Hoffmann, and K. Henkel, EMRS Spring Meeting (May 28 - June 1, 2007; Strasbourg, France).

4. **"No interfacial layer for PEDOT electrodes on PVDF: Characterizations of reactions at interface P(VDF-TrFE)/Al and P(VDF-TrFE)/PEDOT:PSS"**, K. Müller, D. Mandal, and D. Schmeißer, MRS Spring Meeting 2007 (9-12 April, 2007; Sanfrancisco, CA,USA).

5. **"Dipole orientation of the P(VDF-TrFE) co-polymer films: A NEXAFS study"**, D. Mandal, K. Müller, and D. Schmeißer, Annual Meeting of the Deutsche Physikalische Gesellschaft and DPG(25-29 Feb., 2008; Berlin,Germany).

6. **"Interface reactions of ferroelectric copolymer layers with different electrode materials"**, K. Müller, D. Mandal, K. Henkel, I. Paloumpa, and D. Schmeißer, Annual Meeting of the Deutsche Physikalische Gesellschaft and DPG(25-29 Feb., 2008; Berlin,Germany).

7. **"Electrical and spectroscopic characterization of ultra-thin (<100nm) organic ferroelectric films"**, K. Müller, D. Mandal, K. Henkel, and D. Schmeißer, EMRS Spring Meeting (2008; Strasbourg, France).

8. **"Electrical investigations on MIFS structure consisting P(VDF-TrFE) as ferroelectric layer"**, K. Henkel, D. Mandal, B. Seime, I. Paloumpa, K. Müller, D. Schmeißer, I. Lazareva, and P. Müller, Congress Materials Science and Engineering (2008; Nürnberg, Germany).

9. **"Electrical and spectroscopical characterization of P(VDF-TrFE) ferroelectric layers, prepared by spincoating solutions"**, K. Müller, D. Mandal. I. Paloumpa, K. Henkel, and D. Schmeißer, 11th Europaen Conference on Organized Films (2008; Potsdam, Germany).

10. **"Electrical investigations on MIFS structure consisting P(VDF-TrFE) as ferroelectric layer for non-volatile memory applications"**, K. Henkel, D. Mandal, B. Seime, I. Paloumpa, I. Lazareva, K. Müller, P. Müller, and D. Schmeißer, 15th Workshop on Dielectric in Microelectronics (2008; Bad Saarow, Germany).

11. **"No interfacial layer for PEDOT electrodes on PVDF: Characterization of reactions at the interface P(VDF/TrFE)/Al and P(VDF/TrFE)/PEDOT:PSS",** K. Müller, D. Mandal, and D. Schmeißer, European Conference on Molecular Electronics (ECME) (05-08 Sept., 2007; Metz/France).

12. **"Organic ferroelectrica for non-volatile memory devices",** K. Müller, D. Mandal, K. Henkel, B. Seime, and D. Schmeißer, Euromat (10-13 Sept. 2007; Nürnberg).

13. **"Study of reactions at the interface P(VDF/TrFE)/Al and P(VDF/TrFE)/PEDOT:PSS"**, K. Müller, D. Mandal, O. Seifarth, P. Hoffmann, K. Henkel, and D. Schmeißer, Workshop on Integrated Electroceramic Functional Structures (IEFS) (14-15 June, 2007; Berchtesgaden).

Acknowledgments

Germany is the motherland of Einstein, Plank, Schrödinger, Heisenberg, Laue, and many other physicists. I had the dream to visit this great country to take part of my academic carrier since my childhood. Therefore first of all, I would like to thank Prof. Schmessier for giving opportunity to pursue my doctorate programme in his group.
The topic *"Ultrathin Films of a Ferroelectric Copolymer: P(VDF-TrFE)"* was suggested by Prof. Schmessier to me. I am very grateful to him for his valuable advice, suggestions, and many other new ideas. It is a pleasure to discuss with him.

I would like to thank Dr. Klaus Müller and Karsten Henkel for their constant encouragement and valuable suggestions.

I would like to appreciate the support of all my colleagues who have made the completion of this work possible: Guido Beuket, Karsten Henkel, Dr. Olaf Seifarth, Dr. Patrick Hoffman, Dr. Klaus Müller ,Dr. Massimo Tallarida, Mr. Fridricd, Dr. Rakesh Sohal and Dr. Mohamed Torche for their technical assistance and scientific discussions.

I would like to express special thanks to Mrs. Ioanna Paoumpa and Carola Schwiertz for valuable suggestions for sample preparations.

I would like to acknowledge Mrs. Kersten for fast solving of all aspects in administrative work.

I would also like to acknowledge the technical support of the BTU mechanical workshop and the BESSY staff.

I appreciate the support of all of my family members and friends. Their understanding and encouragement have sustained me through many difficult and challenging moments.

Finally, I greatly appreciate the financial support from the DFG under the project DFG-SCHM 745/9-2.